NTNU
Det skapende universitet

Ultra høyfast betong med fiberarmering og testing av Da Vinci brumodell

Linda Landbø

Bygg- og miljøteknikk
Innlevert: juni 2014
Hovedveileder: Terje Kanstad, KT

Norges teknisk-naturvitenskapelige universitet
Institutt for konstruksjonsteknikk

Department of Structural Engineering
Faculty of Engineering Science and Technology
NTNU- Norwegian University of Science and Technology

ACCESSIBILITY

MASTER THESIS 2014

SUBJECT AREA:	DATE:	NO. OF PAGES: 89
Concrete structures	10.06.14	

TITLE:

Non-linear analyses and laboratory testing of the Leonardo da Vinci bridge in Ultra High Performance Fibre Reinforced Concrete.

Ikke-lineære analyser og laboratorietester av Leonardo da Vinci brua i Ultrahøyfast Fiberbetong

BY:

Linda Landbø

SUMMARY: In 2010 a group of students built a bridge in Ultra High Performance Fibre Reinforced Concrete as part of a group project. This is a slender structure that spans 3 meters without conventional reinforcement. The bridge is fibre reinforced with 2vol-% steel fibres of 3.5cm. In 2010, standard material tests were executed and the flexural strength was calculated to 16.2MPa and the compressive strength to 113.7MPa. The bridge's true capacity was never tested. This master thesis consist of a theoretical report about Ultra High Performance Fibre Reinforced Concrete, a laboratory report and non-linear finite element analyses of the bridge using the software DIANA. The research also includes testing and numerical analyses of smaller elements of the same material.

The purpose of the thesis is to determine material tensile properties of the material, by using a curve fitting principle and inverse analyses. The research presented concludes with a stress-strain relationship for the material and the flexural capacity of the da Vinci bridge. Conclusions also concerns non-linear analyses in DIANA and time dependent material effects.

RESPONSIBLE TEACHER: Terje Kanstad

SUPERVISOR(S): Terje Kanstad, Max Hendrix

CARRIED OUT AT: Department of Structural Engineering

Preface

This master thesis is carried out at the Department of Structural Engineering at Norwegian University of Science and Technology (NTNU), spring 2014.

The thesis consist of non-linear analyses and failure testing of a small-scale footbridge built in Ultra High Performance Fibre Reinforced Concrete. The goal is to verify the material properties of the concrete used in the bridge using the concept of inverse analyses and curve fitting. Also, the thesis includes a somewhat extensive theory report.

My personal basis for starting the thesis was limited, with no previous knowledge to DIANA and with only basic courses covering numerical solutions and FEM. A considerable amount of time has been put into finite element theory, theory on concrete technology and learning the software.

During the project I have gained extensive knowledge about UHPFRC, non-linear analyses of concrete and I have become acquainted with the FEM program DIANA. I am personally very satisfied with the learning outcome of the thesis.

I would like to express my gratitude towards my teaching supervisor Terje Kanstad for his professional support and guidance during the project. He has been genuinely interested and encouraging throughout the process. There has been many obstacles along the way, mainly considering the software and non-linear analyses. I have received advice and help from several people and I would like to give special thanks to Max Hendriks, Morten Engen, Elena Vidal Sarmiento and Jan Øverli for all technical support. The time you have generously spent with me on this project have speared me many hours of troubleshooting.

Testing was done in the concrete laboratory at NTNU, and i would like to thank laboratory personnel Steinar Seehus for help executing the tests.

Linda Landbø Trondheim, June 2014

Abstract

In 2010 a group of students built a bridge in Ultra High Performance Fibre Reinforced Concrete as part of a group project. The structure is slender and spans 3 meters without conventional reinforcement. The bridge is fibre reinforced with 2vol-% steel fibres of 3.5cm. In 2010, standard material tests were executed and the flexural strength was 16.2MPa and the compressive cylinder strength was 113.7MPa. The bridge's true capacity was never tested. This thesis consist of a theoretical report about Ultra High Performance Fibre Reinforced Concrete, a laboratory report and non-linear finite element analyses of the bridge using the software DIANA. The research also includes testing and numerical analyses of smaller elements of the same material. All additional mathematical calculations throughout the thesis, and the plotted results are carried out in MATLAB.

The purpose of the thesis is to determine material tensile properties of the material, using a curve fitting principle and inverse analyses. The research presented concludes with a stress-strain relationship for the material and the flexural capacity of the da Vinci bridge. Conclusions also include general comments concerning non-linear analyses in DIANA and time dependent material effects of UHPFRC.

Conclusions:

- The final material model defines the cracking strength as 3.0MPa and the residual strength as 4.0MPa. A hardening and a softening tensile behaviour is determined and the compressive strength is defined as 113.7MPa based on previous cylinder testing.
- The flexural capacity of the da Vinci bridge built in 2010 was 12.1kN.
- Number of integration points, a strict force convergence norm and avoiding shear stresses in the cracks prove important for the accuracy of the results in DIANA. The non-linear model is quite sensitive to modifications in the stress-strain behaviour especially after crack localization.
- The behaviour in the analyses is stiffer than in the experiment. Ageing and time dependent effects as shrinkage and drying have a negative impact on the stiffness of the structure and changes the cracking behaviour.
- For slender constructions which are designed for small service loads, UHPFRC shows rather good quality in strength and ductility. This master thesis proves that mixing and casting of Ultra High Strength

> Concretes must be executed with great care and a reduction in stiffness over time should be expected due to autogenous shrinkage and drying.

Due to a number of sources of error, the material model is not considered to be a conservative result.

Sammendrag

I 2010 bygget en gruppe studenter ved NTNU en bru i ultrahøyfast fiberbetong som en del av et studieprosjekt. Brua er slank og spenner over 3 meter. Den er fiberarmert med 2 vol-% stålfiber på 3.5cm. I 2010 ble det utført standariserte materialtester i forbindelse med bruprosjektet. Bøyefastheten ble målt til 16.2MPa og trykkfastheten til 113.7MPa. Den egentlige styrken til brua ble aldri testet. Denne masteroppgaven inneholder en teoretisk rapport som omhandler ultrahøyfast fiberbetong, en laboratorierapport og ikkelineære FEM analyser av brua ved bruk av analyseprogrammet DIANA. Studiet inkluderer også testing og numeriske analyser av mindre elementer av samme materiale. Alle andre utregninger og alle plottede resultater er gjort i MATLAB.

Målet med oppgaven er å bestemme materialegenskapene til da Vinci brua, ved bruk av kurve-tilpassing og invers analyse. Studiet konkluderer med en spenning-tøynings kurve og bruas bøyefasthet. I tillegg trekkes frem ikke-lineære analyser i DIANA og tidsavhenginge virkninger på ultrahøyfast fiberbetong.

Konklusjoner:

- Materialmodellen defineres med en risstyrke på 3.0MPa og en residual styrke på 4.0MPa. En herdende og en avherdende oppførsel er bestemt og trykkfastheten er antatt å være 113.7 slik som i tidligere forsøk.
- Bøyestyrken til da Vinci brua ble målt til 12.1kN.
- Antall integrasjonspunkter, et strengt lastbestemt konvergenskrav og å unngå lokale skjærkrefter i rissene viser seg viktig for resultatene i DIANA. Modellen er også sensitiv for små endringer i spenning-tøyningsdiagrammet, speiselt etter risslokalisering.
- Den analytiske oppførselen er stivere enn den reelle. Alder og tidsavhenginge virkninger har en negativ effekt stivhet og endrer rissoppførsel i en konstruksjon.
- For slanke konstruksjoner som er designet for små nyttelaster, viser ultrahøyfast fiberbetong ypperlige egenskaper i styrke og duktilitet. Denne masteroppgaven viser at om det kreves nøyaktighet når man støper en ultrahøyfast betong. En kan også forvente en redusert stivhet som følge av autogen svinn og uttørking.

På grunn av en rekke mulige feilkilder er ikke materialmodellen regnet som konservativ.

Contents

List of Figures

Acronyms

ACM Advanced Cementitious Materials.

AFGC The Association Francaise de Génie.

CMOD Crack Mouth Opening Displacement, crackwidth.

COIN Concrete Innovation Centre, SINTEF.

CRC Compact Reinforced Composites.

CSH Calsium Silicate Hydrate.

FDN Functional Design NL.

FEM Finite Element Method.

fib The International Federation for Structural Concrete.

FRC Fibre Reinforced Concrete.

GGBS Ground Granulated Blast-furnace Slag.

NSC Normal Strength Concrete.

RCP Reactive Concrete Powder.

RHA Rice Husk Ash.

RILEM The International Union of Laboratories and Experts in Construction Materials, Systems and Structures.

SF Silica Fume.

SP Superplastifisizer.

UHPC Ultra High Performance Concrete.

UHPFRC Ultra High Performance Fibre Reinforced Concrete.

w/b ratio Water-Binder ratio.

Chapter 1

Introduction

Ultra High Performance Fibre Reinforced Concrete (UHPFRC) is a material developed over the last 30 years combining the high compressive strength of Ultra High Performance Concrete (UHPC) and the ductility and tensile strength of fibre reinforcement. UHPC is a very brittle material and with only conventional reinforcement the application of the material is limited. By using fibre reinforcement the concrete obtains ductility both in compression and in tension and the material can be applied in structural elements.

With France and Japan in the lead, researchers around the world have developed, tested and analysed varieties of UHPFRC. Last year, in 2013, the second international symposium on UHPFRC was held in Marseilles. The first conference was held in 2009. Between then and now, the global interest and use of UHPFRC in construction has grown significantly.

For advocates of UHPFRC, the increasing international interest in the material is very positive. One of the reasons this material has not been largely implemented in the industry is the lack of quantitative experimental data and internationally approved building codes that contain calculation methods and national requirements.

The properties of UHPC and UHPFRC make it ideal for use in repair of structures. Also it is suitable for developing new structures where deterioration will be an issue, e.g. in infrastructure.

1.1 Objective

In 2010 a group of students at the Norwegian University of Science and Technology (NTNU) built a model bridge based on the original design of Leonardo da Vinci's bridge over Golden Horn as part of a project on Fibre Reinforced Concrete (FRC). The material used was an Ultra High Performance Fibre Reinforced Concrete. There was done several simplified calcu-

lations and sample testing of the concrete during the project, but the bridge was never tested to its full capacity.

The objective for the thesis is to carry out a failure test of the bridge and use FEM analyses to determine the tensile properties and behaviour of the material.

1.2 Outline

This thesis will consist of two parts. The first part will be literary on the subject: Ultra High Performance Fibre Reinforced Concrete, describing the matrix composition, material properties and the application of the material. In the second part of the report the model bridge from 2010 will be tested in the laboratory, and analysed in the FEM software DIANA. The analysis and test results will map the material properties and tensile behaviour of the UHPFRC used in the model.

Part I

Ultra High Performance Fibre Reinforced concrete (UHPFRC)

Chapter 2

History and development of UHPFRC

2.1 Ultra High Performance Concrete

One can define Ultra High Performance Concrete (UHPC) as concrete with extraordinary compressive capacity. Generally the term UHPC refer to concrete with a compressive strength of 150-250MPa. Without fibre reinforcement UHPC is a brittle material with relatively low tensile capacity. The concrete can have an elasticity modulus up to 60 000MPa which can lead to very brittle behaviour at failure. This makes UHPC without fibre reinforcement an undesired material and the applications of it is restricted. (Sandven, 2009)

2.2 Fibre Reinforced Concrete

The standard method of reinforcement is reinforcing the concrete with steel bars where it is necessary to resist tension or shear in the concrete. The building codes demands minimum reinforcement and a certain concrete coverage to the re-bars. In slender structures or structures where only minimum reinforcement is required an alternative method of reinforcement may be applied.

Fibre Reinforced Concrete (FRC) is concrete reinforced with fibres, randomly distributed in the concrete matrix. The different fibres used are carbon, polypropylene, alkali-resistant glass and steel among others. Fibre reinforcement can be used as a replacement to conventional re-bars, but often the strength of FRC is not sufficient enough to act solely in large structures. In that case the two methods of reinforcement are used in combination. The use of FRC will normally not affect the strain at cracking but fibres can transfer stress across cracks leading to a significant improvement

of the residual strength and ductility. The combination of the reinforcement methods can reduce the amount of necessary re-bars, reduce the crack widths and increase stiffness.

Typical applications of FRC is in foundations, pre-cast shell and disc elements, beams, pipes and ducts and sprayed concrete for strengthening purposes. FRC is applied e.g. as rock support in tunnels. The concrete is sprayed on to strengthen the tunnel lining between the bolts used to prevent large rocks to fall. Because of low workability and a lack of documentation and regulations FRC is not a widely used material in Norway today. However, there are currently several research projects working to promote it e.g. COIN - the COncrete INnovation Centre lead by SINTEF.

(Sandbakk, 2011; COIN, 2013)

2.3 Ultra High Performance Fibre Reinforced Concrete

Ultra High Performance Fibre Reinforced Concrete (UHPFRC) is a fibre reinforced high performance concrete. An often referred to definition is a fibre reinforced concrete with a compressional strength higher than 150MPa and tensile strength larger than 8MPa. UHPFRC is not widely used in Norway, mainly because of the reasons mentioned for FRC and UHPC. However, world wide there is a growing interest for the material and there are several projects built entirely in UHPFRC. There is a shifting focus and new solutions are required by the industry. (Sandven, 2009)

2.3.1 Research

The international symposium on UHPFRC

France is one of the countries that are ahead in researching UHPFRC. In October 2013 the International Symposium on Ultra High Performance Fibre Reinforced Concrete was held in the Museum of European and Mediterranean Civilizations in Marseille. The conference was organized and hosted by The Association Francaise de Génie (AFGC), The International Federation for Structural Concrete (fib) and RILEM - The International Union of Laboratories and Experts in Construction Materials, Systems and Structures. The objective was to review recent research and the knowledge gained since the last UHPFRC conference in 2009. The latest achievements in civil engineering using UHPFRC in infrastructure, construction and rehabilitations were presented, evaluated and analysed with respect to structural design, reliability and sustainability. (AFGC, 2013)

COIN

Concrete INnovation Centre (COIN) is a research initiative for increased innovation in the concrete industry. Lead by SINTEF the project was granted 200 million Norwegian kroners for research in the period 2007-2014.

COIN works to:

- Further develop fundamental research to be able to make advanced and environmental materials combined with effective and viable methods of production and construction.
- Increase concrete reputation as the environmental material first choice.
- Increase expertise and innovation.
- Stand out in Europe as a leading research centre.
- Contribute to increased research and education.

(COIN, 2013)

COIN annually reports results from their ongoing research projects. Focus area 2.2: Ductile High Tensile Strength Concrete (Fibre Reinforced Concrete), is lead by project manager Terje Kanstad. The objective has been to achieve a ductile concrete with a flexural residual strength of 15MPa and in general make the use of fibres possible in load bearing structures. The 2013 annual report also presents results from tests considering the issues of low flowability while obtaining high residual strength. A solution is a superflowable and stable self-consolidating concrete with fibres. Some pictures and load-deflection diagrams from the testing of the da Vinci bridge in Part II of this thesis are also presented in the annual COIN report from 2013.

As a result of Focus Area 2.2 COIN has published a State of The Art on UHPFRC and a proposition to calculation of fibre reinforced concrete. Both papers are cited several times in this thesis.

(COIN, 2013; SINTEF, 2013)

Chapter 3

Material Characterization

3.1 Matrix

The main differences between the UHPFRC and the conventional concrete matrix are the amount of binder, the size of the aggregate and the presence of fibre.

3.1.1 Water/binder ratio

To achieve high strength and high durability, there are several aspects of the concrete matrix that differs from conventional concrete. In conventional concrete the water/binder ratio lies between 0.35-0.5. The w/b ratio in a UHPFRC matrix should lie close to 0.2. The typical w/b ratios are shown in Figure 3.1. A higher content of binder leads to the absence of capillary pores, higher density and increased strength. The matrix is more compact and the pores in the UHPFRC concrete are smaller than in normal concrete. (Sandven, 2009; COIN, 2013)

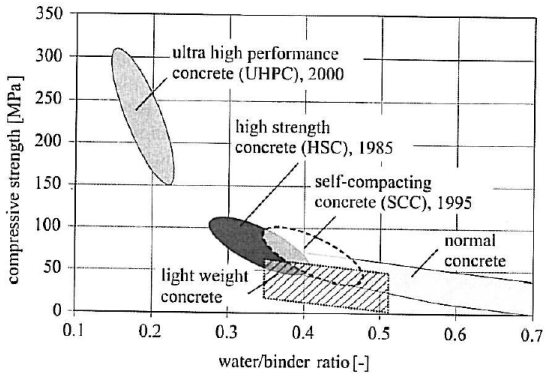

Figure 3.1: Typical areas of water/binder ratios for the different types of concrete. (COIN, 2013)

3.1.2 Packing of particles

Packing density is defined as the volume percentage of solids for each volume unit. When the particles are optimally packed, the volume of air in the mix is minimized. The challenges to obtain high density and stabilize the mix is solved by adding large amounts of fine particles to fill the voids between the larger particles as described in Figure 3.2. When fibres are introduced in the matrix high packing density positively affects the bond between the matrix and the fibres.

Some materials in the concrete matrix function as packing density enhancing additives. Particle packing is crucial for concrete. The way the cement paste encloses the aggregates is largely affected by the particle packing.

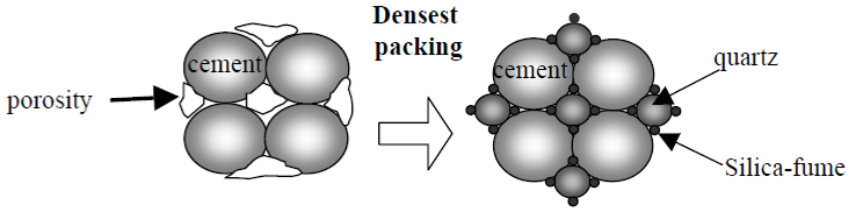

Figure 3.2: Particle packing. (COIN, 2013)

A completely dense packed matrix is not optimal as it will not flow easily during casting. To obtain a densely packed mix as well as maintain required workability, water-reducing agents are added. This ensures that the concrete matrix is flowing despite a high density.

(COIN, 2013)

3.1.3 Cement

The binder used in concrete is cement. In UHPFRC, double the amount of cement is used in the matrix compared to conventional concrete. When choosing cement it is favourable to choose on the grounds of low water demand. Because of the low w/b-ratio, a part of the cement will remain unreacted. This will act inertly and contribute to the particle packing. Several studies suggest part of the cement content to be replaced by additives with certain qualities to improve the properties of UHPFRC.(COIN, 2013)

3.1.4 Additives

Silica fume

Silica fume (SF) is an ultra-fine powder collected as a by-product when producing silicon and ferrosilicon alloys. It contains 85-98 % SiO_2, has a mean particle size of 0,1-0,2 μm and an amorphous structure.

UHPFRC usually has a high content of silica fume, typically 25% of the cement weight. It acts as a micro filler as well as it is a pozzolan which reacts with calcium hydroxide which is the product of cement hydration. The reaction of SF and calcium hydroxide produces calcium silicate hydrate, a binder with higher strength than calcium hydroxide. This reaction increases strength and improves the bond between binder and aggregates and the interaction between binder and steel fibres.

Silica fume should be used in combination with water-reducing admixtures for best performance. Water reducing agents decrease the voids in the matrix leading to a decreased water demand. Further water reduction is then possible by filling the present voids with silica fume.

(Habel et al., 2006; COIN, 2013)

Fly ash

Fly ash is a bi-product of the combustion process of coal, typically from coal fired electric generating plants. It can consist of either an aluminosilicate or a calcium silicate and it has, similar to silica fume, pozzolanic properties and serves as a water reducer.

Using fly ash in concrete will effect the concrete properties in several ways. If cement is replaced by fly ash the concrete obtain a longer setting time and the hardening at an early age is decreased.

(COIN, 2013)

Other additives

In addition there are several alternative supplements that may be added to the matrix or replacing part of it.

Ground Granulated Blast-furnace Slag (GGBS) is made from molten iron slag from blast furnace, a by-product from the iron and steel industry. It can be added to any concrete matrix containing ordinary cement, and may be used in combination with other pozzolanic materials. The slag is composed of limestone, silica and alumina, with small amounts of alkali and iron oxides

as well as magnesia. GGBS enhances the durability of concrete structures and it has a positive influence on flexural strength. Due to improvement in the binder phase both compressive strength and the bonds between the fibres and the matrix are enhanced. GGBS reduces the risk of damage caused by alkali-silica reactions and gives higher resistance to chloride penetration and to attacks by aggressive chemicals, improving the durability. (COIN, 2013)

Rice Husk Ash (RHA) is the by-product of burning rice husk which is used as a fuel in the milling industry or as a fuel for power generation. RHA is similar to silica fume and has a high content of amorphous silica which gives it good pozzolanic properties. Compared to silica fume, which has spherical particles, RHA has angular and porous particles. RHA can replace SF successfully with respect of durability of the concrete and compressive strength. (COIN, 2013)

Van Tuan et al., performed a study in 2012 indicating that RHA has good properties in reducing the autogenous shrinkage of UHPC. RHA has a porous structure and affects both the rate and extent of hydration when added to cement. The study shows that shrinkage is decreased with higher added amounts of RHA, whereas shrinkage increase with increased amounts of SF added. (COIN, 2013; Tuan et al., 2011)

Nanosilicas contribute to denser packing of the matrix by being smaller particles able to fill the voids between cement and finer additives. A denser matrix will have improved mechanical properties due to a higher content of calsium silicate hydrate(CSH). The concretes durability is also enhanced. A study performed by Qing et al in 2007 showed that the pozzolanic activity of nanosilicas is greater than that of SF. It thickens the cement paste and improves the bond between aggregates and paste, in addition to speeding up the hydration process of the matrix. (COIN, 2013; Qing et al., 2007)

3.2 Aggregates

The coarsest aggregate in UHPFRC is 0.5-4mm, but the mean particle size often lies under 1mm. If the maximum aggregate size is 0.5mm or less, the matrix can be defined as Reactive Concrete Powder (RCP) It is very important that the aggregates possess high mechanical strength like granite or bauxite, so it does not become the weakest part of the concrete. (Habel et al., 2006; COIN, 2013)

3.3 Super-plasticizer

UHPFRC is characterized by a high content of cement, silica fume and superplasticizer (SP). Superplasticizer is a high range water reducer and is

highly required in UHPFRC to obtain acceptable workability. It is added to the matrix to improve flow characteristics, casting abilities and to reduce the required volume of water. (Habel et al., 2006; Sandven, 2009; COIN, 2013)

3.4 Fibres

The most commonly used fibre material is steel. There are also other materials used in fibres such as carbon, polypropylene and alkali-resistant glass, but they are often ousted by steel because of it's many favourable properties. Figure 3.3 shows the different types of steel fibres used in FRC.

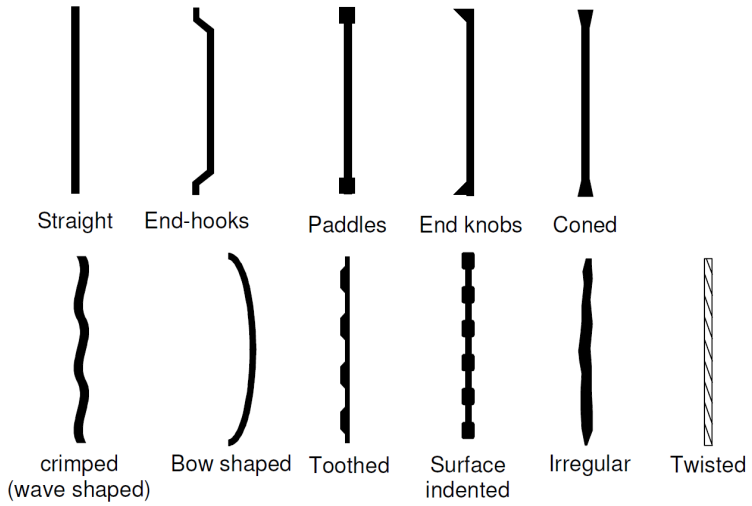

Figure 3.3: Typical steel fibre geometry used in FRC. (Löfgren, 2014)

The amount of fibres added to the concrete matrix is measured as a percentage of the total matrix volume. The fibres aspect ratio is the length of the fibre divided by fibre diameter, l/d. When multiplying fibre percentage with aspect ratio we get fibre factor which is a way to characterize the properties of fibre reinforced concrete. The amount of steel fibres in UHPFRC can be up to 11 vol-%. It has been proven that 2,5 vol-% with an aspect ratio of 40-60 leads to the best result both in view of fresh and hardened concrete properties. (COIN, 2013)

Since there has to be acceptable workability when working with UHPFRC the amount of long fibres cannot be too high, but the fibre content can often include both long and short fibres. Today, we have three main types of fibre reinforced concrete:

- Compact Reinforced Composites (CRC)

  CRC contains 5-10 vol-% fibres and the fibres are fairly short (less than 6mm). Fibres of this length do not contribute largely to ductility, but increase the tensile strength. The concrete is therefore often used in addition to traditional bar reinforcement.

- Reactive Powder Concrete

  RPC contains 2-3 vol-% fibres with length between 13 and 20mm. These fibres improve both the tensile strength and ductility of the concrete. The fibres are intended to replace all traditional reinforcement.

- Multi Scale fibre Reinforced Concrete

  The matrix contains a mixture of short and longer fibres. It can contain up to 11 vol-% fibres and is intended to replace all reinforcement.

(Mehta and Monterio, 2013)

When choosing fibres there are several aspects to consider. The size and geometry of the structure is of importance when deciding fibre size because the crack openings may differ. Also, the largest diameter of the aggregate particles must be evaluated. To ensure low porosity the fibres length should be ten times the maximum aggregate diameter.

Direction and distribution of the fibres will affect how much of the reinforcement that is effective. There will always be an uncertainty of the distribution so large quantities of testing data are necessary to know the reliability of the material. The viscosity of the matrix influences the fibres ability to move within the matrix after mixing. It is important that it is not possible for the fibres to fall with gravity in the matrix during casting.

(Sandven, 2009; Graybeal, 2011; COIN, 2013)

Chapter 4

Material Properties

UHPFRC has high tensile strength and ductility due to fibre reinforcement. The ductility continues to develop even after cracking in cooperation with the fibres. Tensile strength is normally higher than 8MPa. A meso-mechanial model has been developed to predict the UHPFRC tensile response as a function of the volume, aspect ratio, distribution and orientation of the fibres and the mechanical properties of the matrix.

4.1 Strength

4.1.1 Compressive strength

As discussed UHPC has a very high compressive strength, typically between 150-250MPa, but higher strength have also been reached. The compressive strength is only moderately influenced by fibre reinforcement, but the stress-strain relationship under compressive loading is considerably affected by the fibre content. After reaching maximum compressive strength the stress-strain diagram of UHPFRC descends. The slope of this descending part of the diagram depends on content, geometry, stiffness and orientation of the fibres in the matrix. (COIN, 2013)

In 2007 Benjamin Graybeal did a research paper on the stress-strain relationship for UHPFRC in compression and the relationship between compressive strength and the modulus of elasticity. In the paper three linear equations describing the relationship between the E-module and the compressive strength at 28 days are presented, the first for normal strength concrete and the second two determined in UHPFRC studies.

$$E = 4730\sqrt{f'_c}[MPa] \tag{4.1}$$

$$E = 3320\sqrt{f'_c} + 6900[MPa] \tag{4.2}$$

$$E = 19000\sqrt[3]{\frac{f'_c}{10}}[MPa] \tag{4.3}$$

The conclusion in the paper however is that it is terribly difficult to achieve the correct stress-strain response and the E-module using predefined formulas due to the fact that concrete is a heterogeneous material without standardised mixture design. In other words, the relationship is highly dependant on the individual matrix. In Figure 4.1 one can see Greybeal's experimentally derived compressive stress-strain diagram compared to the linear elastic response. His research was executed with cylinder compression tests of treated and untreated UHPFRC. His result gives a picture of what a typical response would look like, given that the gradient and plot valued depend on the researched concrete.(Graybeal, 2007)

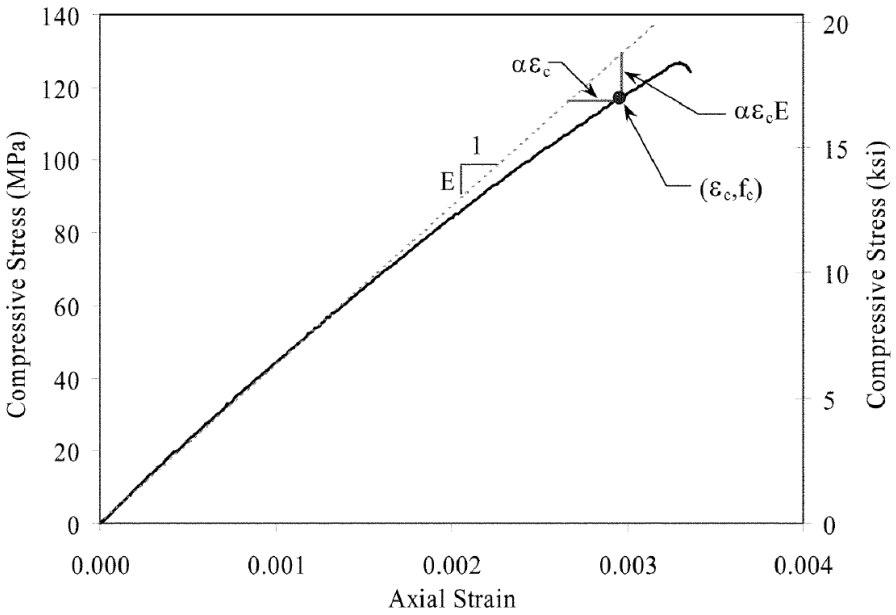

Figure 4.1: Typical stress strain response for UHPFRC(Graybeal, 2007)

4.1.2 Tensile and flexural strength

UHPFRC can be classified as either strain softening of strain hardening in tension. Strain softening is when the maximum tensile capacity decreases after crack opening. This means that the fibres do not contribute to hold the cracks together, although the fibres may increase the tensile strength of the concrete. UHPFRC can also often show strain-hardening behaviour under uniaxial loading. Strain hardening is the strengthening of the material by plastic deformation. In this case the fibres stitch the cracks together. For a material to be strain-hardening in pure tension it requires a very

high fibre content, typically more than 2 volume-%. Even if an UHPFRC exhibit strain hardening behaviour in bending it does not necessarily mean that it exhibits strain hardening in direct tension. Therefore, softening or hardening behaviour cannot be considered to be a material but a structural constructional characteristic. A typical stress-strain relationship is shown in Figure 4.2, where σ_{cc} is the cracking strength, σ_{pc} is the post-cracking strength also known as the residual strength. The curve is divided into 3 domains. From 0 to point A the material behaves linear elastic. At point B, crack localization occurs and softening behaviour is initiated. The softening part of the curve is expressed by a σ-w-curve, where w is the crack width. The size of the different domains depend on the concrete matrix, and for conventional concrete the second domain with strain hardening is close to non-existing. Typical maximum residual tensile strengths of UHPFRC are 6-20MPa. (Habel et al., 2006; Habel, 2004; COIN, 2013)

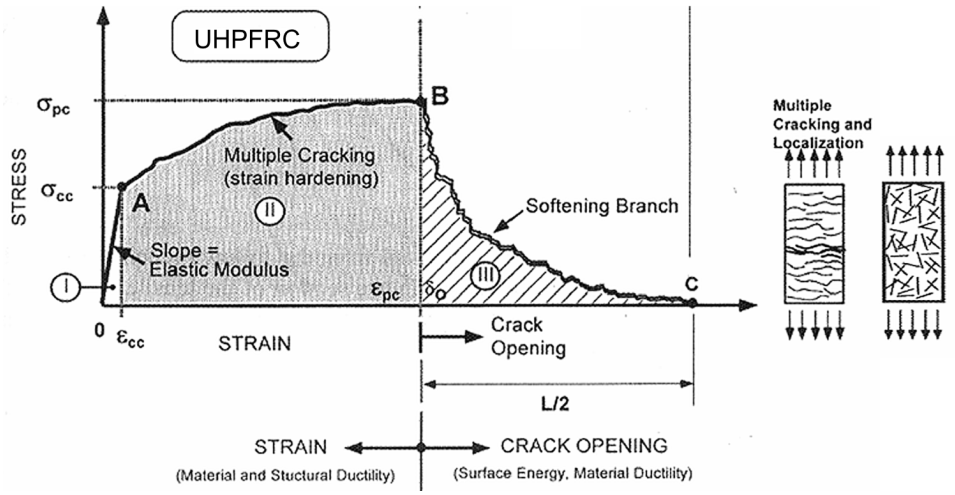

Figure 4.2: Typical stress strain response for UHPFRC(Habel, 2004)

The residual strength may double when fibres are added, depending on the fibre amount, type, distribution and orientation. Distribution and orientation highly depend on viscosity, fibre geometry and casting methods. If the fibres are unevenly distributed it can lead to an inhomogeneous distribution of tensile properties in an element. The orientation of the fibres is also determined by the placing direction, so to obtain higher flexural strength the concrete should be placed parallel to the longitudinal direction of the structure. (COIN, 2013)

There is not a general conclusive way to test flexural and especially direct tensile strength of UHPFRC. To determine the tensile capacity of UHPFRC

the ideal method is uniaxial tensile testing. However, the execution of such tests are challenging and time-consuming. Therefore the tensile behaviour of UHPFRC is often determined by bending tests. The results then have to be interpreted to uniaxial behaviour. During testing the load is measured against the CMOD in a defined notch. See test procedure explanation in Section X and in the following calculations L, b and h are the dimensions of a standard test beam. Four crack widths are predefined and the flexural strength, $f_{\mathrm{R,i}}$ is calculated from the measured load at the given widths with the assumption of linear stress distribution over the cross section. This is shown in Figure 4.3 and 4.4. F_R and M_R refer to applied load and occurring moment.

$$f_{\mathrm{R,i}} = \frac{6M_{\mathrm{R,i}}}{bh^2} \tag{4.4}$$

where

$$M_{\mathrm{R,i}} = \frac{F_{\mathrm{R,i}}L}{4} \tag{4.5}$$

The characteristic values are defined as:

$$f_{\mathrm{Rk,i}} = f_{\mathrm{R,i}} - k \cdot s \tag{4.6}$$

where s is the standard deviation from the data series and k=1.7.

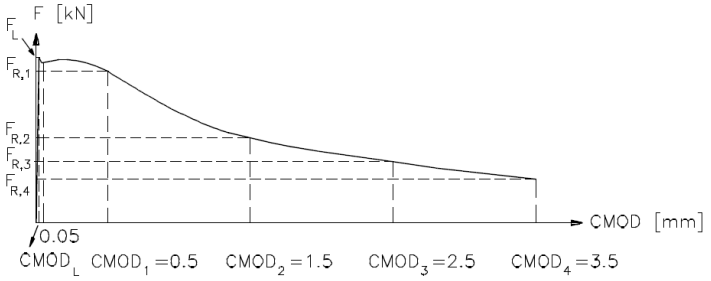

Figure 4.3: A typical test result where the load, F, is measured at predefined crack widths, CMOD. (Kanstad et al., 2011)

Then, the characteristic residual tensile strength, $f_{ftk,res}$ can be derived, based on the assumption that the stress distributions shown in Figure 4.4 are applicable. To calculate the residual tensile strength, characteristic flexural strength at 2.5mm crack width, $f_{\mathrm{Rk,3}}$, is used.

$$f_{\mathrm{Rk,3}} \cdot \frac{bh^2}{6} = f_{\mathrm{ftk,res,2.5}} \cdot b \cdot 9h \cdot 0.5h \tag{4.7}$$

$$f_{\text{ftk,res,2.5}} = 0.37 f_{\text{Rk,3}} \tag{4.8}$$

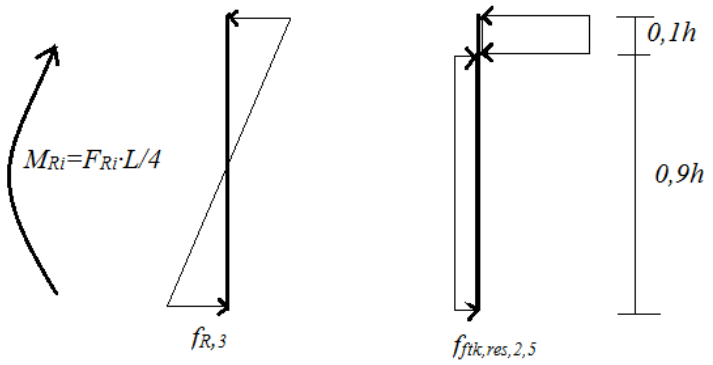

Figure 4.4: Relationship between occurring moment, flexural residual strength at CMOD=2.5mm and characteristic residual tensile strength. (Kanstad et al., 2011)

(Habel, 2004; COIN, 2013; Kanstad et al., 2011)

4.1.3 Cracking

Cracking in UHPFRC starts as a micro crack in the material. Micro cracks are microscopic cracks and can be present in the material already before loading. Under loading they align and form macro cracks which has an effect on the structure. A crack can be active which indicates the crack is changing and deforming, or dormant, where the crack width, length and direction is constant. When loading continues macro cracks become critically active and concentrated stresses and local strains originate in the material. Fibres suppress the formation of cracks and abate their propagation and growth. Strain-hardening UHPFRC has a larger post-cracking strength, where the fibres bridging the cracks contributes to a greater strength than the true cracking strength of the cementitious matrix.

In Figure 4.5, domain I represent micro cracking, domain II and III represent critically active macro cracks originating and expanding. The domains coincide with the domains in the stress strain diagram in Figure 4.2 and domain IV represent the range beyond point C where there are no longer stresses transferred through the localized macro cracks. These cracks are called *real cracks*. The propagation of cracks as a function of the stress-strain relationship is also shown in Figure 4.6

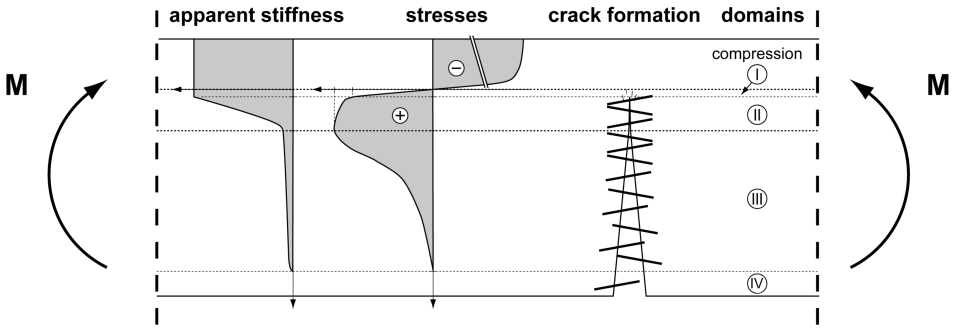

Figure 4.5: Crack formation for UHPFRC. (Habel, 2004)

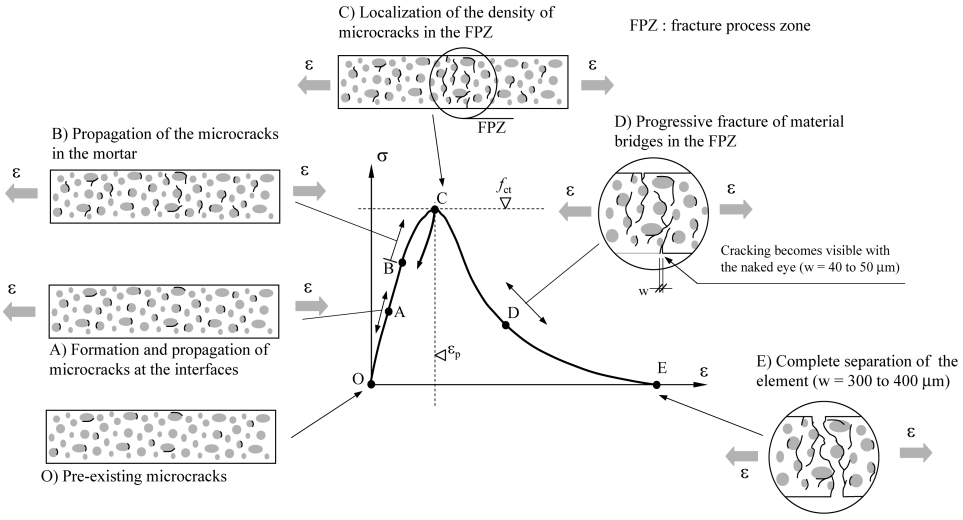

Figure 4.6: Crack formation during the stress-strain progress. (Habel, 2004)

(COIN, 2013; Banthia, 2008; Graybeal, 2011; Habel, 2004)

4.1.4 Time dependent effects

Shrinkage and creep

Plastic shrinkage occurs when the concrete is fresh, the phase from mixing to early setting. Plastic shrinkage is caused by surface evaporation. When water evaporates at a higher rate than the concrete can transport water to the surface (concrete bleeding) the surface will dry out and an underpressure in the pore water causes contraction forces between the particles. The contraction of the concrete result in shrinkage and cracks. These cracks can range from micro to active macro cracks.

In concretes with lower w/b-ratio and small distanced between the particles, like UHPFRC, the capillary forces are greater and the bleeding is

reduced. This increase the rate of plastic shrinkage. It has been shown that matrices that require considerable amounts of plasticizing additives such as SP to achieve workability experience greater plastic shrinkage. The tendency is that such matrices loose their workability quickly and become semi-plastic almost immediately after casting a phase where plastic shrinkage often occur.For UHPFRC with low porosity and w/b-ratio the surface evaporation should not only be reduced, but prevented completely. This could be done by using plastic covers or curing membranes.

Autogenous shrinkage is the concretes inner shrinkage. When the concrete components react with each other the reaction product has a smaller volume than the reactants. During concrete hydration the concrete therefore experience autogenous, or chemical shrinkage. When the inner volume is reduced pores in the binder are created in addition to the external shrinkage. On further hydration these pores are emptied, a process called self-desiccation or self-drying. The consequence of self-desiccation is that the relative humidity within the concrete drop, especially for high strength concretes with low w/b-ratio, and capillary forces are created resulting in external shrinkage. Due to the capillary under-pressure, autogenous shrinkage will be larger in concretes with finer particles and smaller pores, e.g. UHPFRC. This may lead to micro cracks in the material, but can be reduced by using certain additives as described in Section 3.1.4.

Autogenous shrinkage may contribute to plastic shrinkage cracking. This is a theory based on the fact that plastic shrinkage cracks often occur despite many efforts to avoid plastic shrinkage.

After curing, concrete exposed to air will experience drying shrinkage. UHPFRC will, due to small pores and an under-hydrated state not experience as much drying shrinkage as conventional concrete. Drying shrinkage begin on the surface and spread inward through the cross section. Similar to the process of plastic shrinkage tensile stress is created by drying out capillary pores and cracks are originated. The drying state can be presented by the relative humidity in the concrete and the stress is somewhat inverse proportional to the relative humidity. At the concrete surface the relative humidity is low and the tensile stress is high.

Drying shrinkage initiates the minute the formwork is removed and will be largest in the beginning. It is the air humidity of the surroundings that will be the reason for drying shrinkage. The additives, the additives' strength and the cement paste's creep properties will also have an effect.

(Bjøntegaard, 2007; COIN, 2013)

Creep is the time-dependent increase in strain under constant load taking

place after the initial strain at loading. In normal strength concrete, the creep coefficient decrease with an increasing strength. Considering this, the creep in UHPFRC is larger than expected and one reason may be the large amount of paste in the matrix. Heat treatment will reduce creep and shrinkage significantly. (COIN, 2013)

4.2 Hydration

The hydration process of concrete is the exothermal chemical reaction between cement and water along with the reaction of pozzolanic additives in the matrix that lead to hardening of the concrete. Pozzolanic additives, such as silica fume, do not possess cementitious properties, but react chemically with calcium hydroxide and form compounds that do. (Wikipedia, 2014)

Calsium Silicate Hydrate (CSH) is a result of the reaction between cement and water and is mainly responsible for the strength in cementitious material. Figure 4.7 shows the process of hydration of conventional concrete divided into 5 stages. The initial reaction of the process is the production of CSH which form a protective layer on the cement grain surface. The hydration process is then slowed down by this CSH layer. Stage 2 is a dormant stage, where the hydration is nearly stopped, and the material is still workable. Then there is an acceleration stage where the protective layer is broken down and the cement begin to hydrate quickly. The concrete is setting and the products of the hydration process increase in volume and bonds are created between them. After the final setting of the concrete the deceleration stage starts. Hydrated layers around the cement grains brings the high rate of hydration to an end. The reaction is finally brought to a stage of steady state. This final stage finishes when there is full hydration or when there is no more water available to react with cement.

The degree of hydration α at time t is defined as the ratio between hydrated cement at time t and initial amount of cement. When alpha = 1 the cement is fully hydrated.

$$\alpha(\mathrm{t}) = \frac{\text{hydrated binder cement at time t}}{\text{initial amount of binder cement}} \tag{4.9}$$

There can normally only be full hydration of cement if the w/b ratio is over 0.42. For any lower ratio there will remain unhydrated cement in the material. The process of hydration will then be referred to as the degree of reaction, where r at time t is the relation between hydration at time t and final expected hydration. The final degree of hydration can be predicted on the basis of the concrete mix composition.

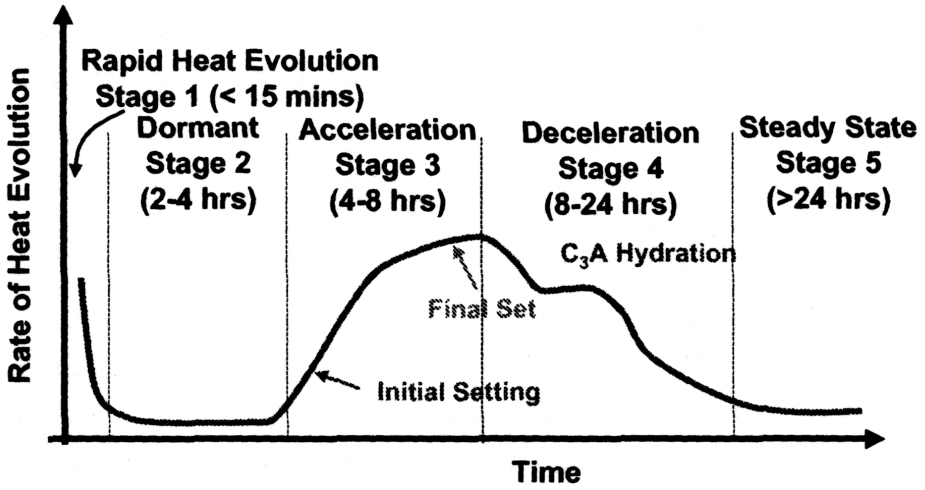

Figure 4.7: The five stages of hydration of normal strength concrete (NSC). (Habel, 2004)

$$\mathrm{r(t)} = \frac{\alpha(\mathrm{t})}{\alpha(\mathrm{t} \to \infty)} = \frac{\alpha(\mathrm{t})}{\alpha_{\mathrm{final}}} \tag{4.10}$$

UHPFRC has a low w/b-ratio and can therefore not fully hydrate. The hydration process is also modified due to a high amount of SP in the material. This delays the setting of material and the dormant period is typically 24 hours or longer compared to 2-4 hours as for conventional concrete. (See Figure 4.7)

(Habel, 2004; Habel et al., 2006)

UHPFRC has significant increase in strength during the first months and has developed most of its final mechanical properties at the age of 90 days approximately. While conventional concrete continues to hydrate and develop properties over several decades, UHPFRC allows only partial hydration which leads to self-drying. The hydration process stops after 90 days. Although the initial degree of reaction is similar, the degree of reaction in UHPFRC develops faster than in conventional concrete, which leads to higher early age strength and stiffness. This may accelerate the construction and prestressing when used in structures. (In UHPFRC the tensile strength develops at a lower rate than for conventional concrete and the fracture energy is 5 times higher.) (Habel et al., 2006)

4.3 Durability and Resistance

The durability of concrete is defined by mechanical properties such as strength, gas permeability and porosity. Autogenous shrinkage in UHPFRC will form micro cracks in the material, reducing the resistance against penetrating substances. Despite this, compared to conventional concrete UHPFRC has improved characteristics in permeability, heat resistance and impact strength. Due to small pores and high density on the material surface, UHPFRC also has high resistance against frost and humidity. Water does not as easily penetrate and the liquid ingress is reduced. It is also very resistant to chloride and other chemical attacks and has high resistance against abrasion. (Sandven, 2009; COIN, 2013)

Chapter 5

Production and Application

5.1 Production Methods

5.1.1 Mixing and casting

Many of the same mixing and casting operations apply for UHPFRC as conventional concrete. However, UHPC requires more energy and increased mixing time. Also, FRC requires special consideration for placement operations and only limited external vibration because of the influence this has on the orientation of fibres have on mechanical properties of the structure. Dispersion and direction of the fibres in the matrix is largely influenced by mixing and casting, the fibres tend to orient in the flow direction. The casting process is therefore very important for the result. (Graybeal, 2011)

5.1.2 Curing procedures

The curing procedure requires little hydration. Heat curing is when the temperature is brought up to accelerate the curing procedure, but no hydration must occur. Surface is sealed of to prevent surface dehydration. Heat treatment, often not necessary, and rarely applied. For practical and economical reasons, mainly UHPFRC without heat or pressure curing is used in field applications. (Graybeal, 2011; Habel, 2004)

5.1.3 Testing

There are different testing procedures. Many of the similar methods can be used to test UHPFRC and conventional concrete, but in some compressive cylinder and cube tests alterations in procedures are required because of high strength. Flow testing, compression testing, modulus of elasticity testing, tensile testing, chloride penetration testing, freeze-thaw durability testing and other durability tests are normal tests to apply the concrete. Examples

of different testing methods to determine material strength are given in Figure 5.1. (Graybeal, 2011)

(a) Cylinder compressive test.

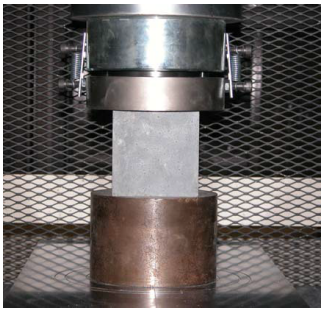

(b) Cube compressive test.

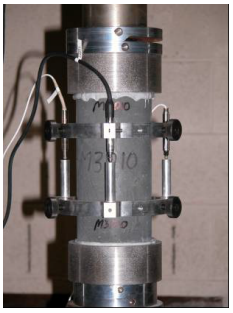

(c) Cylinder tensile test.

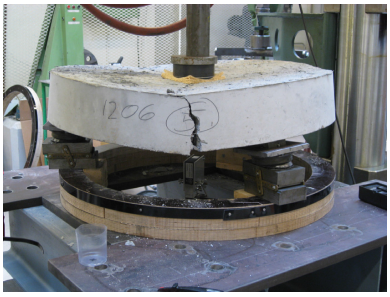

(d) Panel tests.

Figure 5.1: Test methods. (Graybeal, 2005; Sandbakk, 2011)

As mentioned in section 4.1.2, to determine the direct tensile capacity of UHPFRC, bending tests are often applied. The results then have to be interpreted to uniaxial behaviour. Tensile behaviour must be evaluated with care so that the true cracking strength and the post-cracking enhanced strength are recorded separately. Some examples of test procedures for flexural bending are 3-point tests with notch and 4-point test without notch. The crack width is computed as a function of load and flexural strength is calculated according to theory. A three point test with two defined notches was used during testing in 2010 and the calculations are described in Section 6.2.4.

To test fibres explicitly tensile test and pull-out tests on single fibres are practised.

(Graybeal, 2005; Sandbakk, 2011)

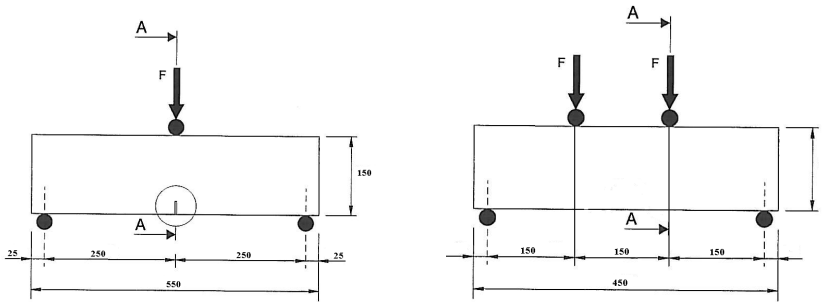

(a) 3-point flexural test with notch under load

(b) 4-point flexural test without notch

Figure 5.2: Examples of flexural beam tests. (Sandbakk, 2011)

5.2 Application

The material costs of UHPFRC are significantly higher than that for conventional reinforced concrete. One can ask if it is economical to build structures solely in UHPFRC. Due to limited validated regulations on the subject and the comprehensive process of casting the use of UHPFRC is not widely applied today, especially not as sole material. However, in several countries in Europe and some places in the US the use of UHPFRC is in focus and newer projects were UHPFRC is the main structural material have been carried out.

Due to the high costs it is necessary to optimize the structural design. Lightweight UHPFRC structures, where necessary concrete is minimized, is a competitive material to steel and concrete and offer an improvement in durability and aesthetic features. In Alicante, a u-shaped truss footbridge spans 45 meters over the Ovejas ravine. The structure is precast and has a thickness of 35mm. The bridge is the first truss pedestrian bridge of its kind, where all the structural elements are made of solely UHPFRC.

(López et al., 2014)

UHPFRC was initially intended for the precast industry. Because of challenges in mixing and casting, pre-casting and on-site assembling was the original area of use. In Amsterdam an innovative consultancy and engineering company, FDN (Functional Design, NL), produce Ultrabridges. The Ultrabridge is made from precast UHPFRC elements pre-stressed together by internal bonded tendons. The concept is shown in Figure 5.4. The bridge can span up to 30 meters and is put together by only two element types, railings and plates. FDN's website market the following promising aspects of their concept:

Figure 5.3: UHPFRC bridge over Ovejas ravine in Alicante

- Maintenance free for 100 years
- Low CO_2-footprint
- Easy to transport
- Minimum concrete
- Constructed in a day
- Design your own railing

...among others.
(FDN, 2014)

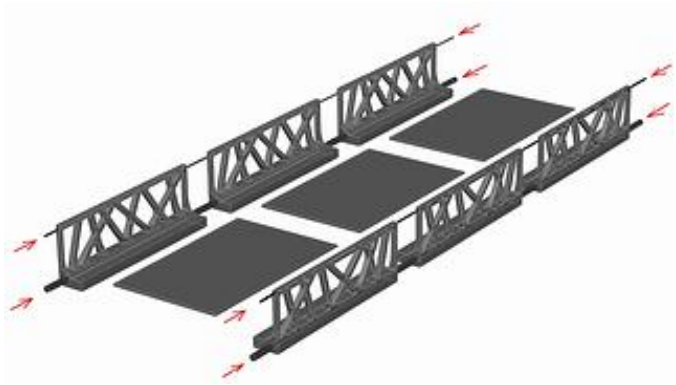

Figure 5.4: The Ultrabridge structure concept

As a product of an international architect contest in 2002 the Museum of European and Mediterranean Civilizations (MuCEM) was designed and built in Marseilles. See Figure 5.5. The architecture is modern and the principle elements of the structure; the columns, long-span beams, façade

and roof, is made of UHPFRC. Also the footbridge linking the structure to the Saint Jean fort is built with UHPFRC. (Nemetschek.Scia, 2013)

(a) The museum and the footbridge linking it to the Saint Jean fort

(b) The UHPFRC façade.

Figure 5.5: The Museum of European and Mediterranean Civilizations (MuCEM)

UHPFRC can more easily be applied in composite materials where the advantages of several materials can be exploited in an optimal way. Katrin Habel documented in 2004 a study on composite materials combining Advanced Cementitious Materials (ACM) and conventionally reinforced Normal Strength Concrete (NSC) where ACM, such as UHPFRC are used in especially vulnerable parts of a structure, for example at points of exposure to detrimental substances or under high concentrated loading. The theory is applicable in cases of both rehabilitation and improvement of existing structures and in the building of new ones. In any case where guaranteed durability is demanded. UHPFRC is, with its high resistance against deterioration processes, often used in parts of a structure subjected to attack of damaging substances or where high strength and stiffness is required. In bridge construction and highway infrastructure development and repairing, UHPFRC is for example used in thin overlays and concrete crash barriers. See Figure 5.6. These are elements exposed to physical abrasion and detrimental substances such as salts containing chlorides. UHPFRC and other ACM are very useful when the mechanical resistance need to be increased without increasing the dead load of the structure. (Habel, 2004)

Footbridges are suitable for trying out new materials and methods, because the actual payload is small. There are several footbridges around the world built with UHPC and UHPFRC today. Other areas of application can be in roads, beams in nuclear power plants, staircases and marine structures. (Habel, 2004)

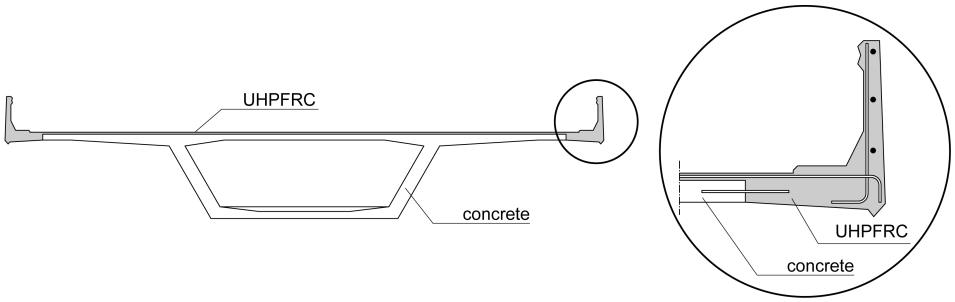

Figure 5.6: UHPFRC is suitable for use in thin overlays and crash barriers on roads and bridges.(Habel, 2004)

Today, the UHPFRC commercial product that is most popular is Ductal. Ductal is a brand of UHPC developed by Lafarge, a french industrial company that focuses on innovative solutions. Ductal is one of their newer concrete products. MuCEM is built with Ductal concrete. (Lafarge, 2014)

Part II

The Da Vinci Bridge Model

Chapter 6

History and Background

6.1 Da Vinci and the bridge

The Golden Horn in Turkey is an inlet that separates the historic center of Istanbul and the rest of the city. In 1502, the Italian Renaissance artist Leonardo da Vinci, designed a bridge with the intetion of participating in a civil engineering project for Sultan Bayezid II. His drawings presented a single-span bridge over the Golden Horn. The designed bridge span was 240 meters, but was never built. (Wikipedia, 2014)

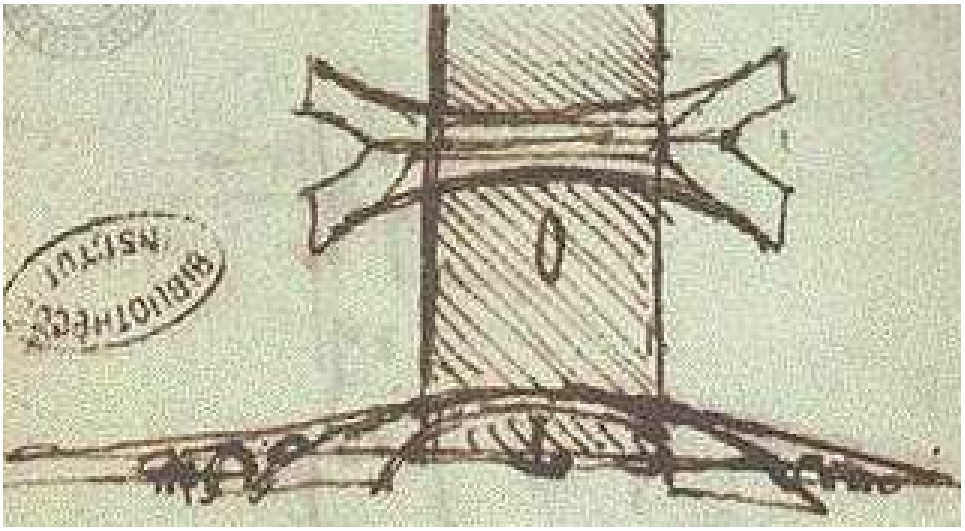

Figure 6.1: Da Vinci's original design drawings

In 2005, the Norwegian artist Aune Sand designed a footbridge inspired by da Vinci's design. It was placed in Ås, constructed by the engineering company Dr. Techn. Olav Olsen. This bridge is made of laminated timber, while da Vinci' original idea was in stone.

Figure 6.2: The da Vinci footbridge in Ås, designed by Aune Sand

6.2 UHPFRC model bridge

In 2010 a group of students at Norwegian University of Science and Technology created a reconstruction of da Vinci's original bridge as part of a project assignment in the course Experts in Team (EiT). The model bridge has a span of three meters and is made of UHPFRC. The students made a simplified 2D structural design in *Focus 2D Konstruksjon* to determine necessary thickness of the bridge. They calculated a necessary thickness of 20,8 mm but with regards to deviations from the 2D model to the actual structure the bridge was built with a thickness of 30mm. The bridge was intended as a footbridge so the width of the mid-span was set to 400mm, enough room for a person to cross.

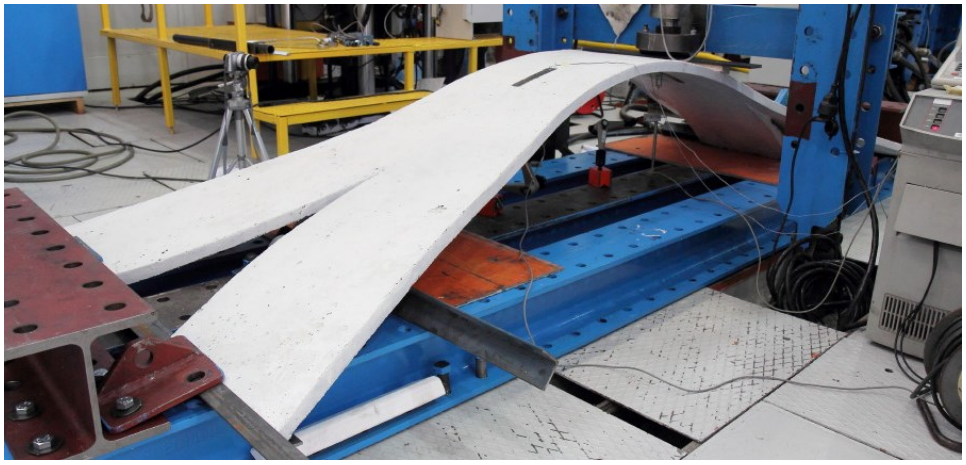

Figure 6.3: The da Vinci bridge built by students at NTNU in 2010

6.2.1 Arch bridge theory

Before the introduction of concrete and steel, stone and brick were the main materials available for construction. These materials had only compressive strength, and offered challenges in design and construction. Arches were a solution to such challenges. Arch bridges were designed to transfer only compressive forces. Under construction an arch had to continuously be supported by scaffolding which made the building of large span bridges very comprehensive work. Da Vinci's bridge was originally designed in stone material, and designed to avoid tensile forces in the construction. As the model bridge from 2010 is built in UHPFRC this criteria was overlooked and the focus was to minimize the flexural bending moment in the arch.

An arch is normally designed as a part of a circle or a parabola. For large spans the arch line will resemble a parabola, while for smaller spans an arch will often be circular. The da Vinci bridge arch is designed as part of a circle. The flexural stiffness EI often varies along the arch due to for example changes in cross section, especially for larger arches. In our case, the arch is relatively small and we assume constant EI.

(a) Zero-hinge arch (b) Two-hinge arch (c) Three-hinge arch

Figure 6.4: Arches

An arch can be a zero-hinge, two-hinge or a three-hinge arch. The da Vinci bridge is a two hinge arch where the main arch is restrained against horizontal and vertical movement at both ends, but are free to rotate. The moment distribution in the arch is dependent of external loading and the ratio between the rising height and the span. An arch's boundary conditions also influences the distribution of forces and deflection of the arch.

When analyzing an arch there are several approaches. Arches are often slim structures and should be calculated with second degree theory where deformations are accounted for. In real life the analysis is often divided into two steps. First, a classical static analysis where deflections are neglected then an additional analysis where the effects of deformations are calculated.

The actual analysis of the da Vinci bridge will be executed in the computer software DIANA, but to find the most unfavourable point of loading we use influence lines for the arch to find the critical points. Influence lines are functions giving the effect, in a determined point in the structure, of a

load placed at an arbitrary location along the structure. To determine the influence lines for a two-hinge arch we follow the method of Bjørn Vik and Norconsult.

In a two-hinge arch there is only one statically undetermined force, the horizontal reaction force H at the hinged ends. For an arch, the influence line for H is η_H. The length of the span is defined as L, rising height as f and x is the distance from left one end.

$$\eta_H = \frac{(x/L - 2 \cdot (x/L)^3 + (x/L)^4)/3}{\frac{8 \cdot f}{15 \cdot L} + \frac{I_0}{f \cdot L \cdot A_0}} \tag{6.1}$$

The equation accounts for axial deformations.

The influence line for moment at a determined point in a vertically loaded two-hinge arch is

$$\eta_M = \eta_M^0 - \eta_H \cdot y \tag{6.2}$$

where η_M^0 is the influence line for the moment at the same point in a simply supported beam with the same span as the arch and y is the arch height:

$$y(x) = \frac{4 \cdot f}{L^2} \cdot x \cdot (L - x) \tag{6.3}$$

The method is illustrated in Figure 6.5

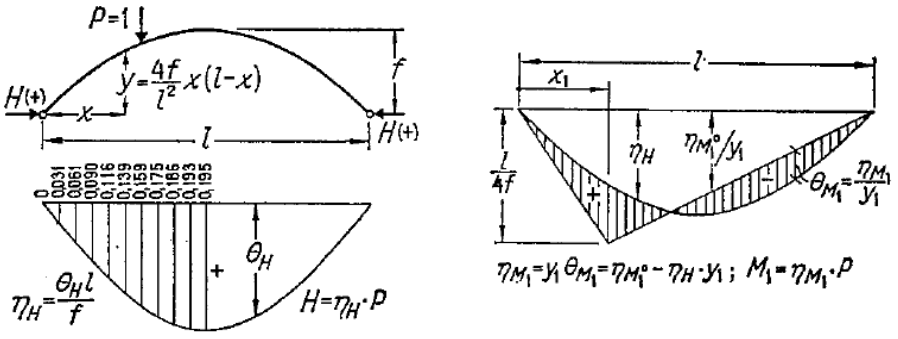

Figure 6.5: Influence line for reaction force H at arch end and for moment at point x_1. (Vik, 2012)

(Vik, 2012)

6.2.2 Geometry

The geometric description given in the project from 2010 was limited. The main values such as span, width and rising height were listed in the report, but the overall geometry was directly measured in the laboratory. The values are shown in Figure 6.6 and 6.7. (Haagensrud et al., 2010)

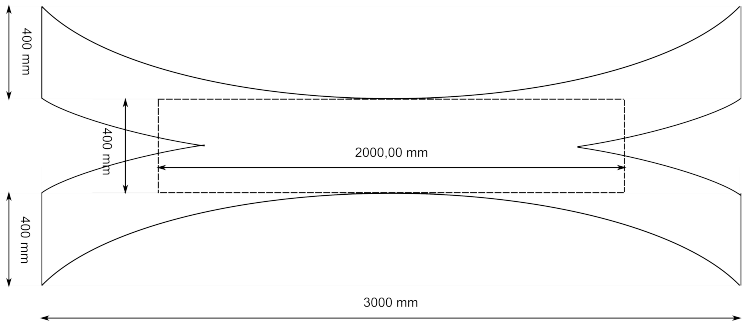

Figure 6.6: Geometry

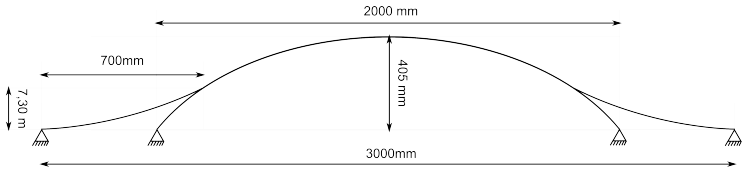

Figure 6.7: Geometry

6.2.3 Materials

The matrix was suggested by Professor Terje Kanstad at NTNU. The result was an ultra high performance, fiber reinforced, self compacting concrete. The matrix contained 2 vol-% steel fibers of 3,5cm.

The matrix consists of:

- Cement: Norcem Anlegg cement. 24,4 weight-%
- Microsilika: Elkem Mikro silica 940U, Elkem Mikrosilika consist of sub-micron, amorphous, non-porous spheres of silicon dioxide (silica, SiO2). Undensified form. 4,9 weight-%
- Water: 6,7weight-% free water. 0,4 weight-% absorbed water
- Aggregates: 0-8mm 45,4 weight-%, 8-16mm 11,4 weight-%
- Superplasticizer: Degussa skyflux 550 0,5 weight-%

- Steel fibers: 3,5cm 6,2 weight-%

The concrete prescription is enclosed in Appendix E.
(Haagensrud et al., 2010)

Casting and comments

The report from 2010 describes the practical execution of the project. Building the concrete formwork turned out to be more challenging than expected. The concrete was very viscous and the formwork cover was divided into smaller parts to cast the bridge in stages. During casting a vibrator was used in order to disperse the concrete inside the thin frame. After three days the most of the formwork was removed and the concrete was moistened with wet burlap sacks in order to have enough water available for the curing process. After 16 days the rest of the frame was removed.

The surface had many open pores due to air trapped in the formwork during casting. (Haagensrud et al., 2010)

6.2.4 Sample testing results

In 2010 there were done several sample tests to determine the capacity of the material. After 28 days of curing three cylinder test were executed to determine the compressive strength of the concrete. The mean breaking load, $\bar{N}$ was used in the calculations.

$$\bar{N} = 892.7kN \tag{6.4}$$

$$A_c = \pi \cdot \frac{d^2}{4} = 7854mm^2 \tag{6.5}$$

$$f_{ck} = \sigma = \frac{\bar{N}}{A_c} = 113.7MPa \tag{6.6}$$

The tensile strength was determined through a three-point bending test. This is one of the test procedures mentioned in Section 5.1.3 where a simply supported beam with dimensions 150x150x500mm is loaded at the centre of the span. Two notches are made in the bottom surface on each side of the loading. During the loading the deformation(Δ) in these notches are measured, the crackwidth (CMOD) is calculated and registered as a function of loading.

$$w = CMOD = \frac{\Delta - 4mm}{0.85} \tag{6.7}$$

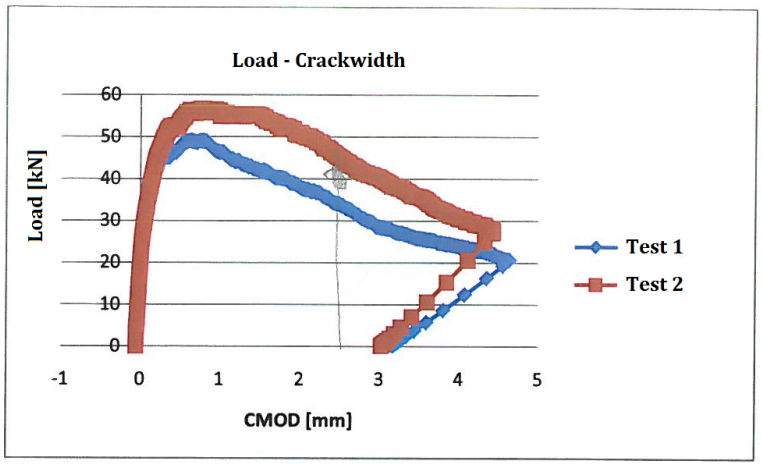

Figure 6.8: The load-CMOD curve from 2010 flexural tests. (Haagensrud et al., 2010)

Figure 6.8 shows the load-crackwidth diagram the students achieved in 2010. The maximum loading was used to calculate the moment.

$$M = \frac{PL}{4} \tag{6.8}$$

The stress distribution over the cross section was in reality more complex at maximum load, but to simplify the calculations linear stress distribution over the element depth was assumed. The stress was calculated as:

$$\sigma = \frac{M}{W} = \frac{P \cdot L}{4 \cdot \frac{1}{6} bh^2} = \frac{3}{2} \frac{PL}{bh^2} \tag{6.9}$$

The load at 2.5mm CMOD is $P = 39.55kN$ gives the following tensile stress during testing. This value is the value that in FRC is used to determine residual tensile strength.

$$f_t = \frac{3PL}{2bh^2} = 12.57MPa \tag{6.10}$$

The maximum load occurring in tests is $P = 51.01kN$ gives the following tensile stress during testing, assumed to be the flexural capacity of UHPFRC:

$$f_t = \frac{3PL}{2bh^2} = 16.2MPa \tag{6.11}$$

(Haagensrud et al., 2010)

Chapter 7

Testing in the Laboratory

7.1 The da Vinci bridge

The bridge was tested in the laboratory at NTNU. Previous to the test the boundary conditions and the location of the load was determined. The bridge is painted white and a superficial inspection before the testing revealed some small cracks in the paint which indicates some micro cracks in the material surface. Possible consequences of this are discussed in Chapter 9.

7.1.1 Loading

The bridge was loaded asymmetrically by a point load to the left of the bridge's centre. The actual location of the load is not important for the material property research addressed in Chapter 8 as the finite element model will only represent the actual test situation. However, it was desirable to check the bridge's capacity during testing and it was therefore decided to determine the weakest point and load the bridge at this location. The weakest point in the bridge is decided on the basis the theory on influence lines in Section 6.2.1.

The line of influence was calculated with a simplified method, where the arch is defined between the connection points of the four legs where the bridge cross section is larger and stronger. These connection points are highlighted in Figure 7.1. When the arch is defined as this, it will in reality be a mix between a two-hinge bridge and a zero-hinge bridge, where the ends are fixed. We have simplified the calculations and are looking at the arch as a two-hinge arch with a span of 1600mm between the two points.

The maximum flexural moment in the influence line as a function of x_1 along the span is plotted in Figure 7.2. From this plot it is determined that $x_1 = 350$mm is the most unfavourable point of loading. In the bridge this

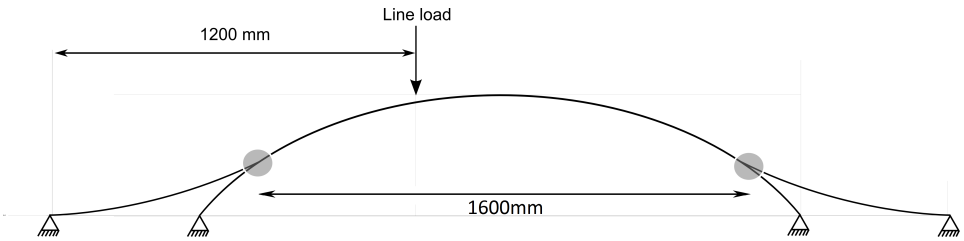

Figure 7.1: Location of load on the model

will be at 1150mm from the end

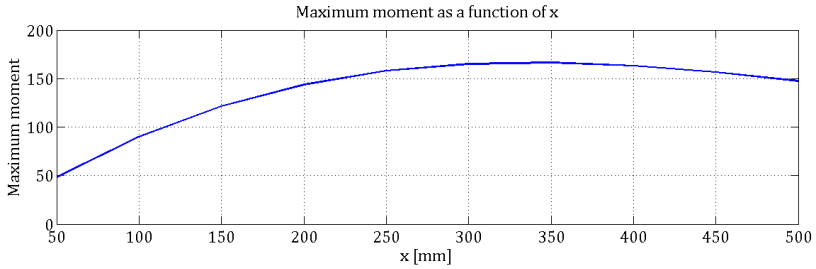

Figure 7.2: Max moment as a function of x_1

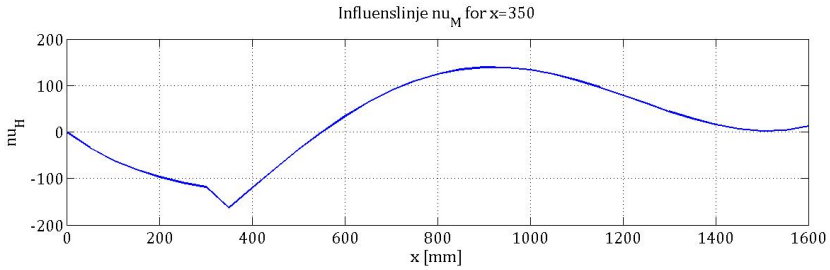

Figure 7.3: Influence line for x_1=350mm

During moving of the bridge, due to incautious action, a crack occured across the top surface approximately 15 cm from the centre of the arch. See Figure 7.4. The crack ran through half the thickness of the bridge. To avoid that the cracking effected the outcome of the analysis, it was necessary to take into account the main arch's line of influence to decide the location of the load and assure compression in the top of the cross section where the cracking was located. The load was applied in the DIANA model and linearly analysed. The results from the simplified influence lines and the linear analysis in DIANA diverge a little, but both results assure compression in crack.

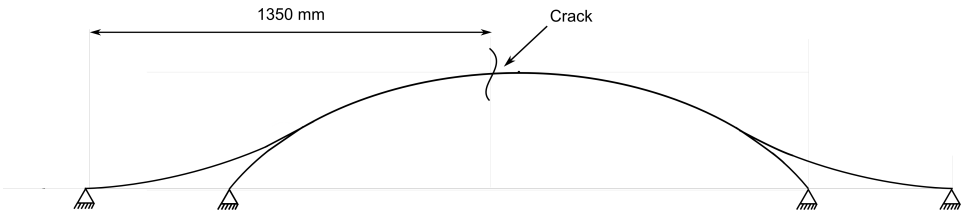

Figure 7.4: Location of crack on the model

Both the influence lines and the DIANA analysis assures compression at the crack when loading is placed at 1200 mm from the outer end, see figure 7.1. During testing, this is the location of loading.

A wooden brick was custom cut and glued to the bridge where the load was to be applied in order to distribute the point load over the width of the bridge. A steel plate was placed on the brick to ensure evenly compression under the point load and avoid deformation of the wood.

7.1.2 Boundary conditions

The six ends of the bridge was clamped in vertical and horizontal directions by bolting steel profiles to the underlying steel beams as shown in figure 7.5.

Figure 7.5: Outer ends fastened

7.1.3 Instrumentation

The test was executed using a 100kN hydraulic servo actuator to load the structure, a Spider 8 to read the measurements and Catman easy AP software to present the data.

To measure the displacement, two W10LVDT (Linear Voltage Displacement Transfuser) were used. One under the load and the other at the point off expected maximum negative deflection. Strain gauges - PL120, to measure the material strain, were placed at the same two positions on the underside of the bridge at loading and on the upper side of the bridge where

the largest strains were expected. The measuring devices can be seen in 7.12a. The applied force was measured by a HBM U2B.

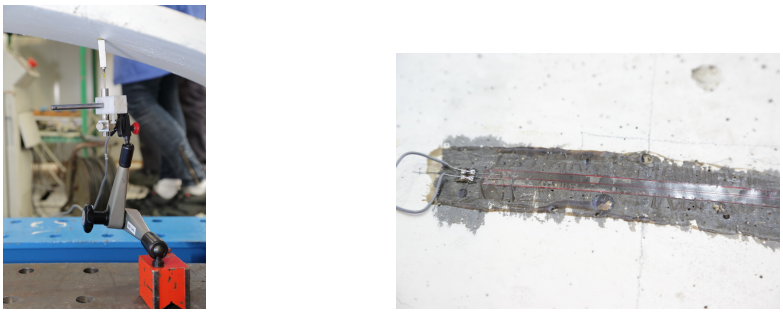

(a) LVDT (b) Strain gauge, PL120

Figure 7.6: Measuring devices used during testing

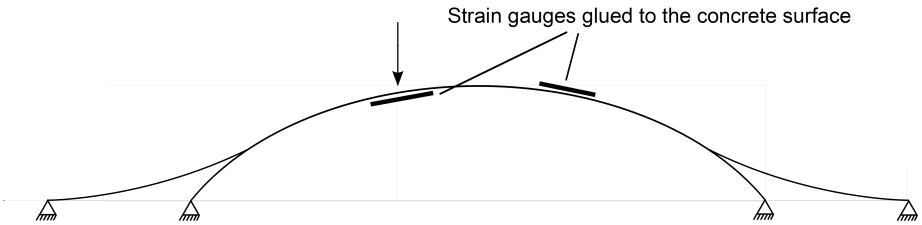

Figure 7.7: Strain gauges shown on figure

7.1.4 Testing

The testing was executed with the assistance and guidance of Steinar Seehuus at the NTNU concrete lab the 24th of March. Present was also teaching supervisor Terje Kanstad, and Giedrius Zirgulis who documented the testing with video and pictures. During the testing several spectators were present.

The test was displacement controlled with a displacement rate of 0.5mm per minute. The log frequency was 1Hz.

7.1.5 Result

The test results for the da Vinci bridge are shown in figure 7.9 and 7.10. Figure 7.8 shows the reference points for the results.

As we can see the flexural load capacity for this load case is 12.1 kN. In the strain diagram the strain gauge under the loading is disabled at 9kN, when the gauge is damaged by crack expansion. In the diagrams there are

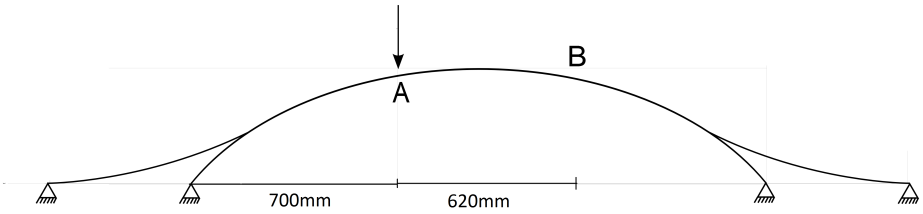

Figure 7.8: Reference points for experimental results

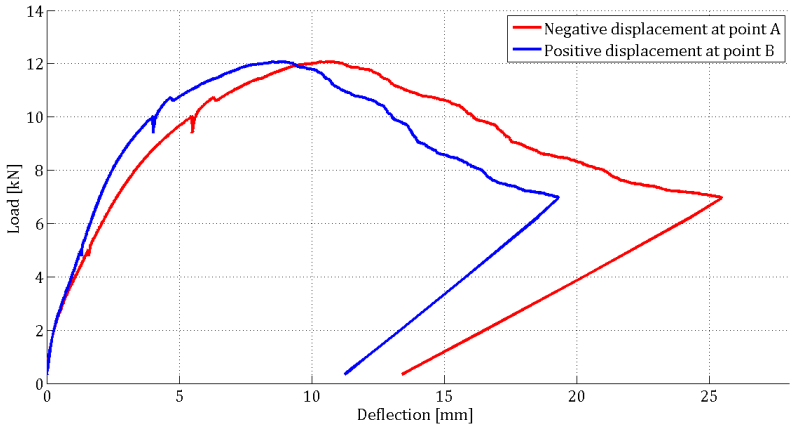

Figure 7.9: Experimental load-deflection curve

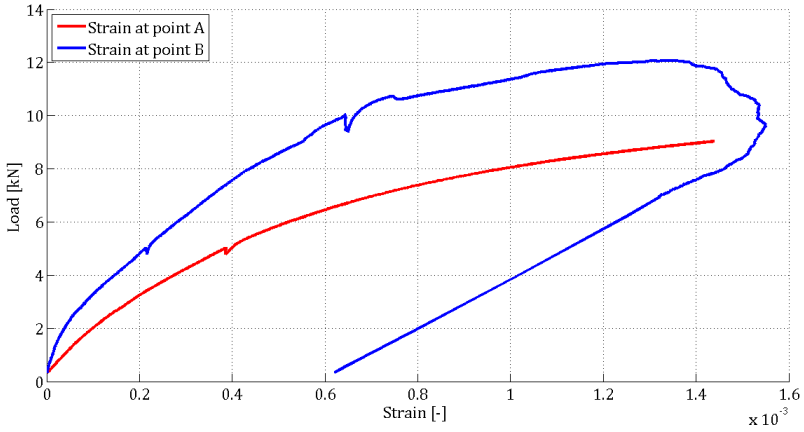

Figure 7.10: Experimental load-strain curve

"dips" in the curve at 5kN and 10kN. The loading was stopped at these values to take pictures and evaluate cracking. Already at 5kN there was a clear crack directly under the loading and several small cracks over a

larger area on the top surface at point B (see Figure 7.8). When the test was terminated there was one prominent crack under the loading and one relatively distinctive crack among several smaller on the opposite side on the top surface. In Figure 7.11 the areas of distinctive cracking are highlighted. Area B is where the load was applied, while area C is where the area that showed most cracking as a result of tension in top surface. There was also some cracking in area A on the top surface. The pictures in Figure 7.12 and 7.13 were taken during testing.

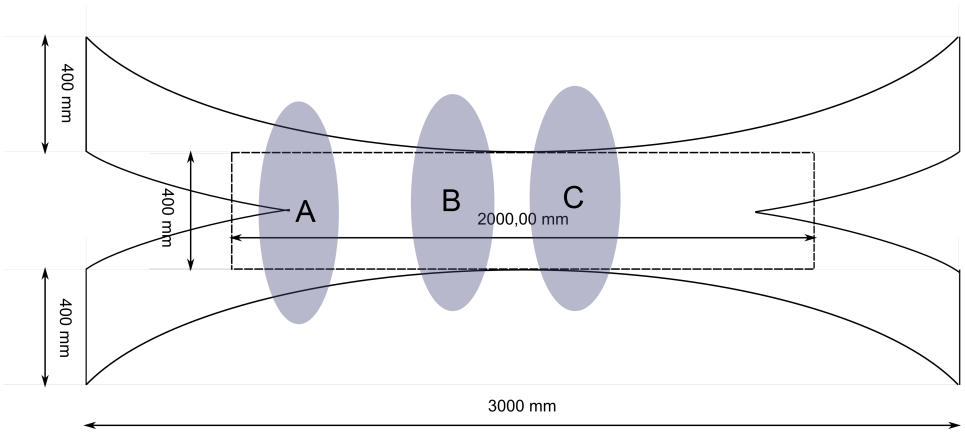

Figure 7.11: Areas with visible cracking on the bridge after testing

(a) Close view of crack under load (b) Prominent crack under load

Figure 7.12: Cracking in area B (Ref: Figure 7.11)

The results were lower than expected. After studying the results and comparing them to the results from the FEM-analysis there were uncertainties about the material properties. The solution was to extrude smaller material samples from the undamaged sections of the bridge and execute standard 4-point tests. These tests would be basis to a new approach of inverse analysis and verification of the material properties.

Figure 7.13: Cracking in area C (Figure 7.11)

7.2 Material samples

Four beams were cut out for testing. The geometry is shown in Figure 7.14. In theory the test beams should be approximately 30mm thick at all points in the beam, according to the assumption of 30mm thickness over the entire bridge, but the four samples had a varying thickness that spanned over 30mm to 50mm. Because of this deviation the thickness in was set to an average of 35mm in the DIANA analyses. This is a source of possible errors in the following analyses. The variations in the thickness is shown in Figure 7.15.

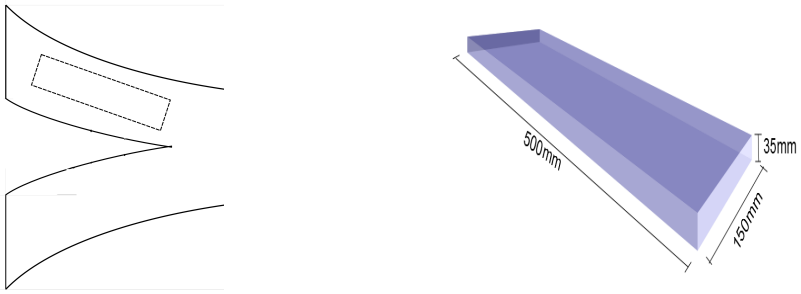

(a) Where the beams are extruded from the bridge

(b) Geometry of beams

Figure 7.14: The beams extruded from the bridge

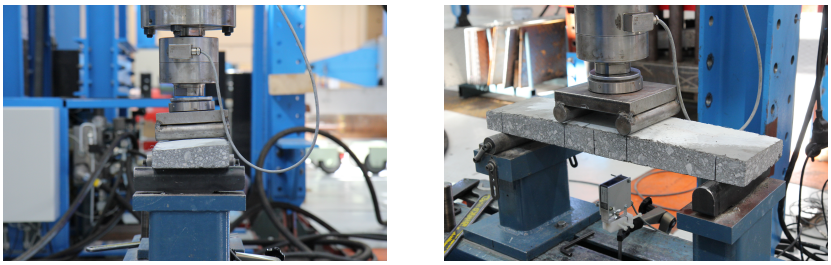

(a) Thickness over the width (b) Thickness over the length

Figure 7.15: The thickness varied over the width and length of the beams

7.2.1 Loading

The test was loaded by two loads distributed over the width of the beam as shown in figure 7.16.

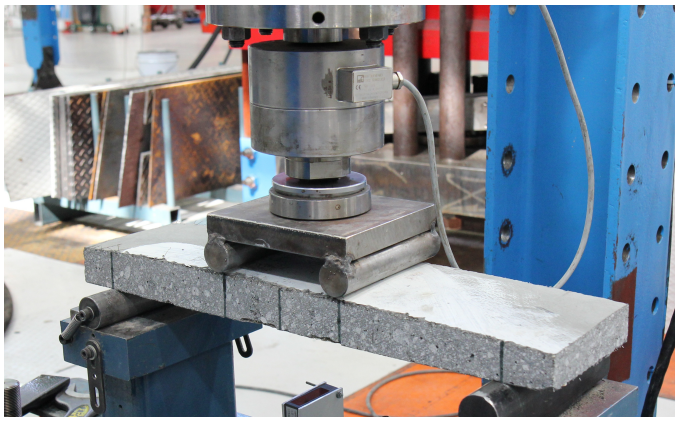

Figure 7.16: Loading of testbeam

7.2.2 Boundary conditions

Boundary conditions and loading is shown in Figure 7.17. The beams were simply supported.

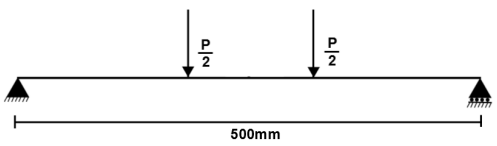

Figure 7.17: Boundary conditions of test beams

7.2.3 Instrumentation

The same instrumentation was used for the the sample testing as for the testing of the bridge with exception of the strain gauges. In the standard beam testing only deflection and load was measured. The instruments are described in Section 7.1.3.

7.2.4 Testing

The testing was executed in the NTNU concrete lab on 16th of May, with the assistance of Steinar Seehuus. The load was deflection fixed and the rate of deflection was 0.2mm per minute. The test was terminated at 3.5mm.

7.2.5 Result

The results for the four standard beams are shown in Figure 7.18. The curves are very rough, which is probably a result of the geometrical unevenness of the beams. All the four beams cracked in one distinctive crack close to the centre of the beam. The beams are shown in Figure 8.17.

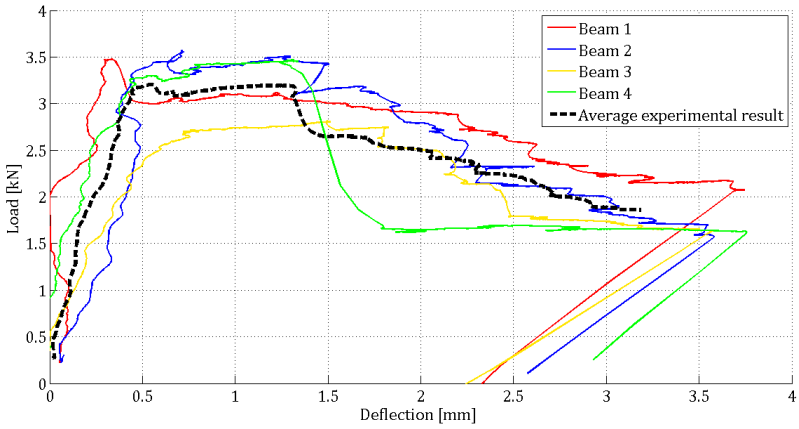

Figure 7.18: Load-deflection curves from experiment and the average curve

(a) Beam 1

(b) Beam 2

(c) Beam 3

(d) Beam 4

Figure 7.19: Standard beams after testing

Chapter 8

FEM Analyses in DIANA

8.1 DIANA

DIANA (DIsplacement ANAlysis) is a finite element software applicable to structural, geotechnical and dynamic challenges within civil engineering. It is also a dedicated tool in tunnelling, earthquake analysis and oil and gas engineering. The software possesses modelling capabilities in 2D and 3D and tools for interoperability with CAD. (TNO, 2014)

In this thesis DIANA is used for non-linear FEM analyses.

8.2 Non-linear Finite Element Analysis

In non-linear analysis the non-linear properties of a material is considered. The cracking and plastic behaviour is taken into account. The change in the geometry influences the response and the displacement is often dependent on the displacement at an earlier stage in the analysis. When solving non-linear analyses the solution method is crucial for accuracy. There is not one unique solution procedure suitable for solving the general non-linear problem. In DIANA one can choose between Secant method, Regular Newton Raphson or Modified Newton Raphson method.

The following input data can affect the nonlinear behavior: Mesh density, integration points over the thickness, stress-strain curves without gradients or local axes.

8.3 Incremental-Iterative method

Non-linear processes must be solved iteratively. The iteration process is a relation between internal and external forces which strives for equilibrium between the two. The process is stopped when convergence is achieved. $\mathbf{f}$

represent the internal and external forces and **g** is the "out-of-balance" force. When **g** is acceptably small convergence is achieved and a new increment may be initiated. This process is illustrated in Figure 8.1 and 8.2.

$$\boldsymbol{f}_{int}(\boldsymbol{u}) = \boldsymbol{f}_{ext}(\boldsymbol{u}) \tag{8.1}$$

$$\boldsymbol{g}(\boldsymbol{\Delta u}) = \boldsymbol{f}_{ext}(\boldsymbol{\Delta u}) - \boldsymbol{f}_{int}(\boldsymbol{\Delta u}) \tag{8.2}$$

In non-linear analysis the internal force vector usually depends non-linearly on the displacement, u. The external vector can also in some cases be displacement dependent. Therefore, to achieve force equilibrium, the displacement vector must be calculated. In order to solve this, the problem must be made discrete both in space (FEM) and in time (incremental). The solution for each increment is found iteratively. This method is called the Incremental – Iterative Solution. In the incremental-iterative solution increments are the load steps applied to the model and can be both force and displacement controlled. When choosing the analysis procedure three choices must be made: Increment control, iterative solution method, convergence criteria.

8.3.1 Newton Raphson Method

In DIANA one can choose the incremental-iterative methods: Constant and Linear stiffness(Secant), Regular and Modified Newton Raphson method.

In the following analysis the Newton Raphson method has been applied to determine the iterative increment of the displacement vector. In a newton Raphson method the stiffness matrix K_i represent the tangential stiffness of the structure.

$$\boldsymbol{K_i} = \frac{\partial \boldsymbol{g}}{\partial \boldsymbol{\Delta u}} \tag{8.3}$$

The difference between regular and modified Newton Raphson method is the point at which the stiffness matrix is evaluated. In the Regular Newton Raphson iteration the stiffness relation is evaluated for every iteration. The prediction is based on the last known or predicted situation. The method yields a quadratic convergence characteristic. This means that the method converges to the final solution within only a few iterations, but the quadratic convergence is only guaranteed if a correct stiffness matrix is used and if the prediction is already close to the final solution. (TNO, 2014)

Modified Newton Raphson method only evaluates the stiffness relation at the start of every increment which means the prediction is always based on a converged equilibrium. Modified method can sometimes converge still when the regular method does not.

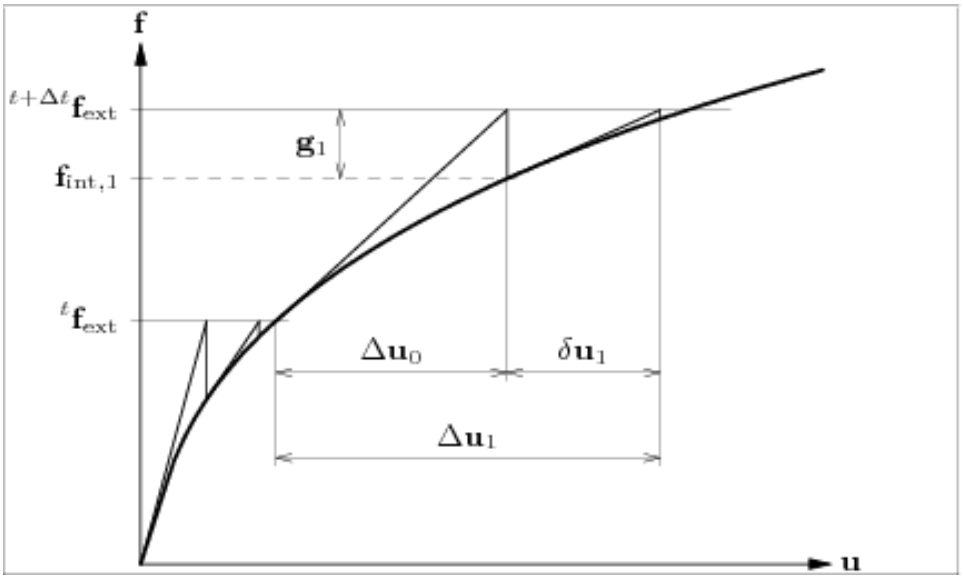

Figure 8.1: Regular Newton Raphson Method. (TNO, 2014)

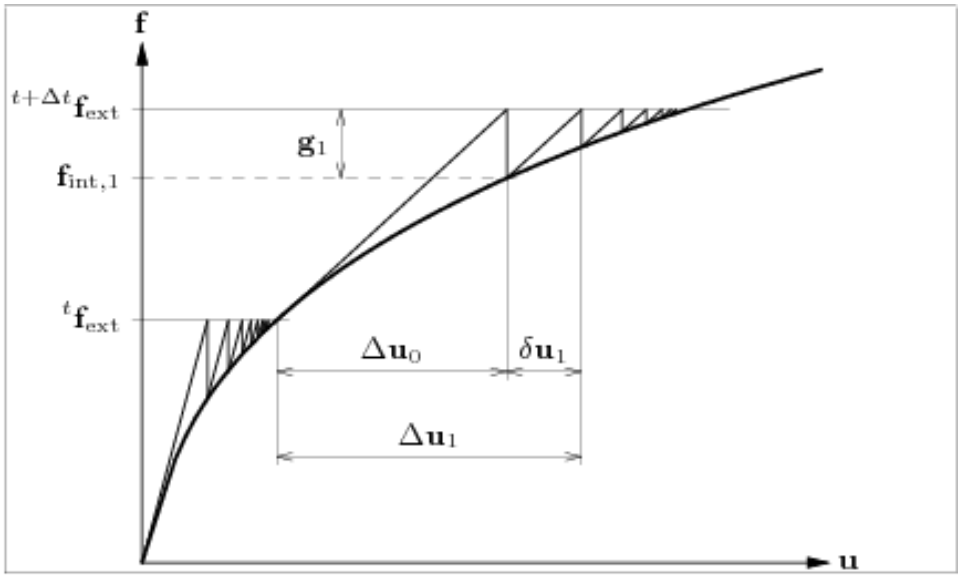

Figure 8.2: Modified Newton Raphson Method. (TNO, 2014)

(TNO, 2014; Palacio, 2013)

8.3.2 Load control

The load incrementation procedure may be either force controlled or displacement controlled. When the analysis is force controlled, the applied

load is increased in every new increment by directly increasing the external force, $\boldsymbol{f}_{ext}$. When the method in displacement controlled the load steps are represented by a fixed prescribed displacement $\boldsymbol{u}^c$.

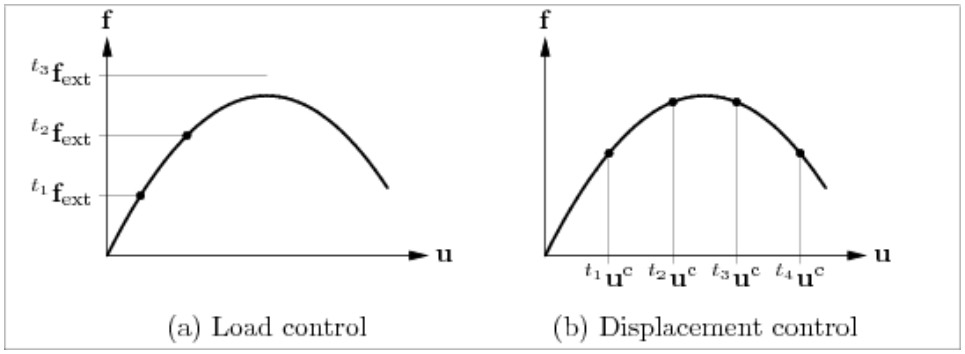

Figure 8.3: Force and displacement control

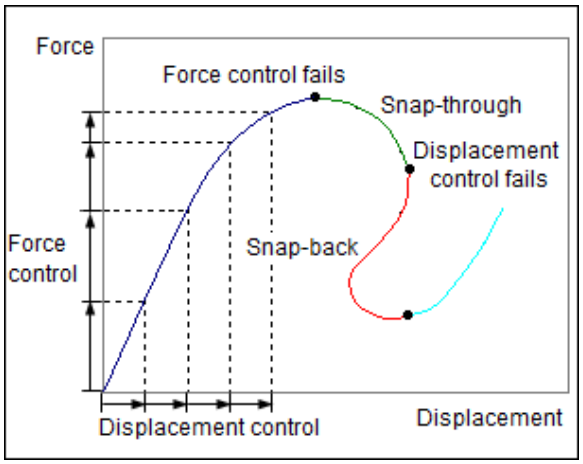

Figure 8.4: Snap-through and snap-back behaviour. (Palacio, 2013)

Force control

In force controlled analyses the force is applied incrementally. As illustrated in Figure 8.3a, the method is best suited for hardening materials as it will fail when the force value exceeds the maximum point on the curve e.g. when softening behaviour is initiated. This type of behaviour, where the curve at one point decrease, is called snap-through behaviour. See Figure 8.4. (TNO, 2014; ?)

Displacement control

When the load is displacement controlled a displacement is applied incrementally. The method solves for snap-through behaviours causing descending curves, but will fail for snap-back behaviours. See Figure 8.4. Displacement control offers an advantage over force control, providing better conditioned tangent stiffness matrix and the capability of computing snap-through behaviour. However, the method is usually restricted to structures with only point load and fails to trace snap-back behaviours. (TNO, 2014; Palacio, 2013)

Arc-length method

To overcome solution failures at snap-through and snap-back behaviours the arc-length control can be applied. Also when the load-displacement curve is close to horizontal, the predictions for the displacement increments can become very large. Arc-length method is capable of passing snap-through and snap-back behaviour as explained in Figure 8.5. Especially in force controlled analyses it is an advantage to apply arc-length control. (TNO, 2014; Palacio, 2013)

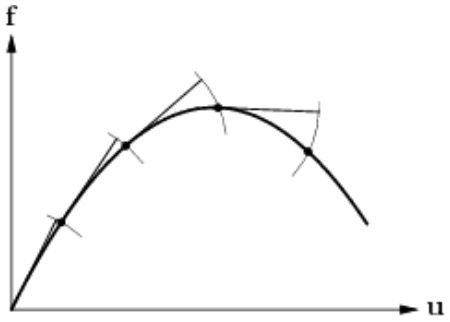

Figure 8.5: The arc-length method

8.3.3 Convergence

If the proper solution procedure is not chosen there may be difficulties converging. Convergence becomes an issue when the iterative solution method is unable to find a solution for the non-linear problem. There are in DIANA four different convergence norms: energy, force, displacement and residual. For every increment the iterations continues until there is convergence or the maximum number of iterations specified have been run.

Force norm is the most demanding norm. The force norm is the Euclidian norm of the out-of balance vector g. Vector g is after every iteration checked against the initial $\boldsymbol{g_0}$.

$$\text{Force norm ratio} = \frac{\sqrt{\boldsymbol{g}_i^T \cdot \boldsymbol{g}_i}}{\sqrt{\boldsymbol{g}_0^T \cdot \boldsymbol{g}_0}} \tag{8.4}$$

Geometrically sensitive non-linear analyses require a tighter tolerance than predominantly material non-linear analyses in order to maintain the solution on the correct equilibrium path. Analysis models with lots of prescribed displacement make the norm displacement criterion less effective, whereas the norm force is less effective for structures that can expand freely where hardly any internal forces can be built up. (TNO, 2014; Palacio, 2013)

8.3.4 Integration points

The default number of integration points over the elements are 2x2 over the element plane and 3 over the thickness for shell elements. In an analysis the exact solutions are calculated in the integration points and extrapolated over the element. The default may not be suitable and the number of points, especially over the thickness due to a non-linear stress distribution, should be considered. The number of integration points necessary over the plane also depends on the element mesh used in the analysis.

8.4 Analysis method

8.4.1 Load control comparison

The choice of load control was made early. With the use of arc-length it was decided to use force controlled analyses. However, because of problems converging, it was decided to run a couple of the analyses with displacement control and look at the different results. The differences were small and the convergence problems were persistent. The analyses were therefore continued with force control together with the arc-length method using updated planes.

8.4.2 Mesh comparison

To begin with a larger mesh than the one presented in the report was used. As an attempt to solve convergence issues the mesh size was reduced. This seemed to have a positive effect on the curves, resulting in a smoother curve and smaller out-of-balance forces, though still not completely converging in all steps.

8.4.3 Integration point comparison

The difference with 3 and 9 integration points over the thickness is astonishing. Figure 8.6 Throughout the following analyses, 9 points over the

thickness have been used to assure the extrapolated stresses do not deviate much from the true value.

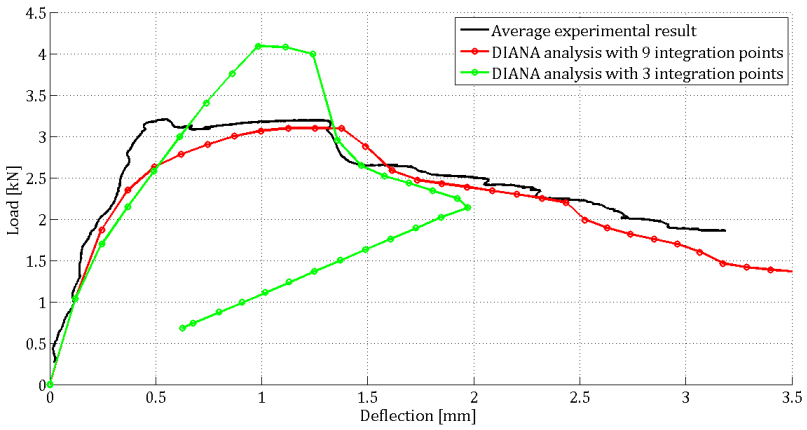

Figure 8.6: Comparing analysis result with 3 and 9 integration points

8.5 Beam analysis

In the initial analysis process of the thesis only the bridge results were considered. The capacity test from 2010 gave an indication of what should be expected. The result from the DIANA analyses did not coincide with the expected results. It was therefore, after some time and consideration decided to test smaller material samples to verify the material properties predicted. The testing procedure and test results are presented in Section 7.2. Although there was done multiple analysis and curve fitting for the bridge FEM model previous to the beam analysis, the results from the latter analysis were used as basis for curve fitting and the inverse process of determining the material properties. It is therefore presented first in this chapter.

8.5.1 Geometry

The beams were sawn out of the actual bridge. The geometry is shown in Figure 7.14 in section 7.2. As discussed, the thickness of the standard beams was varying. In the FE model it was first assumed a thickness of 30mm as in the model bridge. After testing and re-evaluation of the tested elements the thickness in the model was set to 35mm.

8.5.2 Loading and boundary conditions

In the laboratory the beams were tested at two symmetrical points with a distributed load over the width. In DIANA two line loads are placed 75mm

from the center. The two line loads form one unit load of 1kN, two line loads defined as 3.33N/mm. The model beam is simply supported. The supports and loading are shown in Figure 8.7

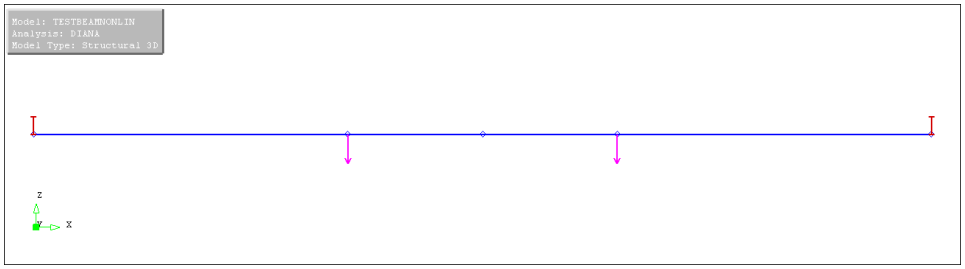

Figure 8.7: DIANA load and vertical constraints

8.5.3 Mesh

The element used in the non-linear analysis is CQ40S. This is an eight-node quadrilateral isoparametric curved shell element. (See Figure 8.8. (TNO, 2014)). It is based on quadratic interpolation and Gauss integration over the $\xi - \eta$ element area, and a Simpson or Gauss integration over the thickness ς. See Figure 8.8. To ensure accuracy the number of integration points is 3x3 over the element surface and 9 over the thickness.

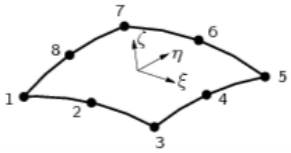

Figure 8.8: Element CQ40S

The mesh is shown in Figure 8.9. A larger mesh was used in initial analyses. It was updated during the process of analysing to better converge. The element area is approximately $13.0mm^2$ on the outer area and $5.5mm^2$ in the centre.

8.5.4 Material Properties

There are two main methods of modelling cracking in concrete: Discrete crack approach and smeared crack model. In discrete crack approach, the concrete is assumed to crack when the nodal force exceeds the tensile capacity. It is beneficial to know exactly where the crack will occur and the approach is for example used in testing of standard beams where the crack is predefined by a notch in the concrete. In the smeared crack model, cracking

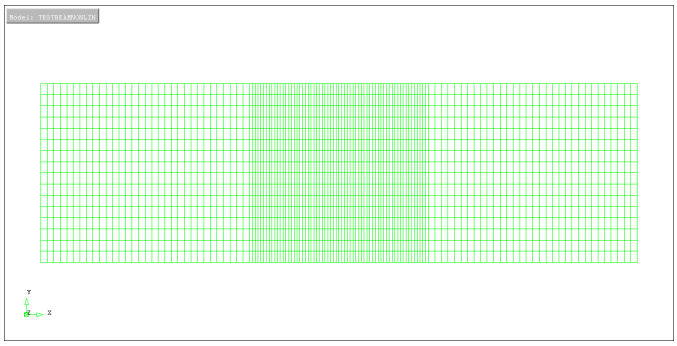

Figure 8.9: The mesh

is divided into the integration points within the elements. For the model bridge, where cracking is uncertain and distributed over the tensile areas in the concrete, smeared cracking is a better suited method.

(Sarmiento, 2012; TNO, 2014)

In a smeared crack model the stress-strain relation is continuous and modified as a reaction to cracking. After the concrete is cracked the strength and stiffness is reduced and depending on the size of the crack there might also be shear resistance in the crack. There have been developed two smeared crack models: Fixed crack model and rotating crack model. The fixed crack model introduces a shear reduction factor and transforms the stresses from principle to local. The shear reduction factor is only assumed and this assumption can be avoided by implementing the rotating crack model, which uses tangential shear stiffness calculated directly from the normal stresses. In the beam analyses it is only interesting to look at flexural behaviour. Therefore, the non-linear analyses may be simplified by choosing the fixed crack and setting the shear retention factor so that shear behaviour in the cracks are avoided. It is generally recommended that the shear retention factor is set to 0.1, but to prevent all shear slip within the cracks this factor is set to 1 in the beam analyses.

(Sarmiento, 2012)

As fiber reinforcement is not an implemented material in DIANA, we are forced to determine the material properties from testing and the simplified calculations executed during the making of the bridge in 2010. During the building of the bridge in 2010 there was executed some standard compression and flexural tests. The compressional capacity is determined from these tests. For the non-linear analysis it is required to define the tensile behaviour. The stress-strain relationship for the material is predicted and simplified based on the results from the linear analysis and later modified to best fit the results attained in the laboratory. The E-modulus is assumed

to be approximately 35 000MPa.

The following material properties are determined in DIANA:

Material name: UHPFRC

- Linear elasticity → Isotropic
  - E-modulus: 35 000MPa
  - Poisson's ratio: 0.2
- Static non linearity → Concrete and brittle materials → Total strain fixed crack → Direct input → Multi-lin. Diag. in tension → Ideal in compression → No lateral confinement behaviour → No lateral cracking reduction → No Poisson reduction
  - File stress-strain diagram: tenpar.dat
  - Compressive strength: 113.7MPa
  - Shear retention factor: 1

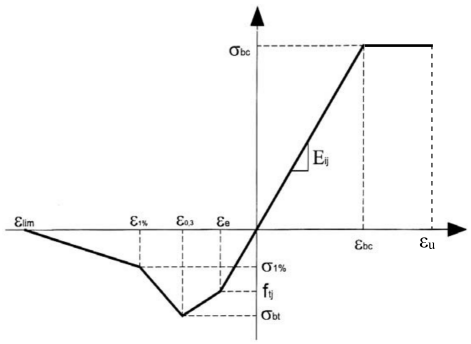

Figure 8.10: A typical stress-strain diagram with multi-linear behaviour in tension and ideal behaviour in compression. (Schmidt and Fehling, 2005)

The stress-strain file tenpar.dat gives the stress-strain diagram for tensile behaviour.

8.5.5 Physical properties

The thickness is in DIANA defined as a physical property:
Physical property name: THICK

- Curved shell → Regular
  - Thickness: 35mm

8.6 Stress-strain diagram fitting

In order to determine a stress-strain relationship for the tensile behaviour of the material the test results and the results from the non-linear analysis in DIANA are compared and the diagram is modified based on the curve fitting principle. An initial prediction of the stress-strain relationship is decided on the basis of the material theory discussed in Section 4.1.2 and expected strength based on material testing in 2010. It is assumed that there is a tensile hardening behaviour after cracking and a softening behaviour after reaching maximum residual tensile stress. Then on the basis of the load-deflection results in the analyses the stress-strain diagram is fitted to achieve best possible results. It is a trail method where the fitted curve that achieve best result is chosen for further analyses. In this process many analyses were executed and only a small portion of the relevant curves that were analysed are presented.

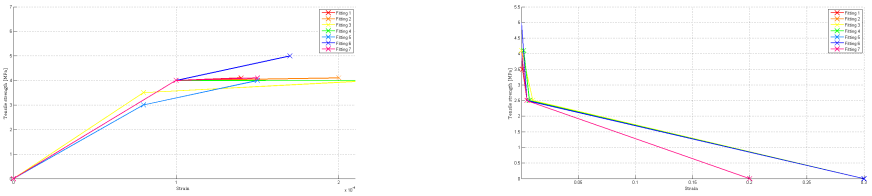

Figure 8.11: The stress-strain diagram, divided into hardening and softening behaviour. These diagrams are enclosed in Appendix A.

Figure 8.11 shows the 7 most relevant trials split into hardening and softening behaviour on the curve. The plotted points are tabulated and plotted in a larger scale in Appendix A.

Figure 8.12 presents the load-deflection results of the different fitting trials. From this diagram fitting 2 and 5 coincides best with the experimental results. Fitting 5 is chosen, because of it's slightly more prominent softening behaviour. This behaviour is desired in the bridge analysis.

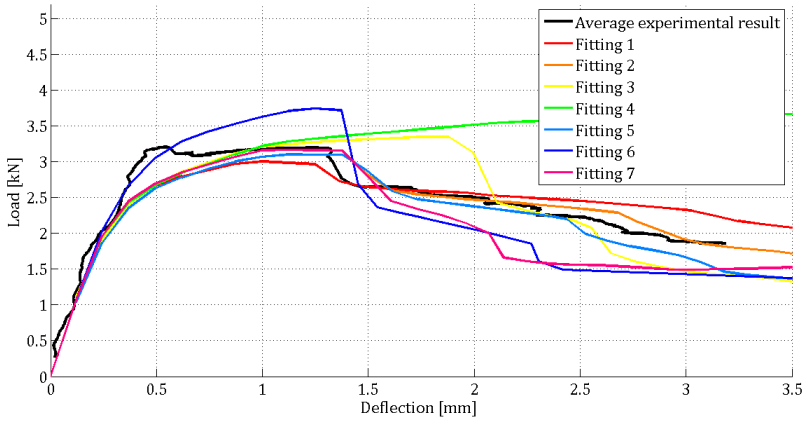

Figure 8.12: Curve fitting

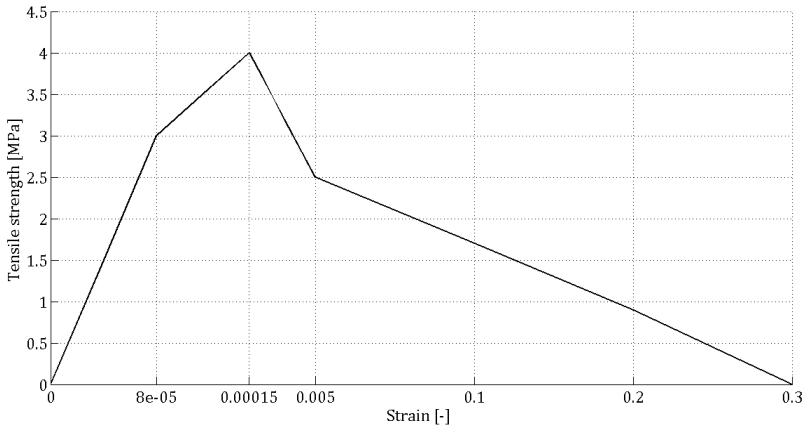

Figure 8.13: Fitting 5: The stress-strain relationship to apply in further FEM-analysis. The x-axis is modified to better present the shape of the curve.

8.7 Non-linear analysis

8.7.1 Result

The non-linear analysis was executed with the tensile multi-linear relationship presented in Figure 8.13. Figure 8.14 shows the load-deflection curve of the centre. This is the same location as the deflection was measured in the laboratory tests. The load steps of the analysis are highlighted with markers on the curve. The curve coincides fairly good with the results from testing and has the same desirable hardening and softening behaviour.

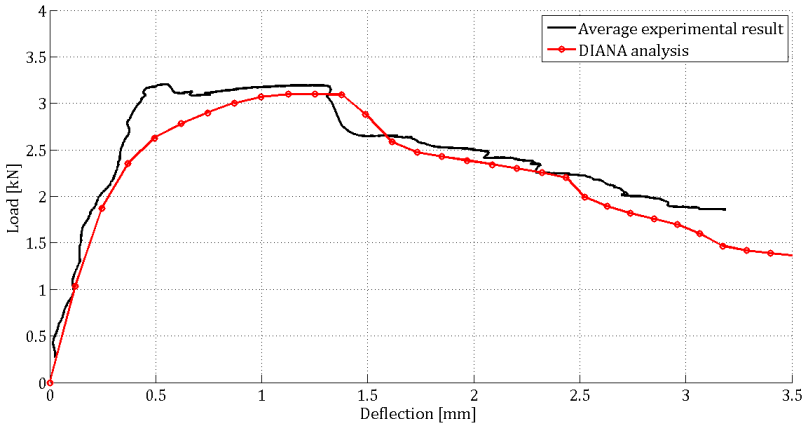

Figure 8.14: The load-deflection curve with analysis steps defined

Deflection

In Figure 8.15 the deflection propagation is presented. The displacement is approximately symmetric up to a point closer to 3.5mm deflection, where the one crack becomes more distinctive than the other. This coincides well with the results where only one crack was clearly distinctive in every beam although, in testing this tendency is revealed earlier. This can also be seen in the crack propagation (Figure 8.17).

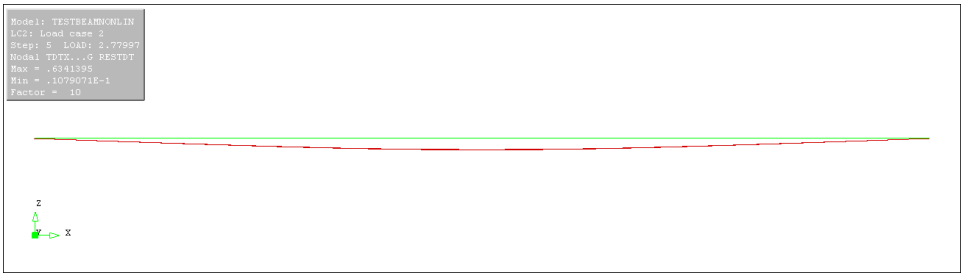

(a) Step 5, load: 2.64kN, deflection: 0.5mm at centre

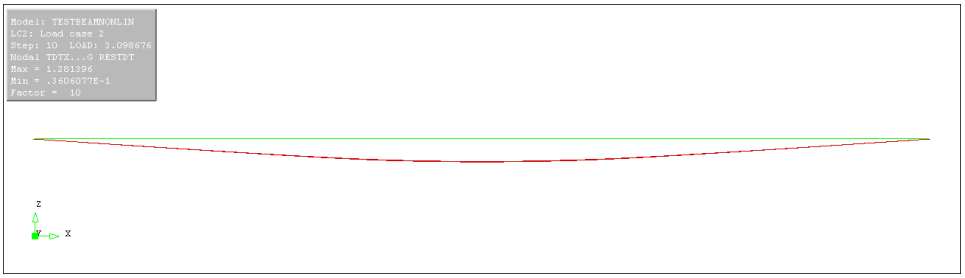

(b) Step 10, load: 3.10kN, deflection: 1.28mm at centre

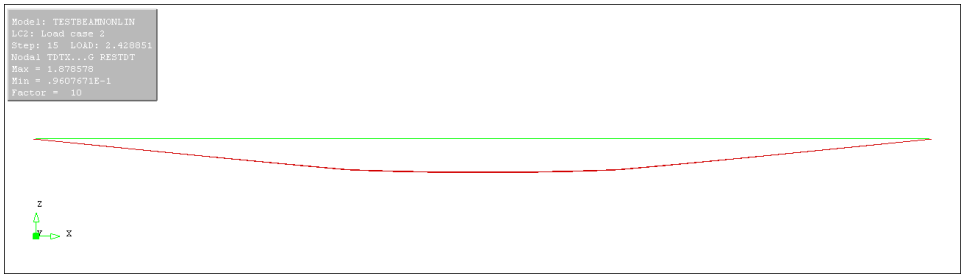

(c) Step 15, load: 2.43kN, deflection: 1.88mm at centre

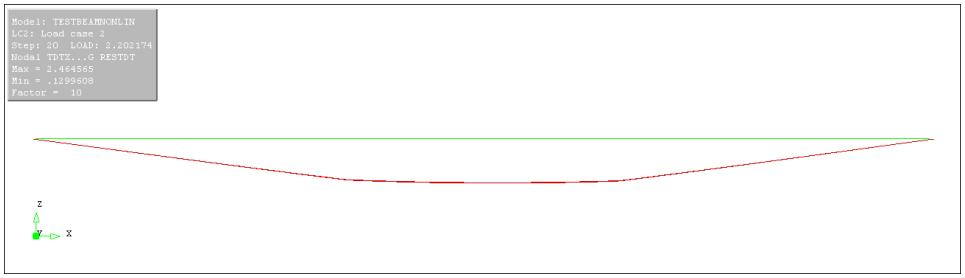

(d) Step 20, load: 2.20kN, deflection: 2.46mm.

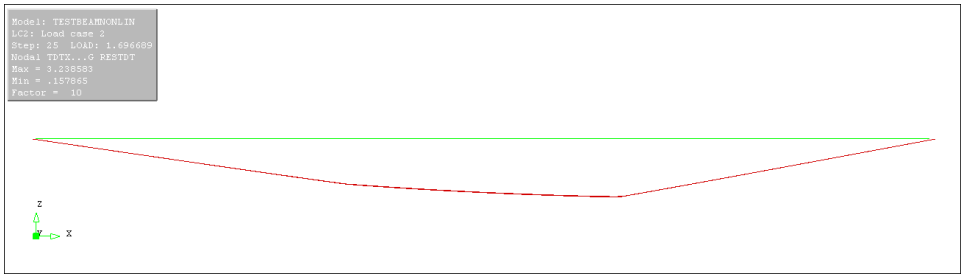

(e) Step 25, load: 1.70kN, deflection: 3.23mm. The largest deflection is now under one of the two loads points.

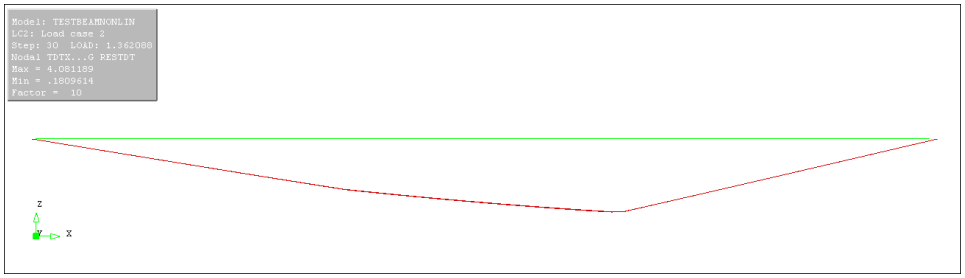

(f) Step 30, load: 1.36kN, deflection: 4.08mm. The deflection continues to grow under one load point

Figure 8.15: The deflection propagation

Crack propagation

The crack propagation in the beams are presented in Figure 8.17. Figure 8.16 gives an explanation to the color coding in the contour plots linking the colors to areas in the stress-strain diagram. The first cracking occur almost immediately and the propagation is symmetric in the beam up to the point where the load has decreased to 1.9kN post cracking. At this point one of the cracks become more prominent than the other. As mentioned this tendency coincides with the real cracking from the laboratory. However, the second crack should according to the analysis also become visible when the deflection approach 3.5mm. This is not the case in reality where only one crack is visible in each beam.

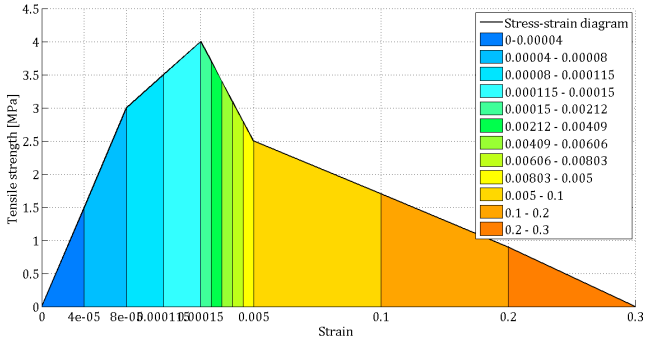

Figure 8.16: Colorcoding of an altered stress-strain diagram

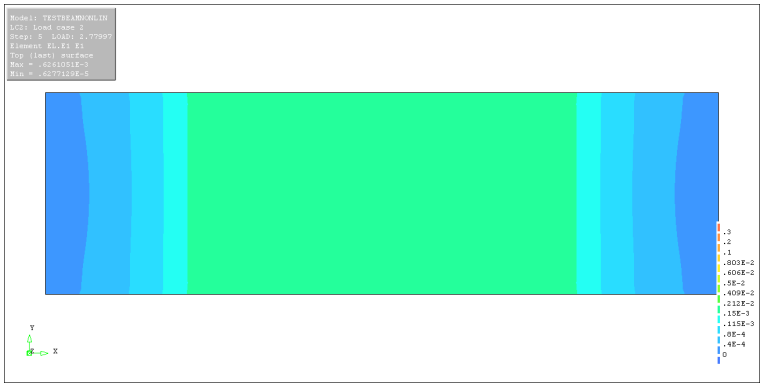

(a) Step 5, load: 2.78kN,

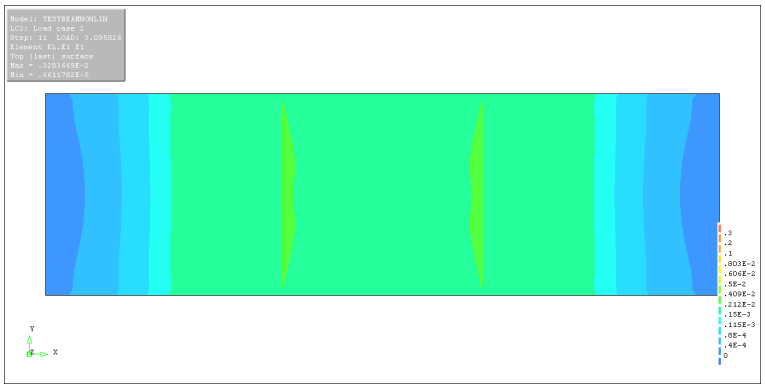

(b) Step 11, load: 3.09kN,

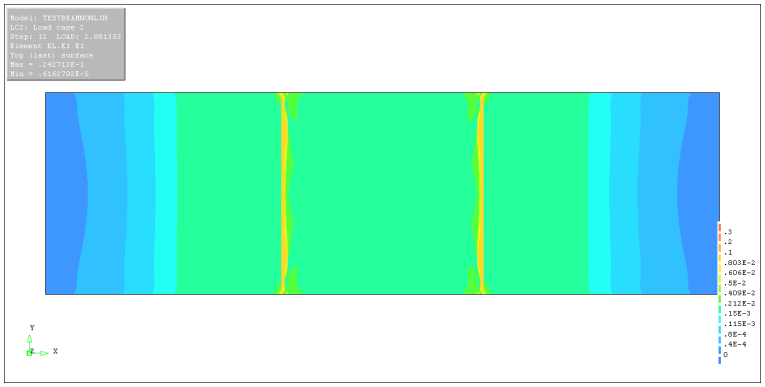

(c) Step 12, load: 2.88kN,

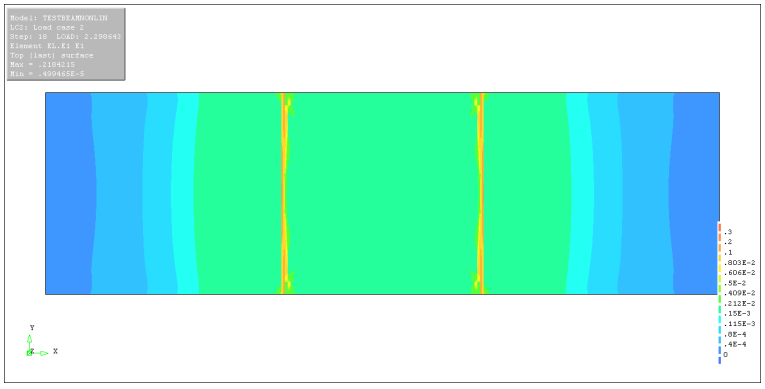

(d) Step 18, load: 2.30kN,

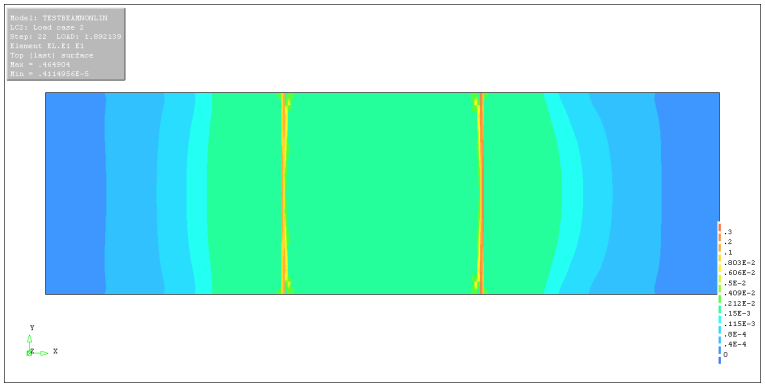

(e) Step 22, load: 1.89kN,

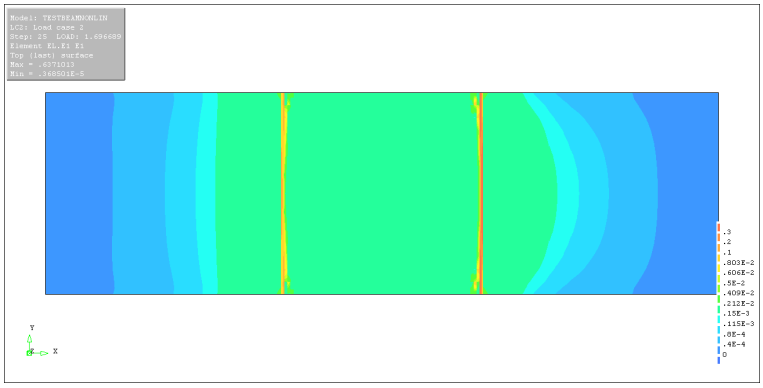

(f) Step 25, load: 1.69kN

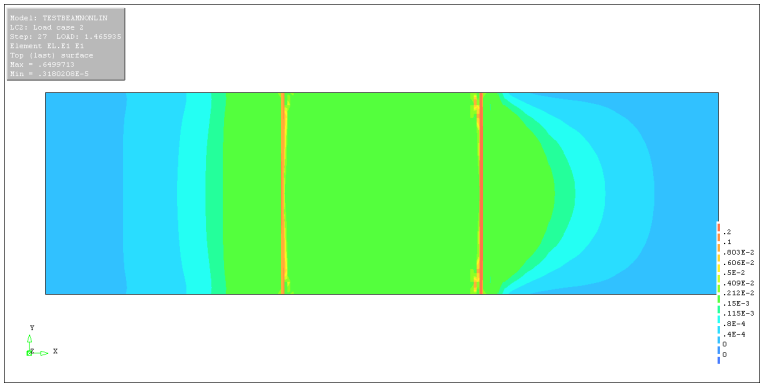

(g) Step 27, load: 1.47kN,

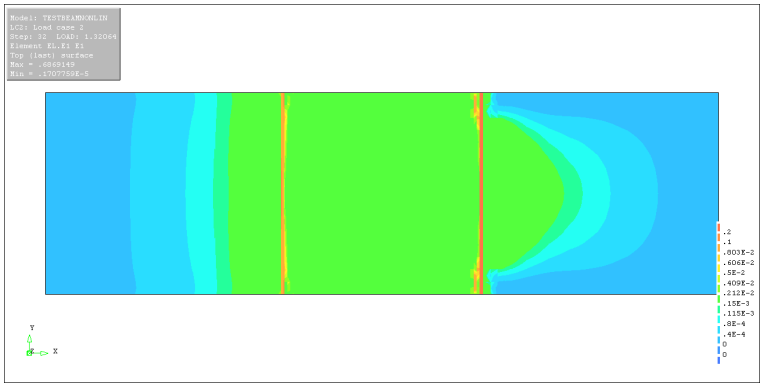

(h) Step 32, load: 1.32kN,

Figure 8.17: The crack propagation

Comments to other results

In the stress propagation the tensile stress after initial cracking is decreasing in the crack locations. In the initial analyses the stress did not decrease after cracking, which does not simulate the reality of material behaviour. In the presented results it is now an obvious reduction in tensile surface stresses in the beam after cracking. Figure 8.18 shows the decreasing stress after crack localisation. Stresses range from zero (blue) to maximum tensile stress 4.0 (red).

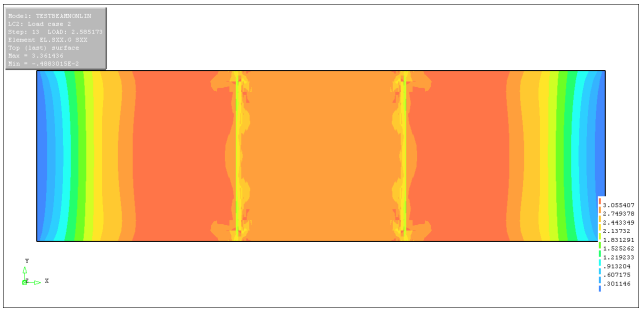

(a) Step 12

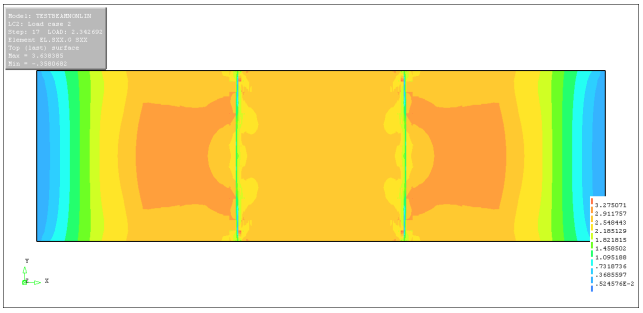

(b) Step 17

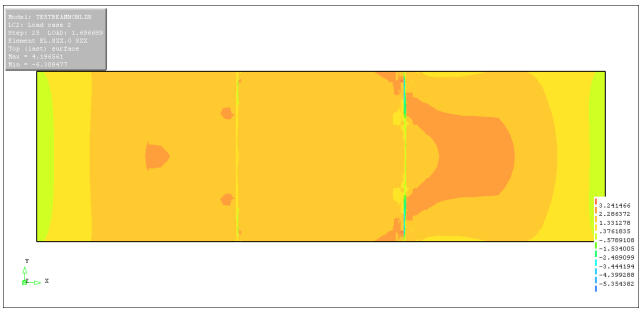

(c) Step 25

Figure 8.18: The decreasing tensile surface stress after crack localisation.

8.8 Bridge analysis

8.8.1 Geometry

The geometric description is given in Section 6.2.2 on page 37. The geometry is idealized in DIANA to simplify the modelling process. The main arch is modelled as part of a circle and the curvature of the outer legs of the bridge is chosen based on assumption. The geometric model, designed in DIANA is shown in Figure 8.19. The figure displays how the model is divided into surfaces.

8.8.2 Loading and boundary conditions

The bridge is loaded asymmetrically, identical to the bridge in the experiment. The load is defined as a line load to indicate even distribution. It is chosen to use unit loading in the analysis. 1kN distributed over the width is 2.3N/mm at this point

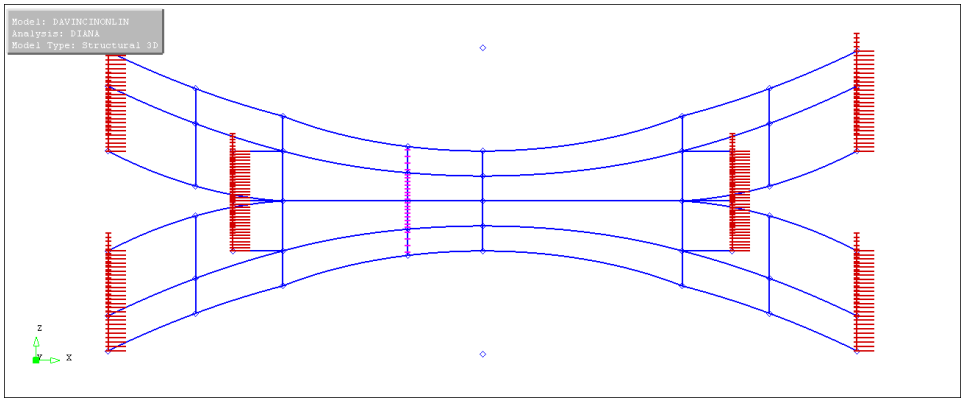

Figure 8.19: Geometry(blue), load(violet) and constraints(red) in DIANA

In Figure 8.19 the constraints and line load is defined. All the ends are constrained against translational motion, but are free to rotate. In order to simulate the real situation it is essential that the boundary conditions in the experiment are ideal and that there is no slip. This is difficult to guarantee, but an approximate accuracy is assumed.

8.8.3 Mesh

The element used in the non-linear analysis is CQ40S which is described in Section 8.5.3. The number of integration points are still 3x3 over the plane and 9 points over the thickness for most accurate results. Figure 8.20 displays the mesh used in the analysis where the largest element size is $1680mm^2$.

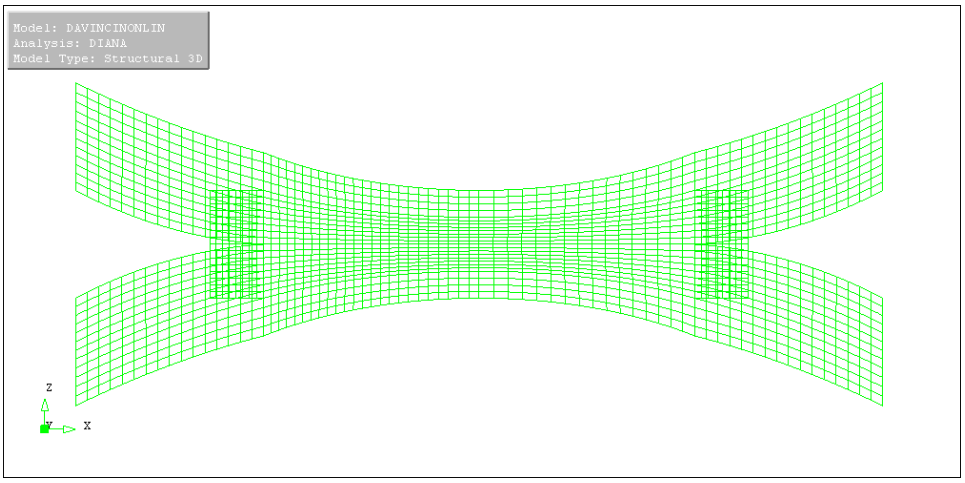

Figure 8.20: Meshing of the model

8.8.4 Material properties

The material is almost identical to the one defined in Section 8.5.4, but because of strict boundary conditions and expectations of a generally more complex cracking behaviour it is decided to use the rotating smeared crack model for the bridge FEM-analysis. See Section 8.5.4 for an explanation of the crack model. Figure 8.13 displays the stress-strain relationship given in tenpar.dat which was determined in Section 8.6.

Material name: UHPFRC

- Linear elasticity → Isotropic
  - E-modulus: 35 000MPa
  - Poisson's ratio: 0.2
- Static non linearity → Concrete and brittle materials → Total strain rotating crack → Direct input → Multi-lin. Diag. in tension → Ideal in compression → No lateral confinement behaviour → No lateral cracking reduction → No Poisson reduction
  - File stress-strain diagram: tenpar.dat
  - Compressive strength: 113.7MPa

8.8.5 Physical properties

In theory the bridge has a thickness of 30mm at all points. When looking closely at the different sections of the bridge it is clear that the thickness deviates from this value, but is measured to 30mm at the most critical

points. Therefore the thickness is set to 30mm and defined in DIANA as a physical property:

Physical property name: THICK

- Curved shell → Regular
  - Thickness: 30mm

8.9 Non-linear analysis

8.9.1 Result

Figure 8.22 shows the load-deflection curve of the two locations, A and B where the displacement was measured during testing. (See Figure 8.21) The load steps of the analysis are highlighted with markers on the curve. The plot coincides well with the material strength, but the softening behaviour is less than expected and the material in the analysis show a much stiffer relationship at initial loading. The first cracks occur much sooner in the test than in the analysis. It is correct that the bridge reaction in point B is stiffer than point A. However, after reaching maximum residual strength, the displacement at point B increase at a much faster rate and show less softening than at point A.

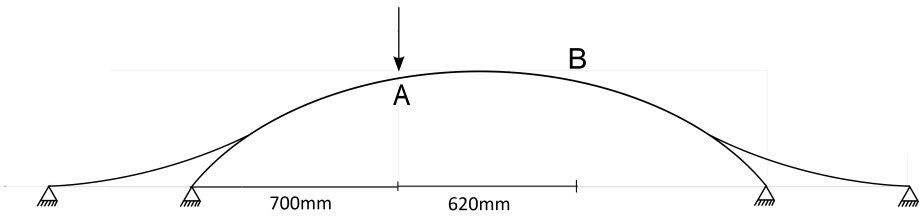

Figure 8.21: Reference points for experimental results

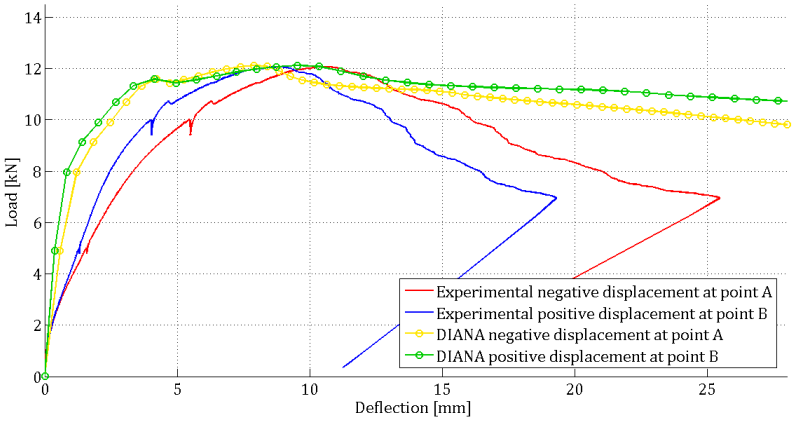

Figure 8.22: Experimental and analytical load-deflection curve

Displacement

The propagation of the negative and positive displacement in the bridge is presented in Figure 8.23. This result does not represent reality as there is a larger positive displacement at unloaded point B than under the load. This was the fact for all analyses performed during the project. It may be seen in the load-deflection curve as well, where the number of load steps on the curve for point B is much lower than the curve for point A

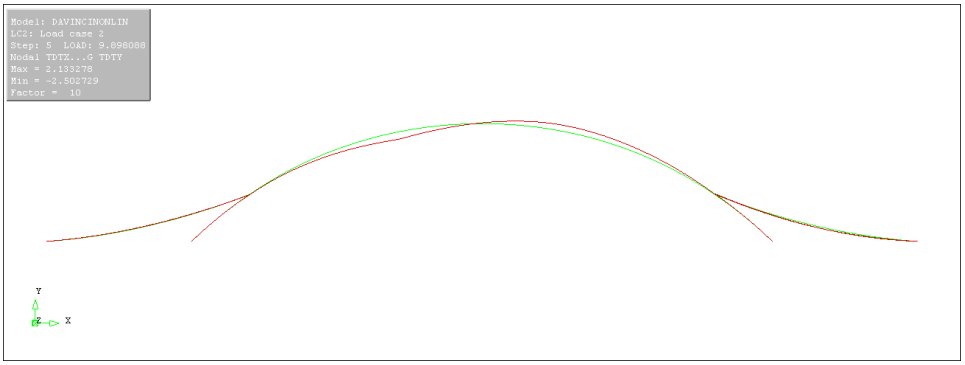

(a) Step 5, load: 9.90kN, Displacement: Max 2.12, Min -2.50

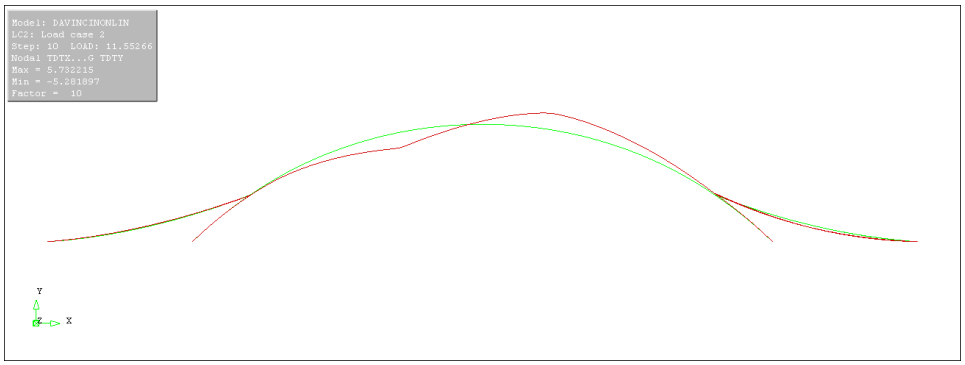

(b) Step 10, load: 11.55kN, Displacement: Max 5.73, Min -5.28

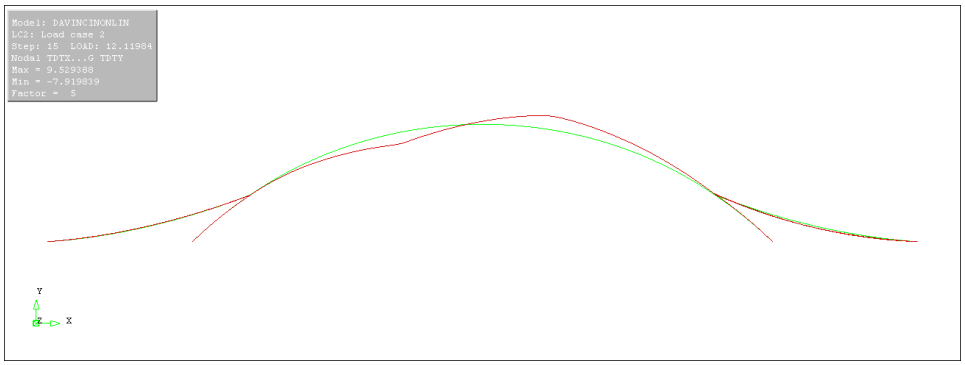

(c) Step 15, load: 12.12kN, Displacement: Max 9.53, Min -7.92

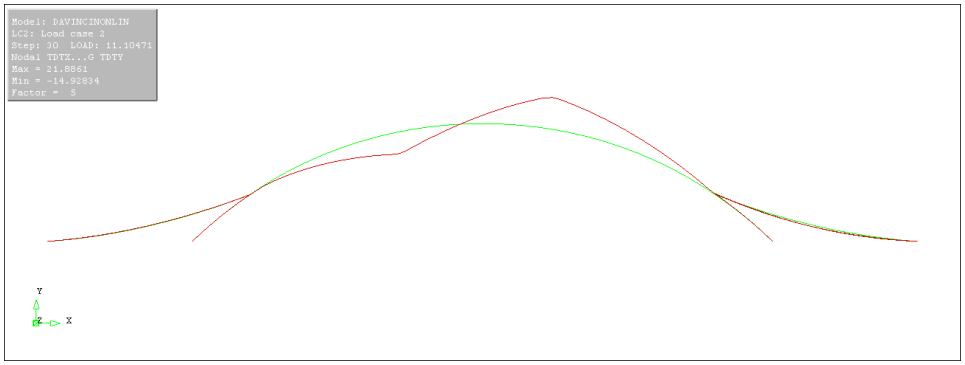

(d) Step 30, load: 11.10kN, Displacement: Max 21.89, Min -14.93

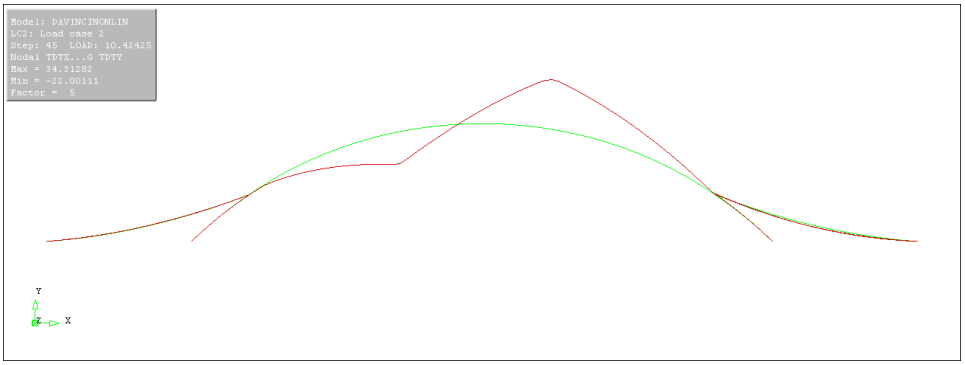

(e) Step 45, load: 10.42kN, Displacement: Max 34.31, Min -22.00

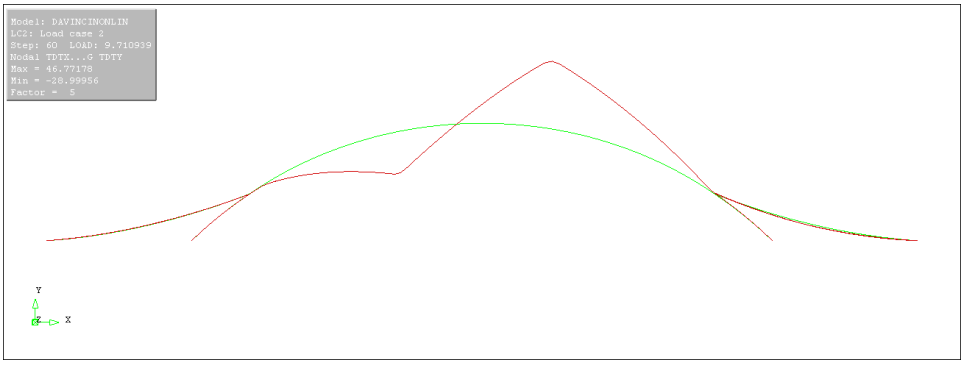

(f) Step 60, load: 9.71kN, Displacement: Max 46.77, Min -29.00

Figure 8.23: The deflection propagation

Crack propagation

Again, the stress-strain relationship is presented with color coding explaining the following contour plots of the bridges crack propagation represented by principle strain E1. (Figure 8.24 and 8.25.) The contour plots show both the strain on both bottom and top surface of the bridge and the colors in the stress-strain diagram indicates where the material is in the hardening and softening part of the curve. The expected crack behaviour is achieved. There is one distinctive crack under loading and one at opposing unloaded point in the top surface. The latter crack was in the experiment closer to the centre and slanting across the width of the arch with a gradient of $\frac{1}{8}$. This slant is probably a result of geometrical or material imperfection that is avoided in DIANA. The cracks at the connection points of the three "legs" on either side are also correctly represented compared to the experimental results.

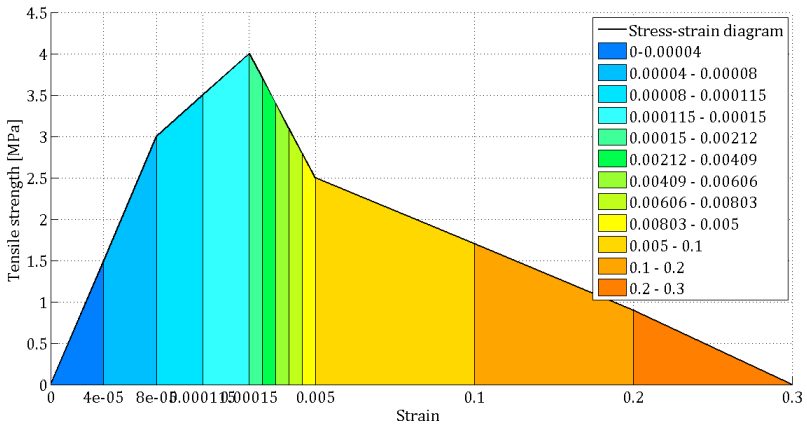

Figure 8.24: Colorcoding of an altered stress-strain diagram

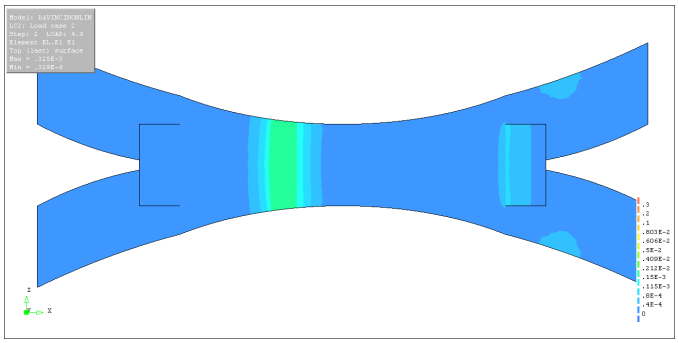

(a) Step 2, load: 4.90kN,

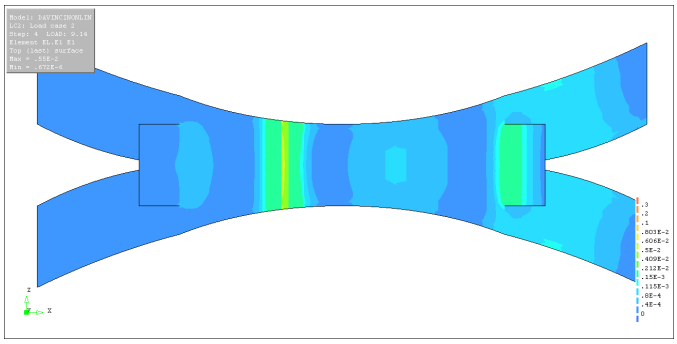

(b) Step 4, load: 9.14kN,

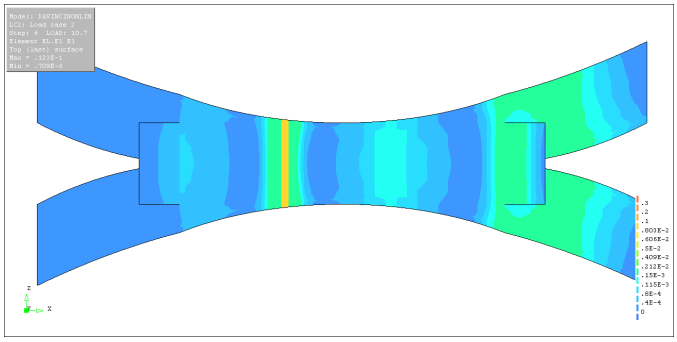

(c) Step 6, load: 10.70kN,

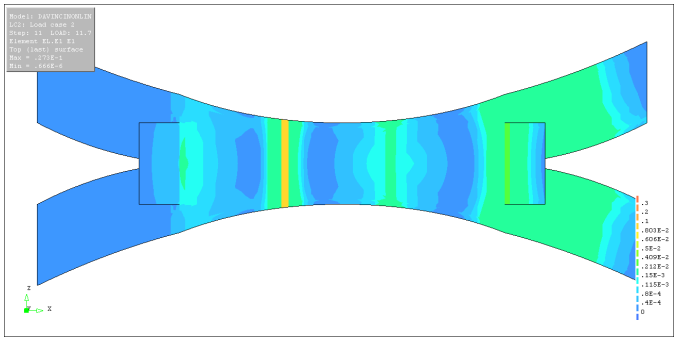

(d) Step 11, load: 11.70kN,

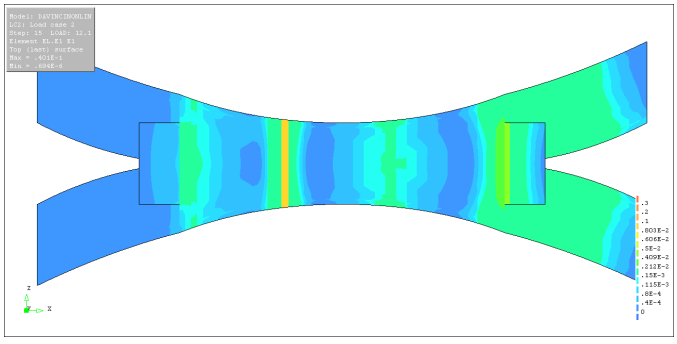

(e) Step 15, load: 12.10

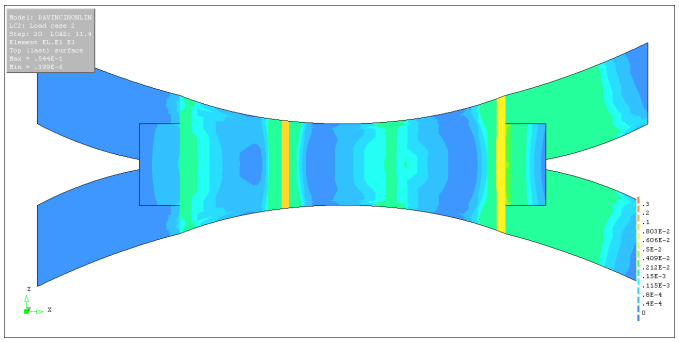

(f) Step 20, load: 11.40kN,

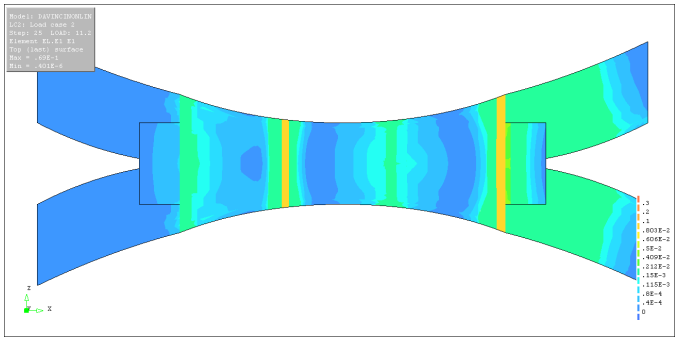

(g) Step 25, load: 11.20kN,

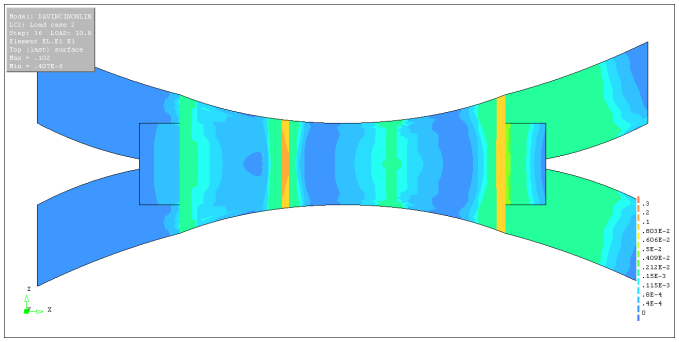

(h) Step 36, load: 10.80kN,

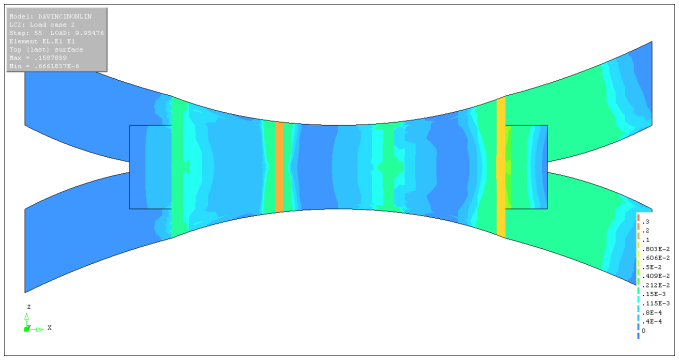

(i) Step 55, load: 9.95kN,

Figure 8.25: Crack propagation on bottom surface in da Vinci bridge

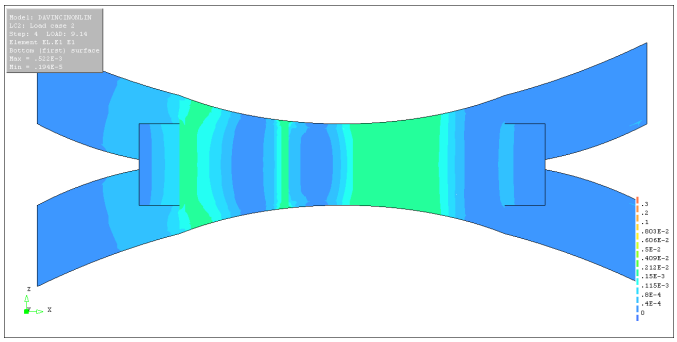

(a) Step 5, load: 2.64kN,

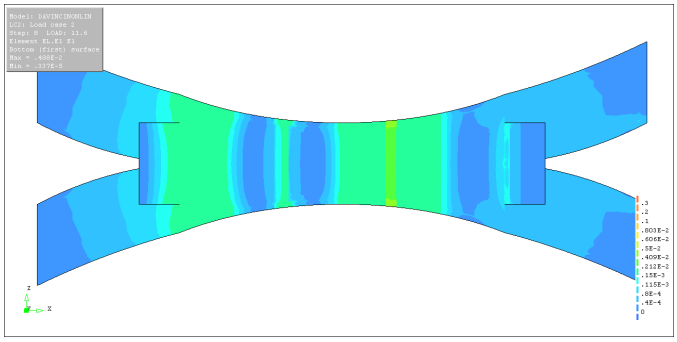

(b) Step 10, load: 3.18kN,

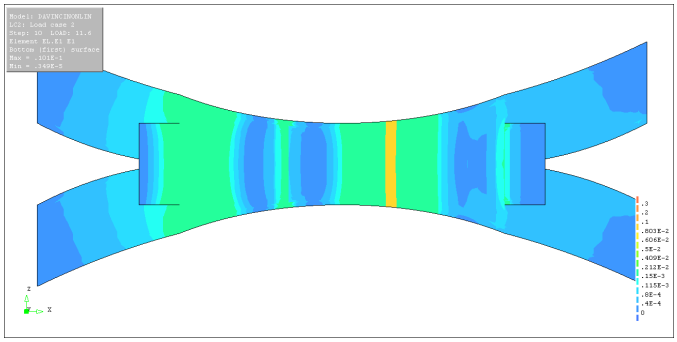

(c) Step 14, load: 3.25kN,

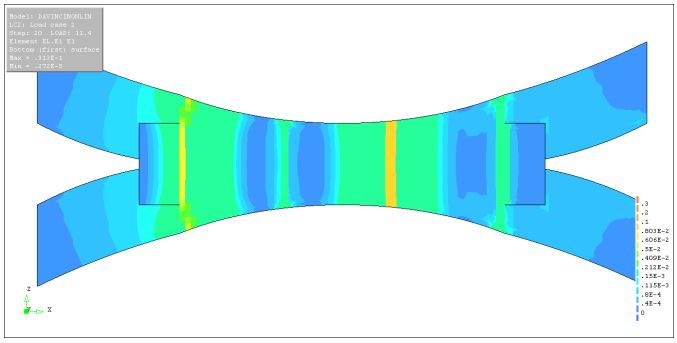

(d) Step 15, load: 2.98kN,

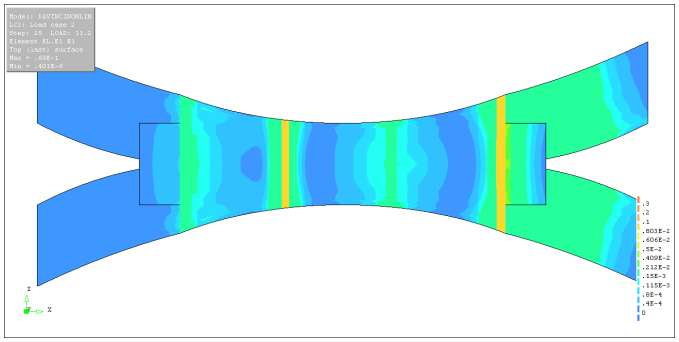

(e) Step 20, load: 2.29kN,

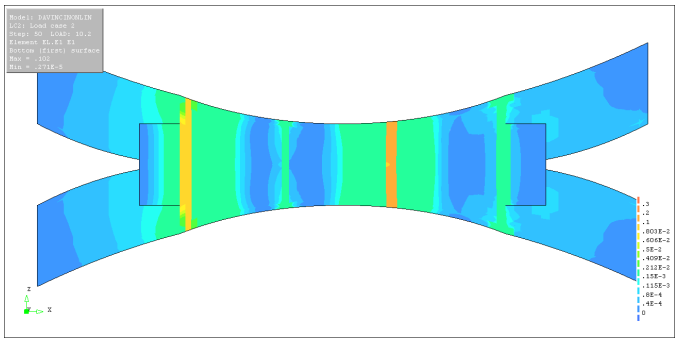

(f) Step 25, load: 1.83

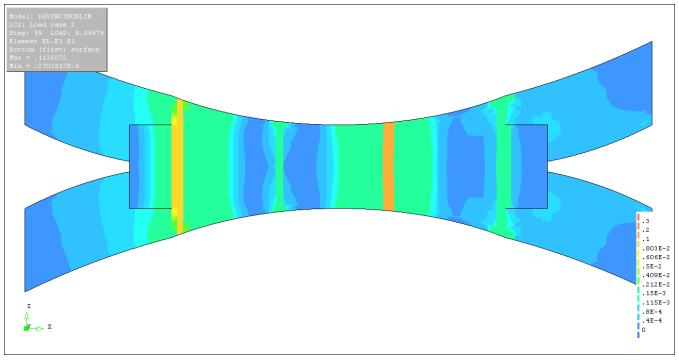

(g) Step 30, load: 1.4kN,

Figure 8.26: Crack propagation on top surface in da Vinci bridge

Chapter 9

Discussion

9.1 Expected results

Based on the theory described in Section 4.1.2 and the data attained from the 2010 testing given in Section 6.2.4 the assumed residual tensile strength is:

$$f_{\text{ftk,res,2.5}} = 0.37 f_{\text{Rk,3}} = 0.37 \cdot 12.57 = 4.65 MPa \tag{9.1}$$

This however is assuming immediate softening behaviour, and concern principally fibre reinforced concrete with normal strength. For UHPFRC some hardening behaviour is assumed and the residual tensile strength is calculated from the flexural strength at maximum load:

$$f_{\text{ftk,res,0.5}} = 0.37 f_{\text{Rk,1}} = 0.37 \cdot 16.2 = 6 MPa \tag{9.2}$$

When the residual strength was set to 6MPa in the stress-strain diagram, the bridges capacity exceeded the true capacity with a factor of two. The original plan was to use the results from the bridge test to decide the tensile behaviour, but after curve fitting, the residual strength giving the best result was 2.9MPa. At this point in the project it was decided to extract material samples from the bridge for additional testing.

Using the beam test results and a beam model in DIANA a higher residual strength was achieved, although the expected value 6MPa was still unachievable.

9.2 Possible source of errors

In both the analyses and in the experiments there are many possible sources of errors causing the results to diverge from what was expected. First, the process of mixing and casting the concrete was rather problematic. As

described in Section 6.2.3 it was challenging to spread the matrix evenly into the formwork and the filling had to be done partially. The final bridge had many large open pores in the surface that indicates an imperfect casting procedure which may have affected the concrete strength.

In the laboratory the bridge supports were clamped to the ground. It is difficult to see in the results if the supports have been 100% constrained. After looking at the correspondence between DIANA and laboratory testing, the reliability of the supports in the testing was discussed. A method of representing this in the model could be to support one end on springs or on an elastic material with a defined stiffness. After the beams were tested however, it was concluded that this possible source of error would have little effect on the results so there were no modifications done to the model.

During testing of the beams it was discovered that the thickness varied over the plane. Due to unevenness at the supports the laser measured varying deflections during loading and the curve was very rough. An average thickness was determined to be 35mm for the DIANA model to simplify the model. For several beams, the thickest point was at the point of loading. Due to this, the average might have been underestimated, resulting in a higher residual strength than what is correct.

It is pointed out early in the master thesis that there are few official standards covering the calculations and dimensioning of UHPFRC. Therefore, altered versions of theory aimed towards FRC have been applied. Due to the wide spectre of results it has been a time consuming process to evaluate the different solution methods especially considering the stress-strain behaviour and the residual strength.

9.3 Issues in DIANA, comments to the software

With no previous knowledge of analyses in DIANA the process of getting to know the software was a somewhat demanding procedure. The DIANA discussion forum on TNO's official web cite was also inconveniently removed at the beginning of the semester, which complicated the process of troubleshooting. The user interface of DIANA is quite unintuitive and the user manual is large, but poorly organized. As a result of this, a large amount of the time put into this thesis have been spent solving different issues in DIANA and troubleshooting errors which are often announced with inconclusive error messages and cryptic coding.

In the early phase of the project, the bridge was modelled in DIANA. Early issues concerning type of elements, element connectivity and direction of local axes lead to challenges in modelling the bridge. These issues

and errors were revealed using linear analyses. With guidance from supervisors and the TNO user manual the issues were one by one solved and the geometric model was finally developed.

For a period, DIANA presented illogical results concerning stress distribution over the cross section. When looking at the stresses in the different integration points over the thickness the cross section was not in equilibrium. The compressive resultant was much higher than the tensile resultant. A modification contributing to a better result was to change the convergence criteria to only fulfil the force norm. After looking at the numbers it was clear that while the displacement norm or the energy norm had converged, the out-of-balance force was unacceptably high which may have been the reason for the equilibrium error.

A problem when looking explicitly at the force norm was to achieve convergence early in the softening domain. This was only a problem for the beam analysis and the bridge had no problem converging. The problem was attempted solved in many ways. Load steps ranged from 0.1-1, the stress-strain curve was continually altered throughout the process and different options of the arc-length method was applied, with little luck. There were also run deflection controlled analyses, but with similar result and similar convergence problems.

In the process of trying to solve the equilibrium problem it was decided to increase the integration points. The default, which is 2x2 over the element plane and 3 over the thickness, was changed to 3x3 points over the plane and 9 points over the thickness. This did not solve the problem, but the alteration succeeded in smoothing out the load-deflection curves and achieving a generally more accurate result. Figure 8.6 in Section 8.4.3 illustrates the large deviation between an analysis using the 3 and 9 integration points over the thickness. The reason for the inaccuracy is that the data calculated in the integration points is extrapolated over the area that the point represent. Increasing the number of points decreases the area to extrapolate over.

In the model it was first decided to use a *smeared rotating crack* model. The model take into consideration the cracks continuously rotation and the shear stress is automatically calculated at all times with respect to rotating local axes. This proved to cause problems when calculating the non-linear flexural effects and might be a reason for the beam analyses' converging issues. It was mainly interesting to look at flexural behaviour in the analyses. Therefore, it was decided to change the crack model to *smeared fixed crack*. This option fixes the cracks stress direction and uses a shear retention factor to consider the shear behaviour in the analyses. The recommended value for this factor is 0.1, but as we were interested in neglecting shear all together

it was set to 1. This solved many of the convergence problems and although some points did not converge the surrounding points fulfilled the criteria and the curves were assumed satisfactory.

9.4 Results

During the process of analysing the beam and bridge only a small percentage of the results have been saved and presented in the report. Many of the analyses have been dismissed due to convergence problems, large deviation from the expected results or other aspects making the result unfit for further discussion.

When it was cast in 2010, the bridge was protected by a burlap sack to reduce evaporation during the hydration process. As mentioned in Section 4.1.4 the surface evaporation of high strength concrete should be completely prevented due to the possibility of large plastic shrinkage. A burlap sac only partly prevents surface evaporation. Post casting, the bridge was painted and therefore somewhat protected against drying. However, under an inspection before testing one could see small cracks in the paint indicating some shrinkage. Poor protection against plastic shrinkage, an expected autogenous shrinkage in addition to possible drying shrinkage over four years of storage may have caused the bridge to develop many micro cracks previous to testing. The thin cross section contributes to the negative effects micro cracks can have to the strength of the bridge. One can see in Figure 8.22 how the DIANA model is stiffer than the bridge. The bridges initial stiffness is similar to the analysis, but cracking and non-linear behaviour occur much faster in the bridge. Time dependant effects can have caused this tendency. The concrete residual strength is however not affected due to the fact that it is the fibres that supply the tensile strength properties. The initial cracking strength might also have been effected by moving the bridge several times over the years.

For the bridge analysis there was little softening after cracking. Extensive softening is more common for FRC than UHPFRC and the high strength concrete reduces the softening. The softening in the laboratory test may be a result of reduction in stiffness caused by time-dependent effects. It may also be a result of poorly casting, assuming the material model is correct. As expected there is a stiffer behaviour at the unloaded point of measuring in the beginning. However, after reaching residual strength the displacement at this point exceeds the displacement under the load. This is not in accordance with test results, but was the tendency in all the analyses executed during the project period.

In the beam testing there was only one prominent crack in the 4-point

test. We can see that this also is the fact in the analyses where there are two cracks under loading. After a certain softening only one crack stands out as prominent which may indicate a correct material model. A result that does not indicate the correct material model is however the displacement in the bridge. As mentioned, in the analyses the positive displacement at the unloaded side of the centre is much larger than the negative displacement under the load. This is not in agreement with the experimental results. A fear amount of time was spent to try to turn that tendency around, with no luck.

The question now is if the material properties are correct. Due to many possible sources of error it is difficult to be certain that the material properties obtained from the analyses are correct. One important question is if the shape of the stress strain diagram is correct. The shape based on a constant or hardening part on the curve after initial cracking and a softening part on the curve giving some softening behaviour after crack localization has proved to be the shape that best correspond with the results from the laboratory.

Chapter 10

Conclusion

10.1 Conclusions

The following conclusions are made based on the experiments and FEM analyses presented in the thesis.

- The research presented in the report concludes with a stress-strain relationship for the material used in the da Vinci brigde. The cracking strength is 3.0MPa and the residual strength is 4.0MPa. A hardening and a softening tensile behaviour is determined and the compressive strength is defined as 113.7MPa based on previous testing.

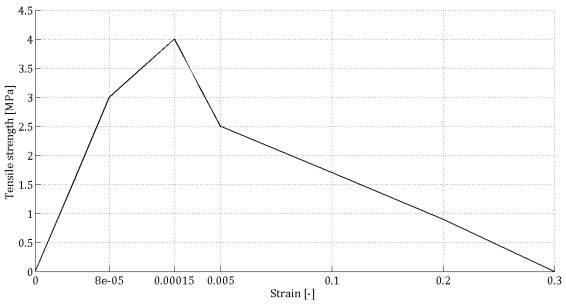

Figure 10.1: Stress-strain diagram of da Vinci UHPFRC. The x-axis is modified to better present the shape of the curve.

- The flexural capacity of the da Vinci bridge built in 2010 was 12.1kN.
- The values of the cracking strength and the post-cracking strength have been determined assuming a thickness of 35mm in the beams. By a possible underestimation of the average value, this can have contributed in an overestimated residual strength.

- Number of integration points, a strict force convergence norm and avoiding shear stresses in the cracks proved quite important for the accuracy of the results in DIANA. The non-linear model is quite sensitive to modifications in the stress-strain behaviour especially after crack localization.

- Ageing and time dependent effects as shrinkage and drying have an impact on the stiffness of the structure and changes the cracking behaviour. This may be avoided to some extent during mixing and casting using methods of protection from shrinkage. Also,certain additives and heat treatment of UHPFRC can reduce time-dependent effects.

- For slender constructions which are designed for small service loads, UHPFRC shows rather good quality in strength and ductility. This was expected from theoretical research. However, this master thesis proves that mixing and casting of such concrete must be executed with great care and a reduction in stiffness over time should be expected.

10.2 Concluding remark and suggestions for further work

It has proven difficult to research and determine material properties of the da Vinci bridge due to many sources of error. The conclusions are based on assumptions and a definite number of curve fittings. One can continue to tweak the analyses until total conformity with experimental results. It would however, not guarantee a more accurate result than the one presented in this master thesis. There are many influencing factors, such as ageing, geometric imperfections, boundary conditions among others resulting in divergence between the analyses and test results.

A disagreement between the deflection in the bridge analyses and laboratory test indicates that there might be errors in the conclusion. For further research in the use of UHPFRC, especially in arches, one recommendation is to use more simple arch models, where geometry and casting is better controlled and easier to reconstruct in a FEM program. Also, it is recommended to obtain material properties by analysing and testing standardized tests before implementing them in an explicit arch model. It might also be of interest to use a different FEM software to analyse the da Vinci bridge and compare it to DIANA analyses.

In time it is also interesting to look at different types of UHPFRC and compare the results considering w/b ratio, fibre content and the use of different additives.

Bibliography

AFGC (**2013**). "Association Francaise de Genie Civil - UHPFRC 2013."

Banthia, N. (**2008**). *Fibre Reinforced Concrete*. Ph.D. thesis.

Bjøntegaard, y. (**2007**). "Volume changes and cracking tendency in concrete." Technical report, Statens vegvesen.

COIN (**2013**). "State of the art - UHPFRC." Technical report, SINTEF NTNU.

FDN (**2014**). "Functional Design NL official website:FDN Ultrabridges."

Graybeal, B. (**2011**). "Ultra High Performance Concrete." Technical report, US Department of Transportation - Federal Highway Administration.

Graybeal, B. A. (**2005**). "CHARACTERIZATION OF THE BEHAVIOR OF ULTRA-HIGH PERFORMANCE CONCRETE."

Graybeal, B. A. (**2007**). "Compressive Behavior of Ultra-High-Performance Fiber-Reinforced Concrete."

Haagensrud, J. S., Jørgensen, H. T. S., Saltnes, M. M., Steinnes, E., and Thorsen, M. L. (**2010**). "EiT - Concrete Innovation." Technical report, NTNU.

Habel, K. (**2004**). *Structural Behaviour of Elements Combining Ultra high Performance Fibre Reinforced Concretes (UHPFRC) and Reinforced Concrete*. Ph.D. thesis.

Habel, K., Viviani, M., Denarié, E., and Brühwiler, E. (**2006**). "Development of the mechanical properties of an Ultra-High Performance Fiber Reinforced Concrete (UHPFRC)." *Cement and Concrete Research*, 36(7): 1362–1370.

Kanstad, T., Juvik, D. A., Vatnar, A., Mathisen, A. E., Sandbakk, S., Vikan, H., Nikolaisen, E., Døssland, s., Leirud, N., and Overrein, G. O. (**2011**). "COIN Project Report: Forslag til retningslinjer

for dimensjonering, utførelse og kontroll av fiberarmerte betongkonstruksjoner." Technical report, SINTEF NTNU.

Lafarge (**2014**). "Lafarge industrial company specialising in cement, construction aggregates and concrete."

Löfgren, I. (**2014**). *Fibre-reinforced Concrete for Industrial Construction - a fracture mechanics approach to material testing and structural analysis*. Ph.D. thesis, Chalmers University of Technology.

López, J., Serna, P., Navarro-Gregori, J., and Camacho, E. (**2014**). "RILEM-fib-AFGC International Symposium on Ultra-High Performance Fibre-Reinforced Concrete." *RILEM Publications S.A.R.L*, pages 77 – 86.

Mehta, P. K. and Monterio, J. (**2013**). "Concrete: Microstructure, Properties and Materials."

Nemetschek.Scia (**2013**). "Reference Projects: Museum of European and Mediterranean Civilizations (MuCEM) - Marseille, France."

Palacio, K. (**2013**). "Practical Reccomendations for Nonlinear Structural Analysis in DIANA."

Qing, Y., Zenan, Z., Deyu, K., and Rongshen, C. (**2007**). "Influence of nano-SiO2 addition on properties of hardened cement paste as compared with silica fume." *Construction and Building Materials*, 21(3): 539 – 545. URL `http://www.sciencedirect.com/science/article/pii/S0950061805002837`. Fracture, Acoustic Emission and {NDE} in Concrete (KIFA-4).

Sandbakk, S. (**2011**). *Fibre Reinforced Concrete*. Ph.D. thesis, NTNU.

Sandven, K. R. (**2009**). "Slim footbridge in composite material of UHPFRC."

Sarmiento, E. V. (**2012**). "Modelling of tension behavior in fibre reinforced concrete beams."

Schmidt, M. and Fehling, E. (**2005**). "Ultra-High-Performance Concrete: Research, Development and Application in Europe."

SINTEF (**2013**). "COIN: Annual report 2013." Technical report, SINTEF Building and Infrastructure.

TNO (**2014**). *DIANA User Manual*.

Tuan, N. V., Ye, G., van Breugel, K., Fraaij, A. L., and Bui, D. D. (**2011**). "The study of using rice husk ash to produce ultra high performance concrete." *Construction and Building Materials*, 25(4): 2030 – 2035.

Vik, B. (**2012**). "Buebruer."

Wikipedia (**2014**). "Golden Horn."

Appendices

Appendix A

Tenpar fitting

Tenpar 1		Tenpar 2		Tenpar 3		Tenpar 4		Tenpar 5		Tenpar 6		Tenpar 7	
0,0	0,0	0,0	0,0	0,0	0,0	0,0	0,0	0,0	0,0	0,0	0,0	0,0	0,0
4,0	0,0001	4,0	0,0001	3,5	8E-05	4,0	0,0001	3,0	8E-05	4,0	0,0001	4,0	0,0001
4,1	0,0001	4,1	0,0002	4,1	0,0003	4,1	0,0021	4,0	0,0002	5,0	0,0002	4,1	0,0002
3,5	0,001	2,5	0,005	2,5	0,01	2,5	0,007	2,5	0,005	2,5	0,005	2,5	0,005
2,5	0,005	0,0	0,3	0,0	0,3	0,0	0,3	0,0	0,3	0,0	0,3	0,0	0,2
0,0	0,3												

Figure A.1: Stress strain diagram coordinates

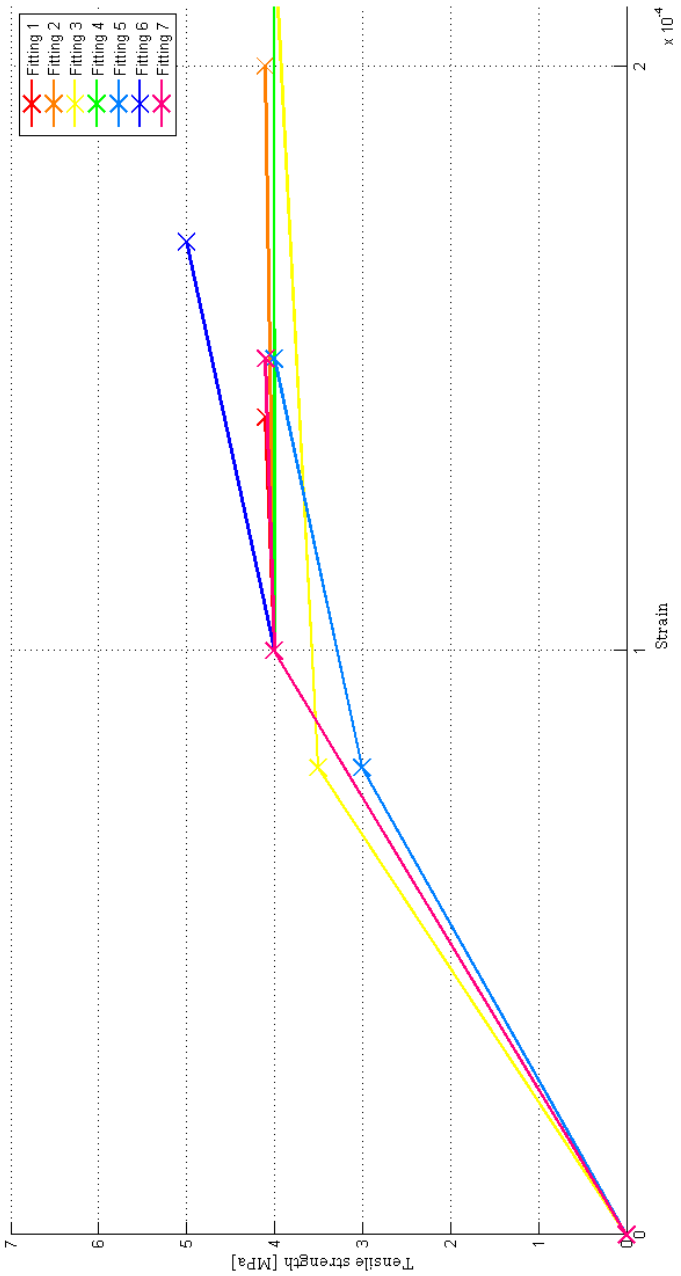

Figure A.2: Stress strain diagrams used in curve fitting, hardening behaviour

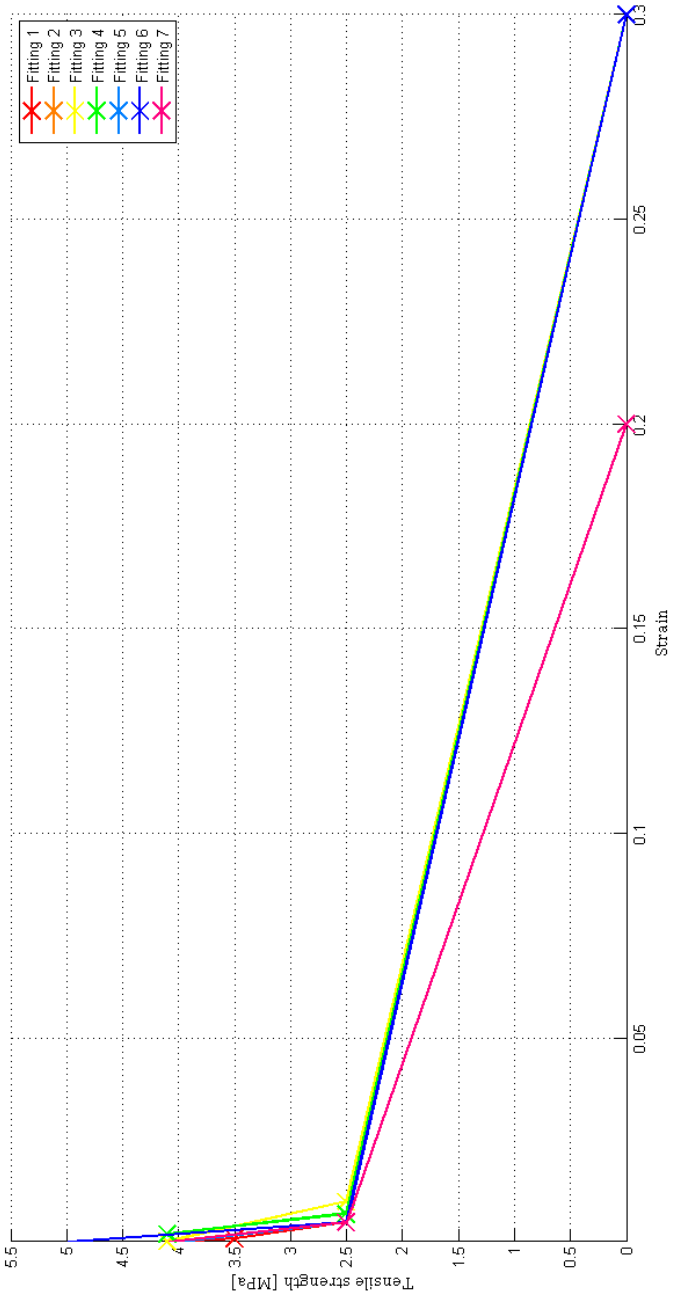

Figure A.3: Stress strain diagrams used in curve fitting, softening behaviour

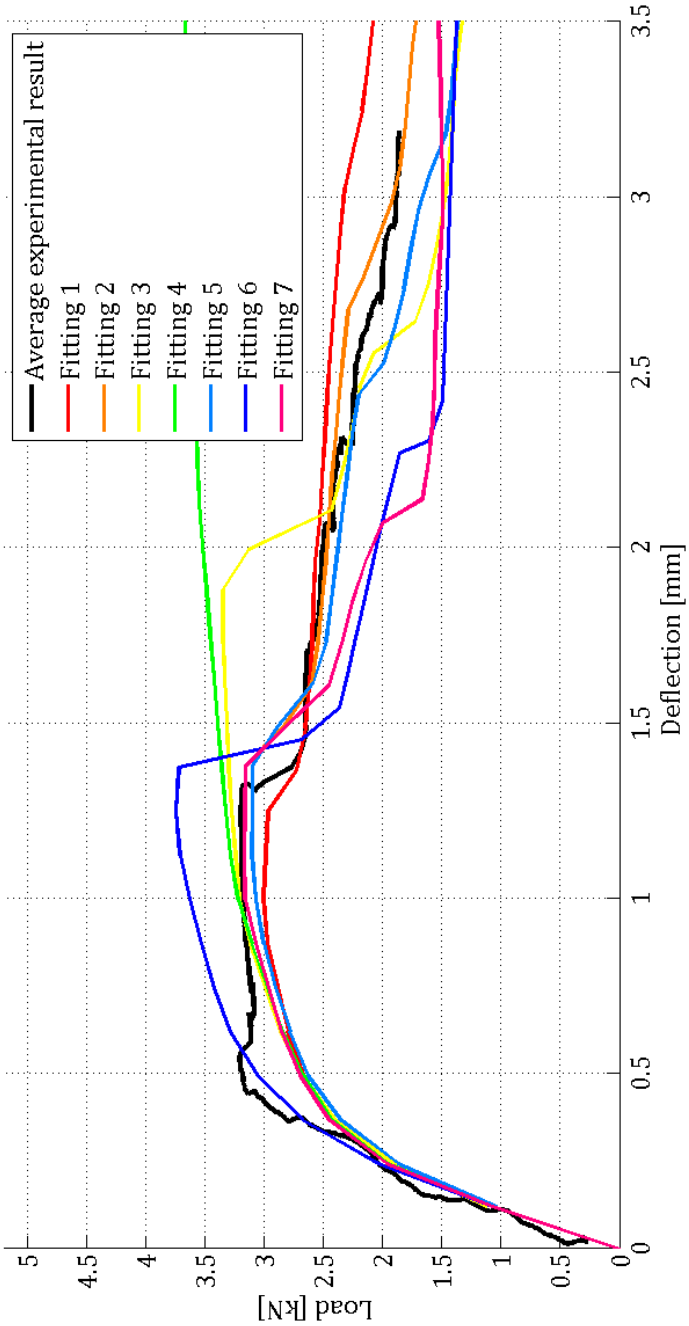

Figure A.4: Results of curve fitting

Appendix B

MATLAB scripts

B.1 Results and curvefitting

```
%-------------------------------------------------------------------------%
%                     MASTER THESIS MATLAB SCRIPT                         %
%-------------------------------------------------------------------------%

clc
clear all
close all

%-------------------------------------------------------------------------
% BEAM TESTING
%-------------------------------------------------------------------------



%-------------------------------------------------------------------------
% Reading the data from experimental testing of beams
%-------------------------------------------------------------------------

tid1 = xlsread('Bjelke1','Tid');
last1 = xlsread('Bjelke1','Last');
nedb1 = xlsread('Bjelke1','Nedboyning');
tid2 = xlsread('Bjelke2','Tid');
last2 = xlsread('Bjelke2','Last');
nedb2 = xlsread('Bjelke2','Nedboyning');
tid3 = xlsread('Bjelke3','Tid');
last3 = xlsread('Bjelke3','Last');
nedb3 = xlsread('Bjelke3','Nedboyning');
tid4 = xlsread('Bjelke4','Tid');
last4 = xlsread('Bjelke4','Last');
nedb4 = xlsread('Bjelke4','Nedboyning');

%-------------------------------------------------------------------------
% Average value
%-------------------------------------------------------------------------

for i = 1:1:890
    last(i) = (last1(i) + last2(i) + last3(i) + last4(i))/4;
end

for i = 1:1:890
    nedb(i) = (nedb1(i) + nedb2(i) + nedb3(i) + nedb4(i))/4;
end

%-------------------------------------------------------------------------
% Sandard deviation
%-------------------------------------------------------------------------

for i = 1:1:890
s(i) = sqrt(1/4*((last1(i)-last(i))^2+(last2(i)-last(i))^2+(last3(i)-
last(i))^2+(last4(i)-last(i))));
end

%-------------------------------------------------------------------------
% Characteristic value
%-------------------------------------------------------------------------
```

```
for i = 1:1:890
    last_k(i) = last(i) -1.7*s(i);
end

%RESULTS OF TEST AND AVERAGE VALUE
figure('Name','Load - Deflection','NumberTitle','off')
hold on
plot(nedb1,last1,'r','LineWidth',2.2)
plot(nedb2,last2,'b','LineWidth',2.2)
plot(nedb3,last3,'color',[1 0.9 0],'LineWidth',2.2)
plot(nedb4,last4,'g','LineWidth',2.2)
plot(nedb,last,'--k','LineWidth',2.5)
hold off
grid on
axis([0,4,0,4])
xlabel('Deflection [mm] ','FontSize',18,'FontName','Cambria');
ylabel('Load [kN] ','FontSize',18,'FontName','Cambria');
% title('Deflection as a function of
loading','FontSize',12,'FontName','Cambria');
legend('Beam 1','Beam 2','Beam 3','Beam 4','Average experimental
result',18,'FontName','Cambria')
legend('Location','NorthEast')


%--------------------------------------------------------------------------
% TENPAR CURVE FITTING
%--------------------------------------------------------------------------


%--------------------------------------------------------------------------
% Reading data from DIANA analysis with force control
%--------------------------------------------------------------------------

DISP_tenpar1 = importdata('DISP_Z_tenpar14_fix.txt');
DISP_tenpar2 = importdata('DISP_Z_tenpar11_fix.txt');
DISP_tenpar3 = importdata('DISP_Z_tenpar12_fix.txt');
DISP_tenpar4 = importdata('DISP_Z_tenpar13_fix.txt');
DISP_tenpar5 = importdata('DISP_Z_tenpar10_2.txt');
DISP_tenpar6 = importdata('DISP_Z_tenpar15_fix.txt');
DISP_tenpar7 = importdata('DISP_Z_tenpar16_fix.txt');
DISP_tenpar5_int = importdata('DISP_Z_tenpar10_3int.txt');


tenpar_1 = [0.0 0.0;
            4.0 0.0001;
            4.1 0.00014;
            3.5 0.001;
            2.5 0.005;
            0.0 0.3];
tenpar_2 = [0.0 0.0;
            4.0 0.0001;
            4.1 0.0002;
            2.5 0.005;
            0.0 0.3];
tenpar_3 =  [0.0 0.0;
```

```
            3.5 0.00008;
            4.1 0.00025;
            2.5 0.01;
            0.0 0.3];
tenpar_4 = [0.0 0.0;
            4.0 0.0001;
            4.1 0.0021;
            2.5 0.007;
            0.0 0.3];
tenpar_5 = [0.0 0.0;
            3.0 0.00008;
            4.0 0.00015;
            2.5 0.005;
            0.0 0.3];
tenpar_6 = [0.0 0.0;
            4.0 0.0001;
            5.0 0.00017;
            2.5 0.005;
            0.0 0.3];
tenpar_7 = [0.0 0.0;
            4.0 0.0001;
            4.1 0.00015;
            2.5 0.005;
            0.0 0.2];

% Stress-strain diagram ------------------------------------------------

% HARDENING BEHAVIOUR
figure('Name','STRESS-STRAIN DIAGRAM, HARDENING
BEHAVIOUR','NumberTitle','off')
hold on
plot(tenpar_1(1:3,2),tenpar_1(1:3,1),'-x','color',[1 0
0],'LineWidth',2.,'MarkerSize',15)
plot(tenpar_2(1:3,2),tenpar_2(1:3,1),'-x','color',[1 0.5
0],'LineWidth',2.,'MarkerSize',15)
plot(tenpar_3(1:3,2),tenpar_3(1:3,1),'-x','color',[1 1
0],'LineWidth',2.,'MarkerSize',15)
plot(tenpar_4(1:3,2),tenpar_4(1:3,1),'-x','color',[0 1
0],'LineWidth',2.,'MarkerSize',15)
plot(tenpar_5(1:3,2),tenpar_5(1:3,1),'-x','color',[0 0.5
1],'LineWidth',2.,'MarkerSize',15)
plot(tenpar_6(1:3,2),tenpar_6(1:3,1),'-x','color',[0 0
1],'LineWidth',2.,'MarkerSize',15)
plot(tenpar_7(1:3,2),tenpar_7(1:3,1),'-x','color',[1 0
0.5],'LineWidth',2.,'MarkerSize',15)
hold off
grid on
axis([0,0.00021,0,7])
xlabel('Strain ','FontSize',12,'FontName','Cambria');
ylabel('Tensile strength [MPa] ','FontSize',12,'FontName','Cambria');
% title('Deflection as a function of
loading','FontSize',12,'FontName','Cambria');
legend('Fitting 1','Fitting 2','Fitting 3','Fitting 4','Fitting 5','Fitting
6','Fitting 7','FontSize',12,'FontName','Cambria')
legend('Location','NorthEast')
```

```
%SOFTENING BEHAVIOUR
figure('Name','STRESS-STRAIN DIAGRAM, SOFTENING
BEHAVIOUR','NumberTitle','off')
hold on
plot(tenpar_1(:,2),tenpar_1(:,1),'-x','color',[1 0
0],'LineWidth',2.,'MarkerSize',15)
plot(tenpar_2(:,2),tenpar_2(:,1),'-x','color',[1 0.5
0],'LineWidth',2.,'MarkerSize',15)
plot(tenpar_3(:,2),tenpar_3(:,1),'-x','color',[1 1
0],'LineWidth',2.,'MarkerSize',15)
plot(tenpar_4(:,2),tenpar_4(:,1),'-x','color',[0 1
0],'LineWidth',2.,'MarkerSize',15)
plot(tenpar_5(:,2),tenpar_5(:,1),'-x','color',[0 0.5
1],'LineWidth',2.,'MarkerSize',15)
plot(tenpar_6(:,2),tenpar_6(:,1),'-x','color',[0 0
1],'LineWidth',2.,'MarkerSize',15)
plot(tenpar_7(:,2),tenpar_7(:,1),'-x','color',[1 0
0.5],'LineWidth',2.,'MarkerSize',15)
hold off
grid on
axis([0.0002,0.3,0,5.5])
xlabel('Strain ','FontSize',12,'FontName','Cambria');
ylabel('Tensile strength [MPa] ','FontSize',12,'FontName','Cambria');
% title('Deflection as a function of
loading','FontSize',12,'FontName','Cambria');
legend('Fitting 1','Fitting 2','Fitting 3','Fitting 4','Fitting 5','Fitting
6','Fitting 7','FontSize',12,'FontName','Cambria')
legend('Location','NorthEast')

%TENPARFITTING: LOAD-DEFLECTION
figure('Name','Load - Deflection','NumberTitle','off')
hold on
plot(nedb,last,'-k','LineWidth',3)
plot(DISP_tenpar1.data(:,3)*-1,DISP_tenpar1.data(:,2),'color',[1 0
0],'LineWidth',2.5)
plot(DISP_tenpar2.data(:,3)*-1,DISP_tenpar2.data(:,2),'color',[1 0.5
0],'LineWidth',2.5)
plot(DISP_tenpar3.data(:,3)*-1,DISP_tenpar3.data(:,2),'color',[1 1
0],'LineWidth',2.5)
plot(DISP_tenpar4.data(:,3)*-1,DISP_tenpar4.data(:,2),'color',[0 1
0],'LineWidth',2.5)
plot(DISP_tenpar5.data(:,3)*-1,DISP_tenpar5.data(:,2),'color',[0 0.5
1],'LineWidth',2.5)
plot(DISP_tenpar6.data(:,3)*-1,DISP_tenpar6.data(:,2),'color',[0 0
1],'LineWidth',2.5)
plot([0;DISP_tenpar7.data(:,3)*-1],[0;DISP_tenpar7.data(:,2)],'color',[1 0
0.5],'LineWidth',2.5)
hold off
grid on
axis([0,3.5,0,5.2])
xlabel('Deflection [mm] ','FontSize',12,'FontName','Cambria');
ylabel('Load [kN] ','FontSize',12,'FontName','Cambria');
% title('Deflection as a function of
loading','FontSize',12,'FontName','Cambria');
legend('Average experimental result','Fitting 1','Fitting 2','Fitting
3','Fitting 4','Fitting 5','Fitting 6','Fitting 7',12,'FontName','Cambria')
legend('Location','NorthEast')
```

```
%RESULT: BEST COINCIDING LOAD-DEFLECTION
figure('Name','Load - Deflection','NumberTitle','off')
hold on
plot(nedb,last,'-k','LineWidth',2.5)
plot([0; DISP_tenpar5.data(:,3)*-1],[0; DISP_tenpar5.data(:,2)],'-
o','color',[1 0 0],'LineWidth',2.5)
hold off
grid on
axis([0,3.5,0,4.0])
xlabel('Deflection [mm] ','FontSize',12,'FontName','Cambria');
ylabel('Load [kN] ','FontSize',12,'FontName','Cambria');
% title('Deflection as a function of
loading','FontSize',12,'FontName','Cambria');
legend('Average experimental result','DIANA analysis','DIANA
loadsteps',12,'FontName','Cambria')
legend('Location','NorthEast')

%COMPARING RESULTS WITH NUMBER OF INTEGRATION POINTS
figure('Name','Load - Deflection','NumberTitle','off')
hold on
plot(nedb,last,'-k','LineWidth',2.5)
plot([0; DISP_tenpar5.data(:,3)*-1],[0; DISP_tenpar5.data(:,2)],'-
o','color',[1 0 0],'LineWidth',2.5)
plot([0; DISP_tenpar5_int.data(:,3)*-1],[0; DISP_tenpar5_int.data(:,2)],'-
o','color',[ 0 1 0],'LineWidth',2.5)
hold off
grid on
axis([0,3.5,0,4.5])
xlabel('Deflection [mm] ','FontSize',18,'FontName','Cambria');
ylabel('Load [kN] ','FontSize',18,'FontName','Cambria');
% title('Deflection as a function of
loading','FontSize',12,'FontName','Cambria');
legend('Average experimental result','DIANA analysis with 9 integration
points','DIANA analysis with 3 integration points',12,'FontName','Cambria')
legend('Location','NorthEast')

%--------------------------------------------------------------------------
% TENPAR 5
%--------------------------------------------------------------------------

colormap jet

tenpar_5 = [0.0 0.0;
            1.5 0.1;
            3.0 0.2;
            3.5 0.2875;
            4.0 0.375;
            3.7 0.4;
            3.4 0.425;
            3.1 0.45;
            2.8 0.475;
            2.5 0.5;
            1.7 0.8;
            0.9 1.1;
            0.0 1.4;];
```

```
x = tenpar_5(:,2);
y = tenpar_5(:,1);
baseline = 0;

%STRESS STRAIN DIAGRAM
figure('Name','Stress-strain diagram','NumberTitle','off')
hold on
plot(x,y,'k','LineWidth',2.,'MarkerSize',15)
hold off
grid on
set(gca,'XTick', [0.0 0.2 0.375 0.5 0.8 1.1
1.4],'FontSize',16,'FontName','Cambria')
set(gca,'XTickLabel', [0 .8E-4 .15E-3 .5E-2 .1 .2
.3],'FontSize',16,'FontName','Cambria');
axis([0,1.4,0,4.5])
xlabel('Strain ','FontSize',16,'FontName','Cambria');
ylabel('Tensile strength [MPa] ','FontSize',16,'FontName','Cambria');

%COLORCODED STRESS STRAIN DIAGRAM
figure('Name','Stress-strain diagram','NumberTitle','off')
hold on
plot(x,y,'k','LineWidth',2.,'MarkerSize',15)
f1 = fill(x([1 1:2 2]), [baseline; y(1:2); baseline],'b');
set(f1,'FaceColor',[0    0.5000    1.0000]);
f2 = fill(x([2 2:3 3]), [baseline; y(2:3); baseline],'b');
set(f2,'FaceColor',[0    0.7500    1.0000]);
f3 = fill(x([3 3:4 4]), [baseline; y(3:4); baseline],'b');
set(f3,'FaceColor',[0    0.9    1.0000]);
f4 = fill(x([4 4:5 5]), [baseline; y(4:5); baseline],'c');
set(f4,'FaceColor',[0.2 1 1]);
f5 = fill(x([5 5:6 6]), [baseline; y(5:6); baseline],'c');
set(f5,'FaceColor',[0.2500    1.0000    0.600]);
f6 = fill(x([6 6:7 7]), [baseline; y(6:7); baseline],'g');
set(f6,'FaceColor',[0    1.0000    0.3]);
f7 = fill(x([7 7:8 8]), [baseline; y(7:8); baseline],'g');
set(f7,'FaceColor',[0.6 1 0.2]);
f8 = fill(x([8 8:9 9]), [baseline; y(8:9); baseline],'y');
set(f8,'FaceColor',[0.7500    1.0000    0.100]);
f9 = fill(x([9 9:10 10]), [baseline; y(9:10); baseline],'y');
set(f9,'FaceColor',[1.0000    1.0000         0]);
f10 = fill(x([10 10:11 11]), [baseline; y(10:11); baseline],'y');
set(f10,'FaceColor',[1.0000    0.8500         0]);
f11 = fill(x([11 11:12 12]), [baseline; y(11:12); baseline],'r');
set(f11,'FaceColor',[1.0000    0.6500         0])
f12 = fill(x([12 12:13 13]), [baseline; y(12:13); baseline],'r');
set(f12,'FaceColor',[1.0000    0.5000         0]);
hold off
grid on
set(gca,'XTick', [0.0 0.1 0.2 0.2875 0.375 0.5 0.8 1.1 1.4])
set(gca,'XTickLabel', [0 .4E-4 .8E-4 .115E-3 .15E-3 .5E-2 .1 .2 .3]);
axis([0,1.4,0,4.5])
xlabel('Strain ','FontSize',18,'FontName','Cambria');
ylabel('Tensile strength [MPa] ','FontSize',18,'FontName','Cambria');
% title('Deflection as a function of
loading','FontSize',12,'FontName','Cambria');
```

```
legend('Stress-strain diagram','0-0.00004','0.00004 - 0.00008','0.00008 -
0.000115','0.000115 - 0.00015','0.00015 - 0.00212','0.00212 -
0.00409','0.00409 - 0.00606','0.00606 - 0.00803','0.00803 - 0.005','0.005 -
0.1','0.1 - 0.2','0.2 - 0.3')


%-------------------------------------------------------------------------
% BRIDGE TESTING
%-------------------------------------------------------------------------



%-------------------------------------------------------------------------
% Reading the data from experimental testing of beams
%-------------------------------------------------------------------------

tid = xlsread('davinci','Tid');
last = xlsread('davinci','Last');
nedb_last = xlsread('davinci','Nedboyninglast');
nedb_strekk = xlsread('davinci','Nedboyningstrekk');
toyn_last = xlsread('davinci','Toyninglast')*10^-6;
toyn_strekk = xlsread('davinci','Toyningstrekk')*10^-6;

% Edit lengths of vectors-----------------------------------------------

editlength = length(toyn_last);

for n=1:editlength
    last_edit(n) = last(n);
end

%-------------------------------------------------------------------------
% Reading data from DIANA analysis with force control
%-------------------------------------------------------------------------

DISP_10_1 = importdata('DISP_Y_tenpar10_1.txt');
DISP_10_2 = importdata('DISP_Y_tenpar10_2.txt');

%LOAD DEFLECTION COMPARISON
figure('Name','Load - Deflection comparison','NumberTitle','off')
hold on
plot(nedb_last*-1,last*-1,'r','LineWidth',2.2)
plot(nedb_strekk*-1,last*-1,'b','LineWidth',2.2)
plot(DISP_10_1.data(1:100,3)*-1,DISP_10_1.data(1:100,2),'-o','color',[1 0.9
0],'LineWidth',2.2,'MarkerSize',8)
plot(DISP_10_2.data(1:100,3),DISP_10_2.data(1:100,2),'-o','color',[0 0.8
0],'LineWidth',2.2,'MarkerSize',8)
hold off
grid on
axis([0,28,0,14.5])
xlabel('Deflection [mm] ','FontSize',18,'FontName','Cambria');
ylabel('Load [kN] ','FontSize',18,'FontName','Cambria');
% title('Deflection as a function of
loading','FontSize',12,'FontName','Cambria');
```

```
legend('Experimental negative displacement at point A','Experimental positive
displacement at point B', 'DIANA negative displacement at point A','DIANA
positive displacement at point B','FontSize',16,'FontName','Cambria')
legend('Location','NorthEast')

%LOAD DEFLECTION EXPERIMENTAL RESULTS
figure('Name','Load - Deflection','NumberTitle','off')
hold on
plot(nedb_last*-1,last*-1,'r','LineWidth',2.2)
plot(nedb_strekk*-1,last*-1,'b','LineWidth',2.2)
hold off
grid on
axis([0,28,0,14])
xlabel('Deflection [mm] ','FontSize',18,'FontName','Cambria');
ylabel('Load [kN] ','FontSize',18,'FontName','Cambria');
% title('Deflection as a function of
loading','FontSize',12,'FontName','Cambria');
legend('Negative displacement at point A','Positive displacement at point
B','FontSize',16,'FontName','Cambria')
legend('Location','NorthEast')

%LOAD STRAIN EXPERIMENTAL RESULT
figure('Name','Load - Strain','NumberTitle','off')
hold on
plot(toyn_last,last_edit*-1,'r','LineWidth',2.2)
plot(toyn_strekk,last*-1,'b','LineWidth',2.2)
grid on
xlabel('Strain [-] ','FontSize',18,'FontName','Cambria');
ylabel('Load [kN] ','FontSize',18,'FontName','Cambria');
% title('Strain as a function of loading','FontSize',12,'FontName','Cambria');
legend('Strain at point A', 'Strain at point
B','FontSize',12,'FontName','Cambria')
legend('Location','NorthWest')
```

B.2 Influence lines

```
%--------------------------------------------------------------------------%
%                            INFLUENCE LINES                               %
%--------------------------------------------------------------------------%

clear all
close all
clc

% Properties
b = 400;            %mm
y = 30;             %mm
E = 35000;          %N/mm^2
L = 1600;           %mm
f = 405;            %mm
I0 = b*y^3/12;      %mm^4
A0 = b*y;           %mm^2

% Influence line for horizontal component of vertical load

dx = 50
N = L
sz = (N)/dx
nu_H = zeros(sz,2);
for j = 1:1:sz+1
    x_1 = dx * (j-1);
    nu_H(j,1) = x_1;
    nu_H(j,2) = ((x_1/L - 2*(x_1/L)^3 + (x_1/L)^4)/3)/(8*f/15/L+I0/f/L/A0) ;
    theta_H(j,1) = nu_H(j,2)*f/L;
    bue_y(j,1) = 4*f*x_1*(L-x_1)/L^2;
end


figure('Name','Influenslinje nu_H','NumberTitle','off')
plot(nu_H(:,1),nu_H(:,2),'LineWidth',1.)
grid on
xlabel('x [mm]','FontSize',11);
ylabel('nu_H','FontSize',11);
title('Influence lines for horizontal reaction');

figure('Name','Influenslinje theta_H','NumberTitle','off')
plot(nu_H(:,1),theta_H(:,1),'LineWidth',1.)
grid on
xlabel('x [mm]','FontSize',11);
ylabel('nu_H','FontSize',11);
title('Influence lines for horizontal reaction');

figure('Name','Buehøyde','NumberTitle','off')
plot(nu_H(:,1),bue_y(:,1),'LineWidth',1.)
grid on
xlabel('x [mm]','FontSize',11);
ylabel('nu_H','FontSize',11);
title('Influence lines for horizontal reaction');

hold on
for k=1:1:10
```

```
    x_1=0+dx*(k)
    for i = 1:1:x_1/dx+1
        c = (i-1) * dx;
        R_a = (L-c)/L;
        nu_M0(i,1)=c;
        nu_M0(i,2)=R_a*x_1 - (x_1-c);
    end
    for i =x_1/dx:1:N/dx+1
        c = i*dx;
        R_b = 1 - ((L-c)/L);
        nu_M0(i,1)=c;
        nu_M0(i,2)= R_b*(L-x_1) - (c - x_1);
    end

for j = 1:1:sz+1
    x = dx * (j-1);
    nu_M(j,1) = x;
    nu_M(j,2) = nu_M0(j,2)-nu_H(j,2)*bue_y(j,1);
    theta_M(j,1) = nu_M(j,2)/bue_y(j,1);
end


m(k,1) = x_1
m(k,2) = max(nu_M(:,2))
 figure('Name','','NumberTitle','off')
 plot(nu_M(:,1),-nu_M(:,2),'LineWidth',2.)
 grid on
 xlabel('x [mm]','FontSize',18,'FontName','Cambria');
 ylabel('nu_H','FontSize',18,'FontName','Cambria');
 title('Influenslinje nu_M for x=350','FontSize',18,'FontName','Cambria');
end
 figure('Name','','NumberTitle','off')
 plot(m(:,1),m(:,2),'LineWidth',2.)
 grid on
 xlabel('x [mm]','FontSize',18,'FontName','Cambria');
 ylabel('Maximum moment','FontSize',18,'FontName','Cambria');
 title('Maximum moment as a function of
x','FontSize',18,'FontName','Cambria');
```

Appendix C

dat files excerpt for DIANA analyses

C.1 Beam analysis

```
FEMGEN MODEL      : TESTBEAMNONLIN
ANALYSIS TYPE     : Structural 3D
'UNITS'
LENGTH   MM
TIME     SEC
TEMPER   KELVIN
FORCE    N
'COORDINATES' DI=2
    1      0.000000E+00     0.000000E+00
    2      0.000000E+00     9.375000E+00
    3      0.000000E+00     1.875000E+01
    4      0.000000E+00     2.812500E+01
    5      0.000000E+00     3.750000E+01
    6      0.000000E+00     4.687500E+01
    7      0.000000E+00     5.625000E+01
    8      0.000000E+00     6.562500E+01
    9      0.000000E+00     7.500000E+01
   10      0.000000E+00     8.437500E+01

……

 2038 CQ40S  5349 6390 5350 6407 5367 6423 5366 6406
 2039 CQ40S  5350 6391 5351 6408 5368 6424 5367 6407
 2040 CQ40S  5351 6392 5352 6409 5369 6425 5368 6408
 2041 CQ40S  5352 6393 5353 6410 5370 6426 5369 6409
 2042 CQ40S  5353 6394 5354 6411 5371 6427 5370 6410
 2043 CQ40S  5354 6395 5355 6412 5372 6428 5371 6411
 2044 CQ40S  5355 6396 5356 6413 5373 6429 5372 6412
 2045 CQ40S  5356 6397 5357 6414 5374 6430 5373 6413
 2046 CQ40S  5357 6398 5358 6415 5375 6431 5374 6414
 2047 CQ40S  5358 6399 5359 6416 5376 6432 5375 6415
 2048 CQ40S  5359 6400 5360 6417 5377 6433 5376 6416
MATERIALS
/ 1-2048 /  1
GEOMETRY
/ 1-2048 /  1
DATA
/ 1-2048 /  1
'DATA'
   1 NINTEG 3 3 9
'MATERIALS'
   1 YOUNG     3.500000E+04
     POISON    2.000000E-01
     TOTCRK FIXED
     TENCRV MULTLN
     TENPAR 0.0 0.0
            3.0 0.00008
            4.0 0.00015
            2.5 0.005
            0.0 0.3
     COMCRV CONSTA
     COMSTR    1.137000E+02
     SHRCRV CONSTA
     BETA      1.000000E+00
'GEOMETRY'
   1 THICK     3.500000E+01
```

```
'GROUPS'
NODES
   1 BOUND / 1-17 562-577 5361-5377 6418-6433 /
   2 DEFL / 2161-2177 3218-3233 /
   3 LOAD / 545-561 1618-1633 3761-3777 4818-4833 /
ELEMEN
   4 BEAM / 1-2048 /
NODES
   5 BEAM_N / 1-6433 /
'SUPPORTS'
 / 1-17 562-577 5361-5377 6418-6433 /   TR     2
 / 1-17 562-577 5361-5377 6418-6433 /   TR     3
'LOADS'
CASE 2
ELEMEN
 / 497-512 /
       EDGE    ETA2
       FORCE     -0.333000E+01
       DIRECT      3
 / 1521-1536 /
       EDGE    ETA2
       FORCE     -0.333000E+01
       DIRECT      3
'DIRECTIONS'
    1   1.000000E+00   0.000000E+00   0.000000E+00
    2   0.000000E+00   1.000000E+00   0.000000E+00
    3   0.000000E+00   0.000000E+00   1.000000E+00
'END'
```

C.2 Bridge analysis

```
FEMGEN MODEL      : DAVINCINONLIN
ANALYSIS TYPE     : Structural 3D
'UNITS'
LENGTH   MM
TIME     SEC
TEMPER   KELVIN
FORCE    N
'COORDINATES'
    1      0.000000E+00     0.000000E+00    -2.000000E+02
    2      0.000000E+00     0.000000E+00    -2.325000E+02
    3      0.000000E+00     0.000000E+00    -2.650000E+02
    4      0.000000E+00     0.000000E+00    -2.975000E+02
    5      0.000000E+00     0.000000E+00    -3.300000E+02
    6      0.000000E+00     0.000000E+00    -3.625000E+02
    7      0.000000E+00     0.000000E+00    -3.950000E+02
    8      0.000000E+00     0.000000E+00    -4.275000E+02
    9      0.000000E+00     0.000000E+00    -4.600000E+02
   10      4.244165E+01     3.226491E+00    -1.784292E+02

……

1974 CQ40S  6107 6219 6108 6224 6112 6227 6111 6223
 1975 CQ40S  6108 6220 6109 6225 6113 6228 6112 6224
 1976 CQ40S  6109 6221 5786 6018 5794 6229 6113 6225
 1977 CQ40S  6110 6226 6111 6231 6115 6234 6114 6230
 1978 CQ40S  6111 6227 6112 6232 6116 6235 6115 6231
 1979 CQ40S  6112 6228 6113 6233 6117 6236 6116 6232
 1980 CQ40S  6113 6229 5794 6034 5802 6237 6117 6233
 1981 CQ40S  6114 6234 6115 6239 2465 2530 2466 6238
 1982 CQ40S  6115 6235 6116 6240 2464 2529 2465 6239
 1983 CQ40S  6116 6236 6117 6241 2463 2528 2464 6240
 1984 CQ40S  6117 6237 5802 6050 2298 2527 2463 6241
MATERIALS
/ 1-1984 /  1
GEOMETRY
/ 1-1984 /  1
DATA
/ 1-1984 /  1
'DATA'
   1 NINTEG 3 3 9
'MATERIALS'
   1 YOUNG     3.500000E+04
     POISON    2.000000E-01
     TOTCRK ROTATE
     TENCRV MULTLN
     TENPAR 0.0 0.0
            3.0 0.00008
            4.0 0.00015
            2.5 0.005
            0.0 0.3
     COMCRV CONSTA
     COMSTR    1.137000E+02
'GEOMETRY'
   1 THICK     3.000000E+01
'GROUPS'
NODES
```

```
   1 BOUND / 1-9 82-89 226-229 262-265 634-642 715-722 859-862 895-
898
             1266-1274 1347-1354 1491-1494 1527-1530 1899-1907 1980-
1987
             2124-2127 2160-2163 2531-2539 2603-2610 2739-2746 2803-
2810
             2994-3002 3131-3138 3195-3202 3323-3330 /
ELEMEN
   2 BRIDGE / 1-1984 /
NODES
   3 BRIDGE_N / 1-6241 /
   4 LOAD / 3406-3410 3551-3554 3675-3682 3931-3938 4059-4066 4315-
4322
            4383-4386 4511-4514 /
'SUPPORTS'
 / 1-9 82-89 226-229 262-265 634-642 715-722 859-862 895-898 1266-
1274
   1347-1354 1491-1494 1527-1530 1899-1907 1980-1987 2124-2127 2160-
2163
   2531-2539 2603-2610 2739-2746 2803-2810 2994-3002 3131-3138 3195-
3202
   3323-3330 /   TR     1
 / 1-9 82-89 226-229 262-265 634-642 715-722 859-862 895-898 1266-
1274
   1347-1354 1491-1494 1527-1530 1899-1907 1980-1987 2124-2127 2160-
2163
   2531-2539 2603-2610 2739-2746 2803-2810 2994-3002 3131-3138 3195-
3202
   3323-3330 /   TR     2
 / 1-9 82-89 226-229 262-265 634-642 715-722 859-862 895-898 1266-
1274
   1347-1354 1491-1494 1527-1530 1899-1907 1980-1987 2124-2127 2160-
2163
   2531-2539 2603-2610 2739-2746 2803-2810 2994-3002 3131-3138 3195-
3202
   3323-3330 /   TR     3
'LOADS'
CASE 2
ELEMEN
 / 1085-1088 /
       EDGE    ETA2
       FORCE     -0.230000E+01
       DIRECT      2
 / 1209-1216 /
       EDGE    ETA2
       FORCE     -0.230000E+01
       DIRECT      2
 / 1337-1344 /
       EDGE    ETA2
       FORCE     -0.230000E+01
       DIRECT      2
 / 1405-1408 /
       EDGE    ETA2
       FORCE     -0.230000E+01
       DIRECT      2
'DIRECTIONS'
```

```
    1   1.000000E+00   0.000000E+00   0.000000E+00
    2   0.000000E+00   1.000000E+00   0.000000E+00
    3   0.000000E+00   0.000000E+00   1.000000E+00
'END'
```

Appendix D

dcf files for DIANA analyses

D.1 Beam analysis

```
*FILOS
 INITIA
*INPUT
 READ  FILE "testbeamnonlin.dat"
*NONLIN
 BEGIN EXECUT
   BEGIN LOAD
     LOADNR 2
     BEGIN STEPS
       BEGIN EXPLIC
         ARCLEN
         SIZES 1E-005 1(30)
       END EXPLIC
     END STEPS
   END LOAD
   BEGIN ITERAT
     BEGIN CONVER
       DISPLA  OFF
       FORCE  CONTIN
     END CONVER
     MAXITE 20
   END ITERAT
 END EXECUT
 BEGIN OUTPUT
   FILE "testbeamnonlin"
   DISPLA  TOTAL  TRANSL  GLOBAL
   ELMFOR  TOTAL  TRANSL
   FORCE  REACTI  TRANSL  GLOBAL
   FORCE  RESIDU  TRANSL  GLOBAL
   NODFOR  TOTAL  TRANSL  GLOBAL
   STRAIN  CRACK  GREEN
   STRAIN  PLASTI  GREEN  GLOBAL  INTPNT
   STRAIN  PLASTI  GREEN  PRINCI
   STRAIN  PLASTI  GREEN  VONMIS
   STRAIN  TOTAL  GREEN  GLOBAL  INTPNT
   STRAIN  TOTAL  MOMENT  GLOBAL
   STRAIN  TOTAL  MOMENT  LOCAL
   STRAIN  TOTAL  FORCE  LOCAL
   STRAIN  TOTAL  FORCE  GLOBAL
   STRAIN  TOTAL  GREEN  PRINCI
   STRAIN  TOTAL  GREEN  GLOBAL
   STRESS  TOTAL  CAUCHY  GLOBAL
   STRESS  TOTAL  CAUCHY  PRINCI
   STRESS  TOTAL  CAUCHY  VONMIS
   STRESS  TOTAL  MOMENT  GLOBAL
   STRESS  TOTAL  MOMENT  LOCAL
   STRESS  TOTAL  FORCE  LOCAL
   STRESS  TOTAL  FORCE  GLOBAL
```

```
  STRESS  TOTAL  CAUCHY  GLOBAL  INTPNT
 END OUTPUT
 BEGIN OUTPUT
   TABULA
   FILE "testbeamnonlin"
   SELECT  ELEMEN 144 136 /
   BEGIN STRAIN
     BEGIN TOTAL
       BEGIN GREEN
         BEGIN GLOBAL
           COORDI
           INTPNT
         END GLOBAL
       END GREEN
     END TOTAL
   END STRAIN
   BEGIN STRESS
     BEGIN TOTAL
       BEGIN CAUCHY
         BEGIN GLOBAL
           COORDI
           INTPNT
         END GLOBAL
       END CAUCHY
     END TOTAL
   END STRESS
 END OUTPUT
 BEGIN TYPE
   BEGIN PHYSIC
     CRACKI  CONSIS
     PLASTI  SECOND
   END PHYSIC
 END TYPE
*END
```

D.2 Bridge analysis

```
*FILOS
 INITIA
*NONLIN
 BEGIN EXECUT
   BEGIN LOAD
     LOADNR 2
     BEGIN STEPS
       BEGIN EXPLIC
         ARCLEN
         SIZES 1e-005 1(100)
       END EXPLIC
     END STEPS
   END LOAD
   BEGIN ITERAT
     BEGIN CONVER
       BEGIN FORCE
         CONTIN
         TOLCON 0.01
       END FORCE
       DISPLA OFF
       ENERGY OFF
     END CONVER
     MAXITE 20
   END ITERAT
 END EXECUT
 BEGIN OUTPUT
   FILE "davincinonlin"
   DISPLA  TOTAL  TRANSL  GLOBAL
   ELMFOR  TOTAL  TRANSL
   FORCE  REACTI  TRANSL  GLOBAL
   FORCE  RESIDU  TRANSL  GLOBAL
   NODFOR  TOTAL  TRANSL  GLOBAL
   STRAIN  CRACK  GREEN
   STRAIN  PLASTI  GREEN  GLOBAL  INTPNT
   STRAIN  PLASTI  GREEN  PRINCI
   STRAIN  PLASTI  GREEN  VONMIS
   STRAIN  TOTAL  GREEN  GLOBAL  INTPNT
   STRAIN  TOTAL  MOMENT  GLOBAL
   STRAIN  TOTAL  MOMENT  LOCAL
   STRAIN  TOTAL  FORCE  LOCAL
   STRAIN  TOTAL  FORCE  GLOBAL
   STRAIN  TOTAL  GREEN  PRINCI
   STRAIN  TOTAL  GREEN  GLOBAL
   STRESS  TOTAL  CAUCHY  GLOBAL
   STRESS  TOTAL  CAUCHY  PRINCI
   STRESS  TOTAL  CAUCHY  VONMIS
   STRESS  TOTAL  MOMENT  GLOBAL
   STRESS  TOTAL  MOMENT  LOCAL
   STRESS  TOTAL  FORCE  LOCAL
   STRESS  TOTAL  FORCE  GLOBAL
   STRESS  TOTAL  CAUCHY  GLOBAL  INTPNT
 END OUTPUT
 BEGIN OUTPUT
   TABULA
   FILE "davincinonlin"
   SELECT  ELEMEN 1336 1344 1512 1520 /
```

```
  BEGIN STRAIN
    BEGIN TOTAL
      BEGIN GREEN
        BEGIN GLOBAL
          COORDI
          INTPNT
        END GLOBAL
      END GREEN
    END TOTAL
  END STRAIN
  BEGIN STRESS
    BEGIN TOTAL
      BEGIN CAUCHY
        BEGIN GLOBAL
          COORDI
          INTPNT
        END GLOBAL
      END CAUCHY
    END TOTAL
  END STRESS
 END OUTPUT
 BEGIN TYPE
   BEGIN PHYSIC
     CRACKI  CONSIS
     PLASTI  SECOND
   END PHYSIC
 END TYPE
*END
```

Appendix E

Concrete recipe used in 2010 (Norwegian)

Prosj./id.:	Navn på serie / blandingsnummer

Blandevolum:	125 liter
Dato:	
Tidspunkt for vanntilsetning	
Ansvarlig:	
Utført av:	

Materialer	Resept kg/m³	Sats kg	Fukt* %	Korr. kg	Oppveid** kg	
Norcem Anlegg	611,5	76,432			76,432	
Elkem Microsilica 940U	122,3	15,286	0	0,000	15,286	
Kalksteinsmel	0,0	0,000	0	0,000	0,000	
Fritt vann	168,8	21,095		-4,299	16,796	18,113
Absorbert vann	10,5	1,317			1,317	
Årdal 0-8 mm	1138,8	142,354	2,1	2,989	145,343	
Årdal 0-2 mm nat. vask	0,0	0,000	0,0	0,000	0,000	
Årdal 8-16mm	285,6	35,695	0,5	0,178	35,873	
Årdal 16-22 mm	0,0	0,000	0,0	0,000	0,000	
	0,0	0,000	0,0	0,000	0,000	
	0,0	0,000	0,0	0,000	0,000	
	0,0	0,000	0,0	0,000	0,000	
	0,0	0,000	0,0	0,000	0,000	
	0,0	0,000	0,0	0,000	0,000	
	0,0	0,000	0,0	0,000	0,000	
Degussa skyflux 550	12,2	1,529	74	1,131	1,529	
	0,0	0,000	100	0,000	0,000	
	0,0	0,000	100	0,000	0,000	
	0,0	0,000	100	0,000	0,000	
Stålfiber	156,0	19,500			19,500	
PP-fiber	0,0	0,000			0,000	

*Se fotnote på delark "Proporsjonering" ** NB! Våte mengder, også for pozzolaner og fillere

Fersk betong					
Tid etter vanntilsetning					
Synkmål					
Utbredelsesmål					
Luft					
Densitet					

Prøvestykker (antall)					
Utstøpningstidspunkt					
Terninger					
150x300 sylindre					
100x200 sylindre					
Bjelker 150x150x550					
Plater 150x600x600					

Delark "Blandeskjema"

Fraksjon I

Type:	Årdal 0-8 mm
Dato:	oktober 2009
FM =	3,25

Åpning	Sikterest (g)		Sikterest
	1	2	(%)
32	0	0	0,0
22,4	0	0	0,0
16	0	0	0,0
11,2	0	0	0,0
8	1,4	0	1,4
4	18,6	0	18,6
2	36,9	0	36,9
1	57,2	0	57,2
0,5	76,4	0	76,4
0,25	87,7	0	87,7
0,125	93,6	0,0	93,6
Bunn	100	0